AOARD-03-4026 / RMO No 2001/1611

Motion adaptation, its role in motion detection under natural image conditions and target detection

Final Report
2 June 2005

THE UNIVERSITY
OF ADELAIDE
AUSTRALIA

David O'Carroll
Discipline of Physiology, School of Molecular & Biomedical Science
& Centre for Biomedical Engineering

Report Documentation Page

Form Approved
OMB No. 0704-0188

1. REPORT DATE	2. REPORT TYPE	3. DATES COVERED
26 JUL 2006	**Final Report (Technical)**	**01-07-2003 to 01-08-2004**

4. TITLE AND SUBTITLE	5a. CONTRACT NUMBER
Motion Adaptation III	**F6256203P0408**
	5b. GRANT NUMBER
	5c. PROGRAM ELEMENT NUMBER
6. AUTHOR(S) **David O'Carroll**	5d. PROJECT NUMBER
	5e. TASK NUMBER
	5f. WORK UNIT NUMBER
7. PERFORMING ORGANIZATION NAME(S) AND ADDRESS(ES) **University of Adelaide,Department of Physiology,S. A. 5005,Australia,NA,5005**	8. PERFORMING ORGANIZATION REPORT NUMBER **AOARD-034026**
9. SPONSORING/MONITORING AGENCY NAME(S) AND ADDRESS(ES) **The US Resarch Labolatory, AOARD/AFOSR, Unit 45002, APO, AP, 96337-5002**	10. SPONSOR/MONITOR'S ACRONYM(S) **AOARD/AFOSR**
	11. SPONSOR/MONITOR'S REPORT NUMBER(S) **AOARD-034026**

12. DISTRIBUTION/AVAILABILITY STATEMENT
Approved for public release; distribution unlimited

13. SUPPLEMENTARY NOTES

14. ABSTRACT
The contractor shall continue investigattion to (1) develop a working model for an elaborated elementary motion detector (EMD) that provides a more robust estimate of local image velocity under natural operating conditions than previous implementations of the Reichardt model and (2) establish a feasible mechanism for producing contrast invariance under real-world conditions that will ultimately provide a blueprint for a robust implementation of an adaptive EMD.

15. SUBJECT TERMS
Biomimetics, Vision, Guidance

16. SECURITY CLASSIFICATION OF:			17. LIMITATION OF ABSTRACT	18. NUMBER OF PAGES	19a. NAME OF RESPONSIBLE PERSON
a. REPORT	b. ABSTRACT	c. THIS PAGE			
unclassified	**unclassified**	**unclassified**		**75**	

1

Introduction

1.1 Background

The control and guidance of movement through a structurally complex world presents enormous computational challenges, yet requires real-time solutions. A hoverfly making a perfectly controlled landing upon a flower moving in the breeze demonstrates these problems are solved by even simple biological systems. Distinguishing complex motions and using this information to control locomotion is an important goal for man-made autonomous flying vehicles, just as it was a strong selective pressure in the evolution of the fly's visual system. Biomimetic approaches to development of electronic guidance and seeker components, based on models of insect visual processing, are now becoming practical due to advances in silicon-based engineering as well as knowledge gained through extensive basic research on the biological system in recent years.

The research program described here advanced this goal through modeling the adaptive properties of the insect motion detection pathway and comparing the model's response with that of the physiological system. This work will lead to insights into neural circuits in the insect brain responsible for guiding and controlling flight, and how these cope with problems imposed by the underlying mechanism used to detect and analyze optical flow. This ability is critical for tasks such as course control during high-speed pursuit, and analysis of the trajectory of moving targets. Since the insect visual system is compact and utilizes relatively sparse coding of the visual input, it provides an ideal model system for a robust, simple and compact guidance and targeting system that could be utilized by small, unmanned flying vehicles.

This report documents an effort to expand understanding the role of the specific phenomenon of *motion adaptation* in the processing of wide-field visual motion detection in insects, particularly in the context of the coding of velocity in natural scenes, and to exploit this knowledge to develop biomimetic computer models capable of performing similar functions. The project is a cross-disciplinary study involving approaches ranging from basic physiological investigation, through algorithm development, to implementation in software. Insect visual neurons display a remarkable ability to respond robustly to the motion of both visual targets and wide-field optic flow, and so this approach has great potential for extension of understanding from basic biology into biomimetic applications where similar tasks need to be solved.

The focus of this project was on *motion adaptation* that occurs in the visual pathway that leads from the retina to tangential neurons in the lobula plate (3rd optic ganglion) of the fly. In particular, we focused on the role of this adaptation in promoting the phenomenon of *velocity constancy*, which we define to mean the dependence of average tangential cell response on velocity of optic flow, in combination with its near-invariance with respect to other parameters of the natural imagery that induces optic flow when the animal moves in its environment. An ability to model the system and reproduce this behavior would provide a basis for robust, simple artificial motion detectors that have a wide variety of applications in both military and civilian environments.

Prior to the commencement of this >3 year program of study, the Principal Investigator (Dr David C. O'Carroll) held a position as Assistant Professor of Neurobiology at the University of Washington, Seattle. Support from this program enabled his re-establishment of a new laboratory in Adelaide, Australia, based in the Department of Physiology, but with strong

cross-disciplinary ties to the Department of Electrical and Electronic Engineering. The first 2 years of this program thus represented a major transition period to this new environment and many technical hurdles in setting up new equipment. The success of experiments during the later period of the program in particular is due in no small part to the support of this program.

In the 1st year, we performed pilot neurobiological experiments and put forth a tentative model for motion adaptation, and by conceptual algorithm development in Matlab, demonstrated the feasibility of a biomimetic implementation. In the 2nd year, we consolidated the basic pilot neurobiological studies in order to begin probing the drivers for motion adaptation and developed an adaptive *elementary motion detector* (EMD) model in Matlab and tested and demonstrated its operation in one- and two-dimensional arrays and a simulation of yaw. In the 3rd year we have concentrated modeling efforts on understanding additional non-linear components of motion processing, in an effort to examine their roles in the phenomenon of velocity constancy.

A major bonus for the program of research carried out was a concurrent program funded as a subcontract from Tanner Research Inc., Pasadena under a Phase I and II SBIR contract (Contract F08630-02-C-0013) from the AFRL/MNGN. The major focus of the latter work was development of analog VLSI hardware based on the adaptive EMD model, and we made substantial progress towards this goal over the same period. An extension of the performance period in this SBIR project until April this year permitted proposal and development of a transition path for the biomimetic models developed under this project, into real-world applications. The interaction between the two PI's, Dr David O'Carroll (Adelaide) and Dr Patrick Shoemaker (Tanner) has been a valuable and collegial collaboration, of immense benefit to the success of the AOARD funded program. In particular, the SBIR effort allowed us to oversee the transfer of ideas from basic neuroscience into real-world circuits. What is, perhaps, most valuable in this kind of interaction is the feedback from the engineering approach that suggests limitations or additions to the experimental approach in determining the underlying algorithms. The usefulness of such interactions during the process of collecting even basic neurobiological data has been of huge value in ensuring that the best experimental approach was adopted.

1.2 Objectives

The project had two central goals: to advance the understanding of early elementary motion detectors (EMDs) in the insect visual system (in particular, the role of adaptation) in those elements, and to develop biologically inspired (and in some cases biomimetic) models for an adaptive EMD. Following are the specific technical objectives that were formulated in support of these goals:

The proposed work would be carried out in 3 overlapping phases:

i. Modeling the EMD using adaptive feedback:
   Develop a conceptual model for a set of operations to implement a bio-inspired adaptive mechanism in a software algorithm for an EMD based on our recently published data. Implement it in Matlab and test its responses to animated natural scenes.

ii. Analysis of physiological responses to broad band images.

Undertake further biological experiments to understand the underlying mechanisms of motion adaptation. Test, modify, and elaborate the algorithm proposed in step I by further neurobiological experiments.

iii. Further experiments to match model parameters to physiological responses:
Elaborate the adaptive EMD model into a two-dimensional adaptive EMD array to mimic the receptive field of a tangential HS neuron and test the model using stimuli that mimic the experiments executed under (ii). Adjust model parameters to explore properties of the adaptive model.

1.3 Executive Summary: Neurobiology

1.3.1 Aims and Approach

Our earlier pilot neurobiological recordings (carried out at the University of Cambridge, UK, in 1998) established a group of tangential neurons in the lobula complex of the hoverflies *Eristalis tenax* and *Volucella pelluscens* as an ideal model for investigating the coding of velocity in insect motion detection and the role that adaptation plays in this process. Our pilot data was strongly suggestive of an unusual degree of 'velocity constancy' - i.e. invariance with respect to both contrast and specific image statistics in the neuron response as a function of velocity. Such robust responses would be a highly desirable characteristic of biomimetic motion detectors in artificial vision applications. Because such robustness is not characteristic of a system based on classical biological models for motion detection, we considered this result to be of vital importance for further study. However, our main experimental approach (in-vivo intracellular recording from single neurons in a flight simulator) is technically demanding and our pilot data reflected the experimental recording error (mainly noise) that characterizes this approach. The stimuli used in those experiments were also relatively primitive, being based on artificially generated random texture patterns rather than true 'natural' images of the kind that would be encountered by either natural or artificial seeing systems in real-world applications. A major aim of our Neurobiological experiments was therefore to verify these earlier observations through repeated averaging of responses a larger set of images obtained from natural scenes, and then to begin the process of investigating the underlying mechanisms and drivers for adaptation through further experiments.

Methods: For our main experimental effort we selected a subset of tangential cells, the HS neurons, which are a yaw-selective element. These HS neurons were selected because they have receptive fields that are believed to be tuned to the yaw component of optical flow (although some recent work questions this interpretation). Using a digital camera, we are able to digitize panoramic scenes and stitch these into a continuous cylindrical projection of the surrounding world that can be animated in prolonged sequences that are reasonably appropriate to the world that would be viewed by such neurons under natural conditions. A major effort by Andrew Straw (a PhD student supported by a Howard Hughes Medical Institute Predoctoral Fellowship) during the earlier part of this period established a new set of experimental stimuli via a suite of open-source function calls built on OpenGL to an animation engine optimized for visual stimulus presentation. Andrew adopted the name "VisionEgg" for this project and development of refined versions of these stimuli continues to date. Although the VisionEgg development had commenced prior to the present project, it became a core component of it and refinement of this software continued throughout the project. The software itself incorporated a number of open-source Python libraries (in particular a module, PyGame, original designed as an API for computer games applications). Andrew's contribution to this effort was a valuable one, and he has released his project under the terms of the open-source LGPL for free download (www.visionegg.org). It has subsequently been adopted by a number of laboratories for experimental stimulus development and applications.

In the experiments forming the basis of this project, VisionEgg animated panoramas were presented on a high-speed CRT monitor mounted within the receptive field of the neuron and subtending approximately 100 degree field of regard, at a frame rate of 200Hz. The real-time rendering of the OpenGL engine permits interpolation of the panoramic images so that even very low speeds of motion can be simulated robustly. We implemented complex spatial and temporal anti-aliasing methods to limit any display artifacts. Additional software allowed us to

synchronize stimulus presentation with the digitization of the membrane potential of HS neurons after pre-amplification.

Experimental design: We used several different stimulus paradigms based on the same cylindrical projections of animated textures. Drifting sinusoidal grating patterns that were ramped in contrast over time permitted estimation of the local contrast gain of the neuron within its receptive field ('local sensitivity') as well as basic spatial and temporal tuning properties of each neuron – a technique that we had used to considerable effect in our earlier studies (e.g. Harris, O'Carroll & Laughlin 2000). Velocity constancy was established through a sequence of interleaved test and adapting 'bursts' of simulated yaw for natural panoramic images, permitting quantitative evaluation of the velocity tuning of the neuron under strongly adapted conditions. Further experiments aimed at testing the underlying drivers of motion adaptation using variants of a 'probe-adapt-probe' protocol that allowed us to evaluate the contrast gain of the neuron before and after application of a specific adapting stimulus.

1.3.2 History

Much initial work on this project also formed a major part of the PhD thesis work of Andrew Straw (with salary support from a concurrent Howard Hughes Medical Institute Fellowship). The main part of his thesis work relevant to this effort focused on documenting velocity constancy in the yaw simulator experiments and primarily in a motion-adapted state (using the interleaved stimulus referred to above). As his tenure reached completion, some experiments were incomplete and were fleshed out through further recordings by Tamath Rainsford (with partial salary support from both SBIR and AOARD funded projects) allowing us to verify the conditions under which velocity constancy was observed. Tamath also completed experiments aimed at evaluating velocity constancy in 'unadapted' neurons. Once this was established Tamath moved on to experiments using the probe-adapt-probe protocol to try and quantify gain changes following adaptation with different drivers (specifically the velocity or contrast of the adapting stimulus). Although we had initially hoped to develop a simplified method to evaluate gain change and thus to explore the adapting stimulus parameter space extensively, experimental recording noise plagued our early efforts on this task. Some effort was put into refining this latter stimulus to optimize our ability to evaluate contrast gain change following adaptation in a minimum of neuron recording time (which is always the limitation on the amount of data that can be obtained in biological experiments) by developing analysis techniques based on a Weibull function fit. While successful, this approach was more time consuming than we had hoped, and so complete exploration of the dependence of gain changes on contrast and the speed of the adapting pattern are ongoing. In the last 6 months of the experimental program, have started looking on more detail at the 'waterfall' effect and the speed of motion adaptation. Briefly, most of our earlier experiments and indeed our modeling efforts have focused on contrast gain control as the primary component of motion adaptation. But since our earlier work on this system had suggested a prominent and apparently separable component of adaptation - the 'waterfall effect' might also play a role in velocity coding, we commenced analysis of its dependence on parameters of the stimulus and its possible effects on effective gain.

1.3.3 Results and Conclusions

1. **Velocity constancy in motion-adapted neurons.** Good velocity constancy was observed in adapted responses to sustained yaw stimuli. Velocity tuning shows a

consistent response up to velocities of ca. 200 degrees/second irrespective of the image selective, providing it is statistically natural. Curves from a variety of such images, including two derived from interior of man-made buildings, nearly overlie one another. Yet when narrow-band (sinusoidal) stimuli with different spatial frequencies are presented, they confound this response in a manner consistent with the classical Hassenstein/Reichardt correlation model.

2. **Velocity constancy in unadapted neurons.** Initially applied as a control stimulus, our attempts to measure responses of unadapted neurons (i.e. those that had viewed a blank display for several seconds prior to stimulation) also showed a surprising degree of velocity constancy. This finding, substantiated approximately half-way through this project, and yet contradicted by any 'simple' models based on the Hassenstein/Reichardt type EMD, raised interesting questions about the role of additional non-linear processing in velocity constancy. As a caveat, our analysis technique requires us to discard transient responses (over at least the time constant of the underlying neural delay mechanisms inherent to any motion detection algorithm) and thus raises questions about the possible role of fast temporal adaptation. Experiments designed to test these ideas were commenced at the end of this project (see 6 below).
3. **Effect of artificially-scaled contrast on velocity constancy:** Our recordings demonstrated velocity constancy with natural images with a large variety of global contrasts, by any of several measures that we applied. One conclusive, yet enigmatic finding is that artificially reducing contrast of any of these images results in a break-down in velocity constancy. Re-scaled images give consistently weaker responses. Interestingly, truly natural scenes still give similar curves to one another, while the artificial (interior) scenes generate less attenuated responses.
4. **Contrast & Velocity dependency of adaptation:** We show that the degree of gain reduction during motion adaptation is dependent on contrast of the adapting pattern. The shape of this dependence is supra-linear in the same manner as that of the EMD response itself. Interestingly, adaptation is also clearly dependent on the velocity of motion, but not in a manner directly predicted by the shape of velocity tuning in the unadapted state. High speeds that excite little net response from the HS neuron cause strong adaptation, suggesting that adaptation is not directly driven by the output of local motion detectors. A caveat to this conclusion is that if (as suggested above) fast components of adaptation play a role in shaping responses that we measure, our attempts to evaluate responses of the unadapted neuron may themselves be confounded by the effects of adaptation. Nevertheless, some pilot experiments using ramps of contrast to produce a 'soft' onset to stimulation and sinusoidal grating stimulus patterns also suggest that adaptation is more prominent at higher temporal frequencies than are optimal drivers for the primary motion response. These data are consistent with a feed-forward gain control mechanism that is, nevertheless, regulated by feedback from motion detector outputs
5. **Role of the Waterfall effect:** Our experiments show that the waterfall effect is much more likely than the gain-reduction to be dependent on the properties of the HS neuron response itself. It appears to contribute a long-lasting, DC potential to the tangential cell output, and antagonistic to the global activity of the neuron during stimulation. Unlike gain reduction, both velocity tuning and contrast dependence of this component match those of the unadapted HS neuron. We thus conclude that the

waterfall component is intrinsic to the motion computation process itself, is a separate mechanism to the gain control and works additively with respect to the effects of the latter. Because of this, this component can exert a global influence on the properties of a tangential cell, while the gain reduction is strictly local phenomenon.

6. **Speed of adaptation:** Our initial experiments show that adaptation may be fast enough to explain the velocity constancy observed in apparently 'unadapted' neurons. Our pilot studies are incomplete and imperfectly designed experiments at the time of writing, and we will seek funds to continue this work in future projects.

1.4 Executive Summary: Simulation and Modeling

1.4.1 Aims and Approach

Our simulation and modeling efforts aimed to achieve two things: to better explain the features observed experimentally in the biological visual motion processing pathway, especially motion adaptation, and to investigate in detail their roles in producing useful information about optic flow / visual motion, particularly with regard to producing a model for velocity constancy. Models were built around a model for an elaborated elementary motion detector (EMD) as we had used in an earlier study of based on the Hassenstein-Reichardt model (Dror, O'Carroll & Laughlin 2000), with the addition of motion adaptation (as will be detailed later). An important feature of this elaborated EMD model that is missing from many earlier modeling studies is that it incorporates models for non-linear coding by "early" visual processing (i.e. by photoreceptors and first order interneurons), and also for non-linearity in spatial integration of local motion signals by tangential cells which collate EMD outputs. This approach allowed us to compare the output of simulations of the entire processing chain which that of the biological system that was subjected to experimental observation (in the form of recordings from tangential neurons). As our earlier work (Harris et al 2000) had identified two distinct components of motion adaptation, our comparison focused primarily on both of these: a motion-dependent gain modulation and a "DC offset" component termed the 'waterfall effect' (persistent hyperpolarization). The latter was modeled primarily in the later phases of this project.

In our concurrent SBIR funded modeling and electronic simulation work, we developed models for gain modulation primarily based on an easily-implemented feedforward contrast gain control. Our modeling for this effort tested an alternative strategy, for which we had some evidence in experimental data, based on feedback of local pooled motion signals. In addition to modeling a feedback gain control mechanism driven by a bi-directional (rectified) sum of local motion outputs, we explored an initial (and somewhat crude) implementation of the waterfall effect as a separate offset introduced into local EMDs based on their individual (unrectified) outputs. Experimental evidence to date is inconclusive as to whether the waterfall component is a local or global property within HS neuron collation of local EMDs, but even a local implementation of this kind produces a global influence on the collated EMD output, and thus is consistent with all experimental data.

The environment used for all modeling in this effort was MATLAB, although we carried out some stages (spatial pre-filtering) using Adobe Photoshop.

Simulations were generally performed with animated natural imagery, in order to maintain the spatial statistics seen by the biological system, and with relatively large arrays of pixels and

EMDs, so that receptive fields of reasonable size could be constructed for wide-field integrating neurons (tangential cells). The modeling approach used the same set of panoramic images as used in the neurobiological experiments.

1.4.2 History

Simulation tools were developed and simulations run throughput the project. Basic implementation of a 2-d EMD array was completed during first 2 years of the project and elaboration of this model to incorporate the waterfall component was complete by the end of the 3rd year.

1.4.3 Results and Conclusions

The feedback modeling approach reproduces a number of interesting aspects of the biological system and certainly provides a much robust estimate of pattern velocity than other variants of the correlational EMD. However, neither the model developed here, nor the concurrent modeling effort in the SBIR funded project fully explain the degree of velocity constancy seen in the biological system, suggesting that further refinement is necessary. Contrast gain control greatly reduces the dependence of response on image contrast, but still not to the degree seen in biological neurons, and it does not explain the fact that adaptation is more pronounced in response to motion signals versus flicker stimuli. As implemented, the feedback model is also relatively sluggish in achieving velocity constancy, whereas our later biological experiments showed that this property is evident in even the first few hundred milliseconds of the response of the neuron to the onset of motion. Furthermore, the feedback approach does not approximate velocity constancy unless assumptions (such as high feedback gain) are made which tend to distort the velocity dependence of response such that it no longer closely resembles that of the neurobiological system. That said, the model incorporates substantial dynamic non-linearity and is computationally expensive in our present simulation environment, making it difficult to fully explore the large range of potential variables that influence the match between model and experimental data. In addition, it does not account for fact that very high-speed motion induces profound adaptation even though motion signals (i.e., tangential cell responses) are weak under these conditions. It does, however, fully explain the difference between motion- and flicker-induced adaptations, a feature that remains inadequately captured by our concurrent modeling efforts with Tanner research (and funded by the SBIR).

There are two possible conclusions of the modeling effort that encourages further elaboration of the models proposed and tested in this effort. The first, and most obvious, is that motion adaptation is not a single process but rather has several separable components operating in parallel. A combination of both feedforward and feedback models, for example, would be consistent with all of the biological data obtained to date. A caveat to this conclusion is that such a complex elaboration might not represent the simplest solution to the task and is not in itself supported by any direct evidence from experiments, so we should thus be cautious in claiming such a hybrid model as biomimetic. The second is experimental evidence for the separability of the waterfall component of adaptation. Inclusion of this effect in our modeling of the feedback mechanism certainly provides excellent fits to the results of probe-adapt-probe experiments. More importantly, this also improves velocity constancy of model outputs. A similar caveat applies to this conclusion, since at this stage the form of feedback used to implement the waterfall effect in our models is not based on any direct experimental evidence, and thus should be considered bio-inspired rather than biomimetic: Much further

neurobiological experimentation is required to clarify the underlying mechanisms of the waterfall component.

2 Project Execution and Results

Details of project execution and results are given in this section for each of the major technical areas of Neurobiology & Simulation / Modeling. They are arranged in approximate chronological order.

2.1 Neurobiology

2.1.1 Year 1

Neurobiological efforts during the first year of activity were dominated by the demands of constructing the new laboratory in Adelaide. By the time of a site visit by AOARD program manager (October 10, 2001) PhD student Andrew had joined the PI (David O'Carroll) in Adelaide, we had been allocated temporary lab space in the Department of Physiology and were beginning to order equipment for the project (aided by AUD$70,000 in setup funds from the University of Adelaide). Construction of the main laboratory space for the neurobiological experiments did not commence until early 2002.

Substantial effort by Andrew Straw on a development setup allowed us to test the emergent VisionEgg software platform however. By mid 2002 we were able to move into the new laboratory and had constructed an initial experimental setup. We also collected a set of panoramic image sets to be used in subsequent experiments and stitched these into single panoramic textures that could be animated in the VisionEgg system. By the time the experimental setup and software were functional, it was, however, mid-winter and thus no animals were available for experiments.

2.1.2 Year 2

With the arrival of Spring (October 2002), our efforts turned to location of a suitable source of experimental animals for initial testing. *Volucella pelluscens* is not available in Adelaide, but the second species studied in the earlier experiments, *Eristalis tenax* was located (with some difficulty) in the hill country surrounding the city. We therefore concentrated our efforts on locating suitable field sites for obtaining experimental animals of this species. We eventually located a consistent source of *E.tenax* in the Mt Lofty Botanic gardens and applied for a collecting permit from the manager. This was granted and we are indebted to the staff of the Botanic gardens who have been very helpful in allowing us access to their gardens for collecting purposes throughout this project.

With a source of flies secured, we ran a number of initial experiments in which adaptation was studied by observation of HS and VS cell responses to the test/adapt/test stimulation protocol used in our earlier work (Harris et al 2000), but utilizing the natural images for the first time. This protocol was, however, extended in an effort to provide data that will help to unconfound the separate effects of EMD gain adaptation and lobula plate cell hyperpolarization (the "waterfall effect"), and to test hypothesis regarding the adaptive mechanism. The modified protocol involved application of adapting stimuli in both the preferred and antipreferred directions, rather than the preferred direction alone. Antipreferred-direction stimuli have been shown to elicit essentially the same gain reduction as preferred-direction stimuli, but without inducing the waterfall effect. This approach was taken in an effort to determine, for example, whether depression of response seen during adapt phases during the test-adapt-test protocol

results from the waterfall effect or of gain reduction, and the degree to which the waterfall effect itself might contribute to velocity constancy (given that it is currently lacking from our models).

2.1.2.1 Confounding effects of pattern noise

Unfortunately, the experiments during this period were not conclusive, due to a second confounding effect. HS cell responses in such experiments display a significant amount of "pattern noise," or dependence on the spatial structure of the stimulus that happens to be passing by the relevant portion of visual space during the relatively short test phases. This is an intrinsically interesting observation, confirming our earlier modeling predictions (Dror et al 2000) that pattern noise remains one of largest potential problems for 'real-world' applications of an elaborated EMD array, despite the statistical predictability of natural scenes in a global sense. The basic phenomenon of pattern noise is exacerbated by our experimental stimulus. Preliminary modeling efforts suggested that the large HS cell receptive field is specifically 'designed' to reduce this effect in nature, by elongation along the axis for the preferred direction of optic flow that the neuron is designed to detect. This elongated receptive field is further extended at the output of the tangential cells in the steering apparatus of the fly thorax, where summation of signals from the two sides of the body serve to extend the effective receptive field even further. In experiments, however, stimuli were presented on a computer display that stimulates only a subset of that receptive field (around 90 degrees in width). When the stimulus was run "backward" during the adapt phases in the antipreferred direction, this structure was different, and the resulting difference in pattern noise masked the effect that we were looking for.

We developed an approach to address the problem by reflecting the images horizontally during each adapting stimulus phase so that the spatiotemporal structure of the stimuli could be made identical for stimuli in either direction. We also 'split' the panoramic images horizontally into 4 segments with 90 degrees 'phase' difference between them. This reduced the effect of vertical phase-aligned features that are prominent in natural images, whilst still stimulating the neurons with images that had basically 'natural' image statistics. Note that the $(1/f^n)$ image statistics that are consistent for all natural scenes ignores such phase correlations within stimuli and that such correlations would have no effect on the behavior of local adaptation (adaptation had been demonstrated to be local in very early work by Maddess & Laughlin, 1986) since they are effects that extend beyond the receptive field of individual EMDs.

Despite our efforts, the presence of "pattern noise" remained a significant confounding influence on the results of the initial experiments. We began working on an elaboration of the test procedure, involving registration of uninverted and mirrored imagery during various portions of the experiments, which we expected to allow better rejection of "pattern noise" when computing the direction-selective portion of adaptation (the "waterfall" effect). Computation of the non-directional effect (i.e., gain reduction) would still require signal averaging over various phases of image presentation. Unfortunately, the condition of uniformity of EMD properties (i.e., connection strength onto the HS cell) across the HS receptive field is not well-approximated in the biological neuron: instead the receptive field is strongly asymmetric, with maximal sensitivity close to the frontal part of the receptive field. Although data loading procedures for the 'Vision Egg' were developed for this modification, it was not ultimately used extensively in future experiments. Instead, we adopted a standard procedure that was much more laborious: By presenting all stimuli at a variety of initial phases and averaging across many repetitions, the effects of pattern noise are mitigated. Unfortunately, this largely insoluble problem leads to a large increase in the total number of experiments

required and, ultimately, to a reduction in the amount of useful data that can be obtained in even the best intracellular recordings (with a duration up to several hours).

2.1.2.2 Elaboration of VisionEgg stimuli

During this period we also completed new stimulus generation techniques relying on the VisionEgg. As before, the stimuli were derived from panoramic images moved in the yaw direction, but using the OpenGL tools and hardware accelerated functions available from the Graphics card in the stimulus PC, we began to predistort them for perspective (rather than projecting them flat on the CRT) so that they corresponded more accurately with pure yaw from the position of the test animal. In this configuration the monitor effectively models a viewport onto a virtual cylinder. Additional advantages include the ability to do real-time interpolation of the imagery on a frame-by-frame basis at the high monitor refresh rate (200Hz) required to overcome flicker sensitivity in the fast fly visual system. This greatly improved animation quality for very low speed animation, where the image needs to move a fraction of a pixel between successive video frames: Our previous display system had been limited to movement of the image by a minimum increment of 2 pixels, introducing 'jumping' artifacts into low speed animations. Other new features included the use of true color (24 bit) imagery.

Initial application of these stimuli to intracellular recordings from 3 HS neurons in *Eristalis* did not appear to support velocity constancy as strongly as earlier data, although it was clear that adaptation resulted in significant compression of the output range relative to the quadratic variation seen in the idealized Reichardt detector. With the approach of winter and associated difficulty obtaining *Eristalis*, emphasis was therefore on experiments to complete analysis of adaptation to natural images in the 'monotonic' velocity tuning experiments as illustrated in figure 1 below:

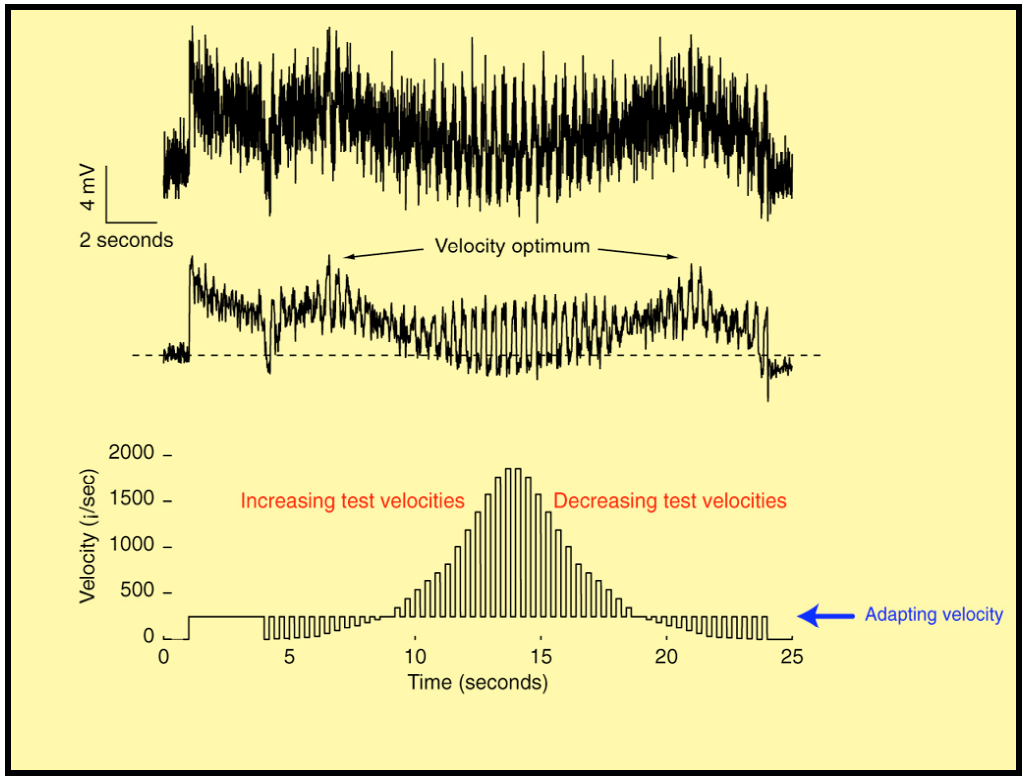

Figure 1: HSNE response to natural images animated to simulate yaw motion in monotonic series.

This stimulus (see lower trace) consisted of an initial 3 second period of motion of an adapting pattern followed by a series of interleaved velocities, presenting in ascending and then descending order, interleaved at 200ms intervals with a ‘burst’ of the same adapting speed as in the initial period. The upper trace in this figure shows the recorded membrane potential of an HS neuron during a single trial presentation of this stimulus, while the middle trace shows the average of several trials, presented at different initial positions of the panoramic image in order to mitigate the effects of pattern noise, as described earlier. Even in the raw data, the velocity sensitivity of the HS neuron is evident, with a pronounced optimum visible in both the increasing and decreasing test series.

One interesting observation came from a rare recording from the 'northernmost' of the set of HS neurons, HSN. We recorded from this neuron infrequently because of the typical orientation of our preparation with respect to the axon position of this cell. Based on preliminary analysis on-line, we noted that there were discrepancies between velocity tuning obtained with an increasing series of test speeds, compared with that on the second half of each series presented, where test speeds are initially high and gradually decrease (over a 12 second period). We previously used the strict 'symmetry' in such curves as evidence that our adapting pattern (interleaved with the tests) maintains a constant adaptation state throughout the experiment, and in typical HS recordings from the more frequently encountered HSNE and HSE neurons, this was the case. Our results for HSN suggested that the time constant for the adaptive process in this cell may be much longer. We tested this by increasing the initial adaptation period from 3 seconds to 8 seconds, and this then produced near perfect symmetry in the responses, confirming that it takes approximately 8 seconds for responses to reach a 'steady state' compared with only 2-3 seconds in HSNE and HSE. The functional significance of this was not clear, given that modeling efforts at the time suggested that that the time taken for response to reach steady state is not necessarily related to time constant of the low-pass filter in the adaptive element, at least not where there is significant feedback in the adaptation process.

The purpose of the monotonic presentation is to evaluate the effect of the test stimuli (i.e. the variable velocities) on the adaptation state of the neuron. The assumption is that powerful motion adaptation by the adapting stimulus ‘clamps’ the adaptation state to a fixed level. This can be evaluated by extracting the response to adapting periods during each interleaved burst and plotting them against the test velocity that precedes them, as in figure 2 below. If adaptation state is kept constant, we should see a flat line for the adapting test patterns. Initially, we considered using a random, rather than a monotonic series of test speeds, but opted for the latter because it would more systematically reveal effects of ‘self adaptation’ to the test patterns themselves. By repeating the whole sequence in reverse, the degree to which the resulting velocity tuning curves are similar confirms the validity of the assumption that adaptation state is clamped constant.

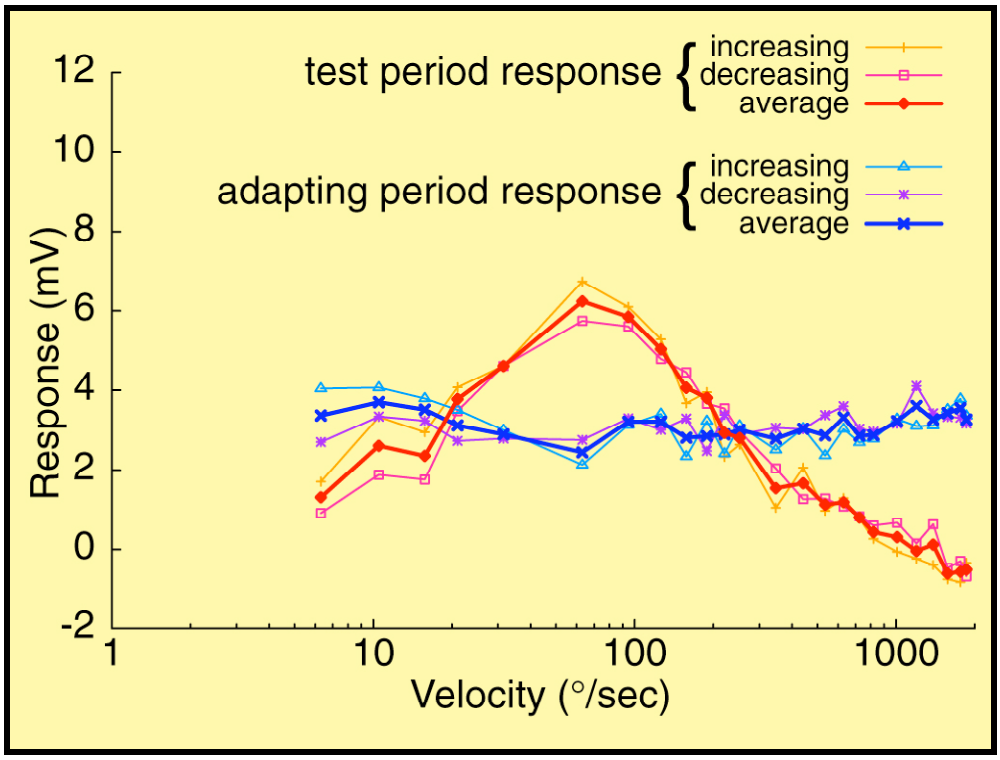

Figure 2: HSNE response to velocity of natural images animated to simulate yaw motion in monotonic series.

2.1.2.3 Testing with a larger set of natural images

We were successful in obtaining several very high quality recordings of long duration (over 3 hours in one case), which allowed us to test responses to many different image sets. In the earlier experiments with this stimulus, we obtained some data that suggested velocity constancy (contrast independence) was not as obvious as in the earlier pilot experiments, at least when contrast was varied by re-scaling the luminance values (color lookup table compression) within an image. An important deficiency in all of these experiments was that our display system, with a maximum contrast ratio of around 250:1, could not come close to matching the dynamic range of 'true' natural scenes, so that simulations of natural motion typically have lower contrast than in nature. We therefore decided to test responses to a larger set of images deliberately selected to display a natural variation in contrast (and possibly in other aspects of natural image statistics) to provide a test for the hypothesis. The image set developed is illustrated below:

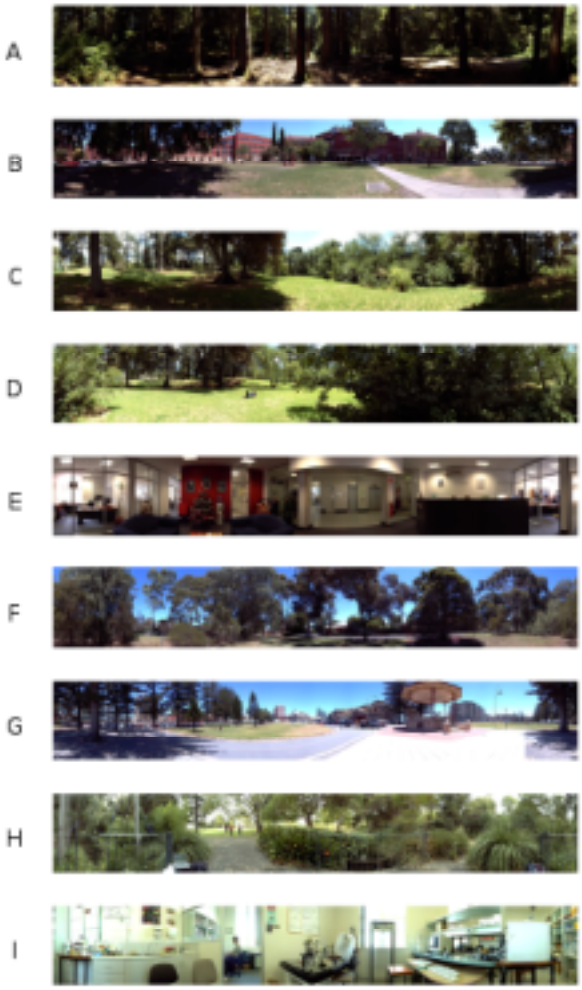

Figure 3: 9 panoramic images selected for testing velocity constancy: Images referred to in subsequent text as follows, A "Hamlin" a contrast scene originally captured in Hamlin woods, near Seattle and captured from the position of a hovering fly located at that time. B: "Barr_sun": captured from the Bar-Smith Library lawns at the University of Adelaide. C: "close": captured from Botanic park, Adelaide and deliberately including close detail of a plant as well as surrounding scenery. D: "Distant" the same scene from further away from the plant foliage. E: "Reception": the reception desk area of the Department of Physiology, University of Adelaide. F: "Linear_park" taken from the Adelaide west parklands. G: "Glenelg" taken from the Glenelg foreshore near Adelaide. H: "Gardens" a scene from the Botanic Gardens in Adelaide on a dull day to deliberately represent a low contrast scene. I: "Lab_pan" captured in the O'Carroll laboratory temporary space, University of Adelaide

The images are illustrated in fig. 3 in an order that matches the approximate variation in natural contrast of this set, evaluated by a simple mean absolute deviation measure. By this measure, the top image has almost 4 times the overall contrast of the lower two (H,I). We deliberately included two artificial enrvironments amonst the image set.

A significant finding was the confirmation that velocity constancy prevails in the response of HSNE neurons with respect to different natural images; i.e., HSNE response was found to be velocity-dependent but invariant when the animated natural images were varied. This is depicted in figure 4 below for the full set of images in 1 recording (blue lines) and a smaller set in a second recording (orange). The degree of velocity constancy is remarkable considering no post-experiment normalization has been applied.

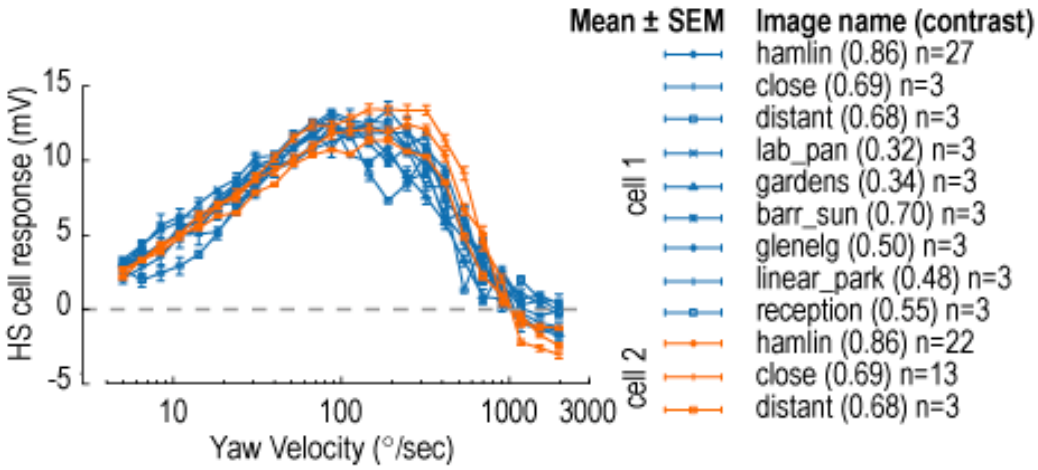

Figure 4: HSNE response to natural images animated to simulate yaw motion. Data are obtained from two different cells. An *ad-hoc* contrast measure, mean absolute deviation as well as the number of trials over which results are averaged, are shown for each image. Recording by A. Straw & D.O'Carroll, University of Adelaide

Contrast of these natural images varied considerably, as indicated in the figure. However, another significant finding is that *artificial* contrast reduction (by rescaling the range of luminance variations while maintaining the same mean luminance) resulted in departure from velocity constancy at higher levels of contrast than suggested by our earlier pilot experiments:

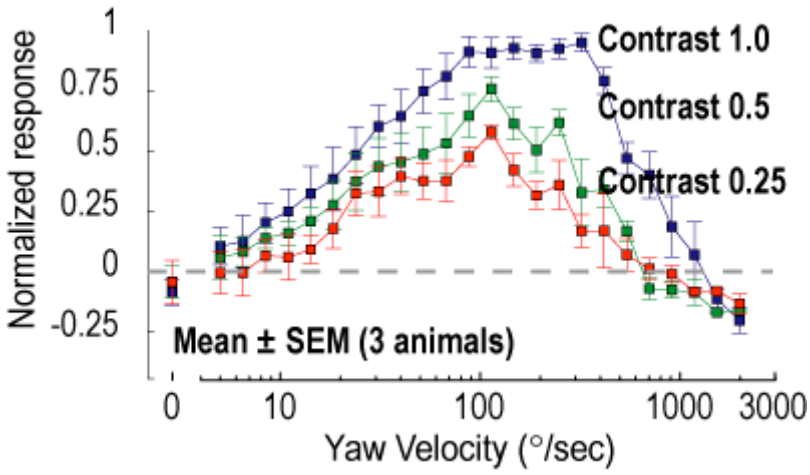

Figure 5: HSNE response to moving natural images under artificial reduction in image contrast. Contrast measures are relative to original image contrast

The reason for the apparent discrepancy between the current and prior results was at this point uncertain; we planned to standardize our methods of computing image contrasts and do a detailed comparison in the future.

2.1.3 Year 3

In our experimental work this period, we made recordings from HS cells in a number of different animals, using the wider variety of images illustrated in figure 3, a larger set of artificially adjusted contrasts, and a greater range of adapting stimuli than in prior work, in order to evaluate the conditions under which velocity constancy holds. These recordings were very successful -- we set a lab record this period for viability of an HS cell following penetration with the recording electrode (over 6 hours). Analysis from these experiments

confirmed basic properties, in particular velocity constancy with different natural images, observed previously.

2.1.3.1 Saturating nonlinearity & velocity constancy in "unadapted" neurons

Although these experiments were not designed specifically to test the mechanisms driving the gain reduction portion of adaptation, preliminary results shed some light on the property of velocity constancy. While it was assumed that adaptive gain reduction / gain control plays a significant role in velocity constancy, we noted other mechanisms that could contribute to this property, that may be in operation in varying degrees in the experimental results we obtained. One such mechanism is a saturating nonlinearity in the EMD correlator outputs, which in combination with high front-end gain results in hard limiting and thus relative insensitivity to changes in input intensity (saturation of these signals is responsible for a significant decrease in contrast sensitivity of the alternate adaptive model under consideration). A second mechanism is the nonlinear and 'normalizing' nature of signal summation in the HS cell itself (somewhat misleadingly referred to as 'gain control' by Borst and co-workers in prior literature).

The relevant results have to do with the response of the HS neurons in the putative 'unadapted' state to full-contrast test stimuli. In this portion of the experiments, a moving test pattern was presented after 'adaptation' to a blank screen of mean luminance for at least 5 seconds, with the pattern appearing in motion for 1s. We discarded the initial 50ms transient then averaged membrane potential across the next 150ms. As always, choosing this averaging 'window' was problematic: Because the images were very high in contrast, adaptation was rapid, so the curves must represent at least a partly adapted state. (On the other hand, if the averaging 'window' were shortened to further minimize this 'self' adaptation, the tuning curves would be distorted because of the transient behavior of the system, which tends to bias curves towards higher temporal frequencies and hence velocities. Our contrast ramp method (developed in the mid 1990s at the University of Cambridge) would have provided a significant improvement in this respect, but would have defeated the purpose of the experiment, which is to estimate responses at the full, un-attenuated image contrast in order to recruit the full range of nonlinearities operating in coding such images, *except* for adaptation). In addition, the variance of responses due to variations in input pattern structure / phase ('pattern noise') was high.

In spite of the complicating effect of these difficulties on interpretation of the results, those results suggested a surprisingly strong degree of velocity constancy even in the unadapted HS cell. Figure 6 below shows unadapted velocity tuning curves averaged across several recordings (4 cells for preferred and 2 for anti-preferred direction) where the initial 'phase' of the panoramic image was altered systematically throughout the recordings to reduce the influence of pattern noise (a particular problem at lower speeds in this experiment). Prior to the application of the adapting stimuli (i.e., after presentation of blank screens of mean luminance), the responses of the HS cells to the test stimuli were recorded in these experiments.

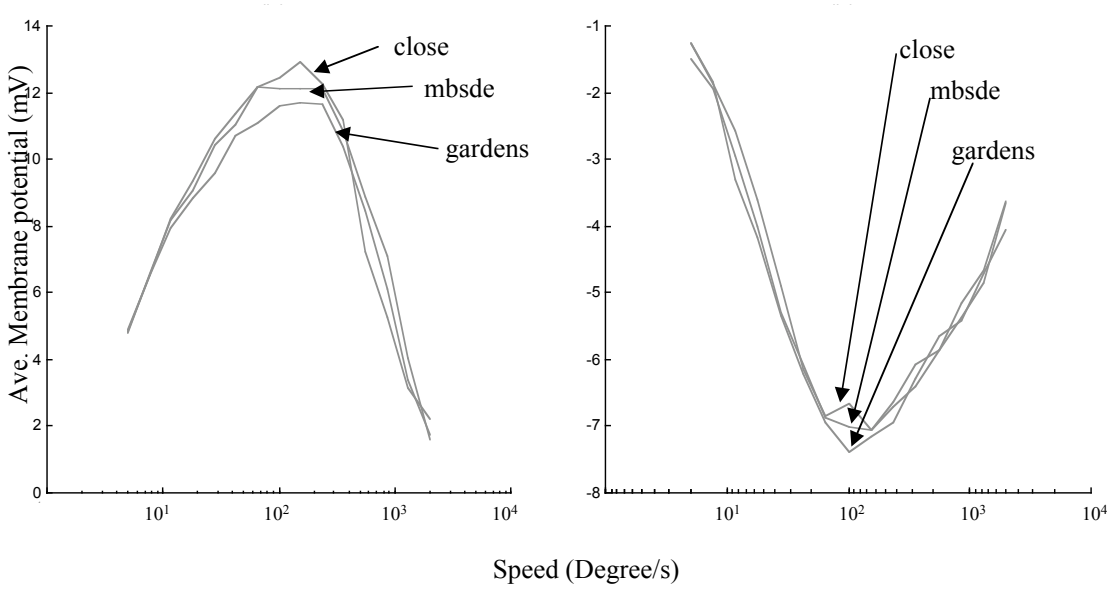

Figure 6: Mean responses of 'unadapted' HS cells to preferred (left) and antipreferred (right) direction yaw motion of natural panoramic stimuli. Responses to three different scenes of varying contrast are depicted and annotated by the name assigned to each as in fig. 3 (except that mbsde=the image "Hamlin" referred to previously). Responses are averaged over several cells and several trials with differing initial phases. Data obtained by T. Rainsford & D. O'Carroll

These initial results encompassed three images (labeled *close*, *gardens* and *mbsde = "Hamlin" referred to earlier*) from a larger set that was presented in similar experiments. These three images represented highest, lowest and an intermediate contrast in the set by various 'traditional' measures of contrast in natural images (e.g. RMS power, mean absolute deviation, etc.). During this period, further analysis was regarded as necessary to quantify how their 'effective contrasts' differed (i.e., contrast with respect to the spatiotemporal receptive field of HS cells): This was performed in concurrent modeling efforts.

From these results, we concluded that mechanisms for velocity constancy, such as EMD subunit saturation and the nonlinear summation of the HS cell itself, must be operational even in the unadapted motion pathway. This naturally raised the question of exactly what the role of contrast gain reduction is in this system (noting that its presence is indisputable based on the results of contrast sensitivity experiments before and after adaptation). It also showed that global mechanisms for velocity constancy in any experiment are likely to seriously confound efforts to infer the effects of contrast gain adjustment. Such global mechanisms have the effect of minimizing the results of changes in the gain at the front end of the system.

2.1.3.2 Test-adapt-test stimuli

In further experimental work, we continued to make recordings from HS cells in specimens of *Eristalis*, and examined adapted as well as unadapted responses to motion. Experiments continued with the three images (*close*, *gardens* and *mbsde*) used in the previous experiments which suggested substantial 'velocity constancy' even in the unadapted system. Using four different contrast measures, *gardens* has between one-quarter and one-third the contrast of *mbsde (="Hamlin")*.

Further tests were done with the interleaved test-adapt protocol. The adapting stimulus was the same image that was presented during the test phases and was always presented at a (maximal) contrast of 1 and at a speed of 100 degrees per second. In the unadapted cases, the adapting stimulus was a blank screen of mean luminance. During the test phases, however, the

contrast of the image was varied artificially by compressing the range of variation around the mean luminance of the raw image. This variable contrast test was presented before and after the adapting stimulus, as in our earlier published work on contrast gain reduction (Harris et al 2000).

Figure 7 & 8 below completely summarize the results of this set of experiments. These new data were consistent with the presence of saturating nonlinearities in the system, supporting the hypothesis that saturation may play a role in velocity constancy. The fact that the unadapted curves (red) were broad and 'flat-topped' (platykurtic) relative to the adapted curves (green) suggested that saturation is more prevalent in the unadapted system (consistent with the hypothesis that adaptation modifies the system gain at the front end of the EMDs). In addition to the difference in shape of the tuning curves, the maximal response in the adapted curves was reached at higher velocities than in the unadapted. The adapted responses decreased in amplitude more rapidly with decreasing contrast than the unadapted, which was also consistent with low contrast gain in the adapted state.

The unadapted velocity response curves at a contrast of 1 were remarkably similar for all images. However, the curves at various artificially reduced contrasts, for each individual image, varied greatly in their amplitude (compare the 3 highest contrasts c=1, 0.75 and 0.5), despite the fact that the range of contrasts was *less* than the variations among the three images themselves at their maximal or 'natural' contrast. This we regarded as very difficult to explain based on any hypotheses at the time. The only difference between the artificially reduced contrast and that seen in the natural variation of the un-attenuated images was the range of luminance values for individual pixels: in an artificially reduced image, the histogram was compressed about the mean luminance. This might be expected to lead to increased gain for such images, due to contrast adaptation of early visual neurons such as photoreceptors and LMCs. Yet, the observed responses were weaker than their counterparts for natural images with similarly low contrast, which however still exercise the full dynamic range of the grayscale image (i.e. 8 bits, or luminance values from 0-255).

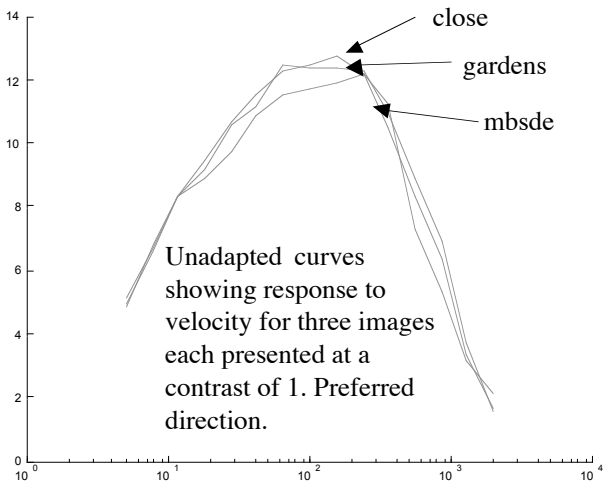

close

gardens

Contrasts 1, 0.75, 0.5, 0.25, 0.12 and 0.1

mbsde

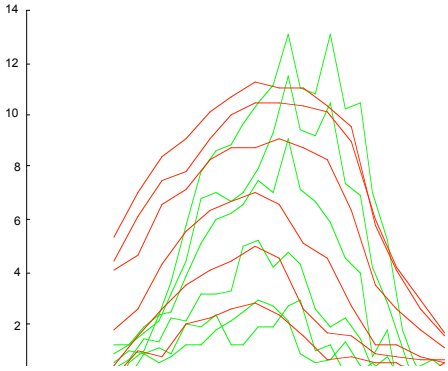

Figure 7: Preferred direction velocity tuning curves from HS cells with the system in the unadapted (red) and adapted (green) states. Responses to three different images are depicted. Contrasts (relative to original image contrast) are varied parametrically. Responses are averaged over several cells and several trials with differing initial phases. Abscissa represents speed in degrees per second in log scale, and ordinate, membrane potential relative to rest in millivolts. Data obtained by T. Rainsford & D. O'Carroll.

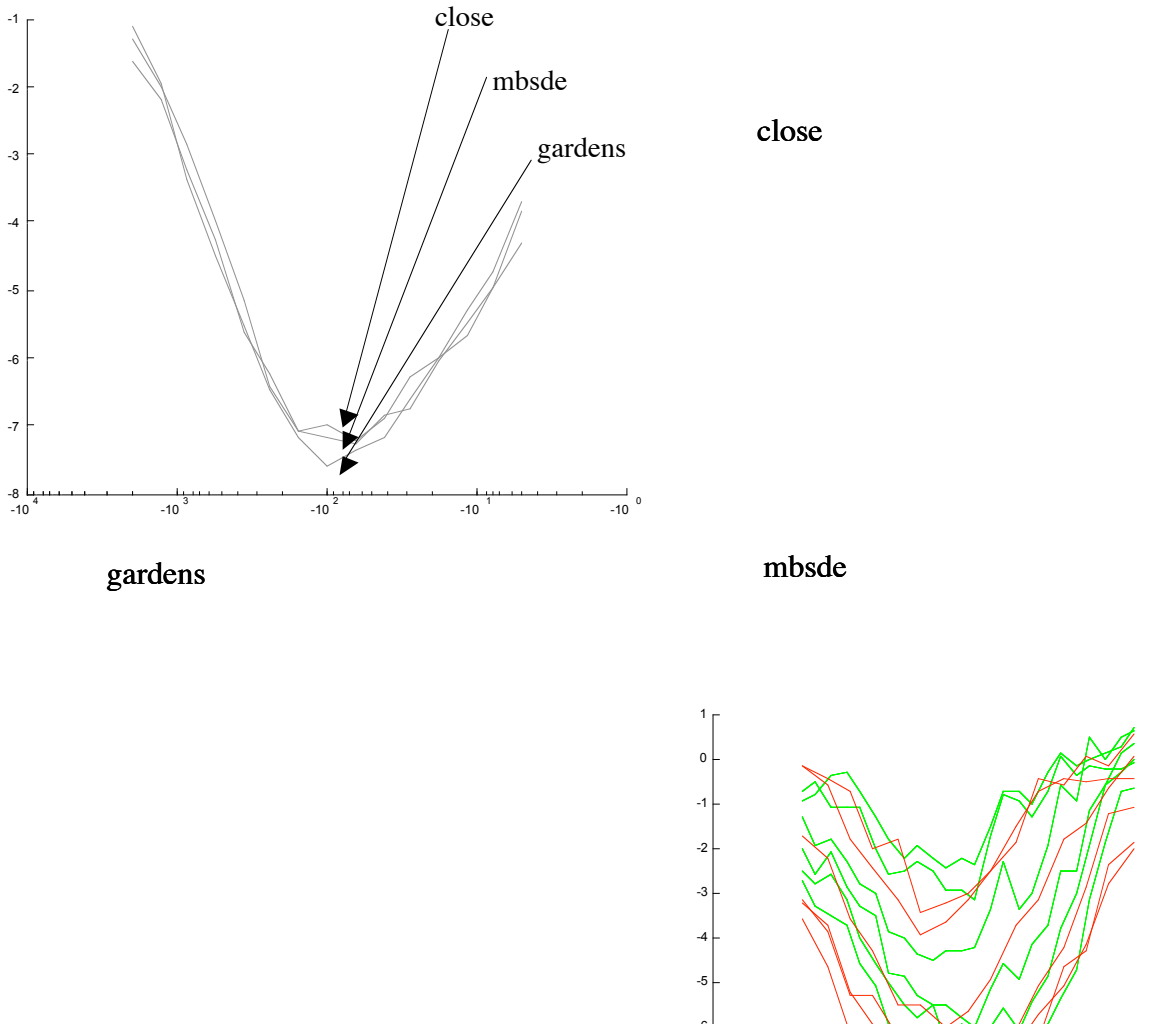

Figure 8: Antipreferred direction velocity tuning curves from HS cells with the system in the unadapted (red) and adapted (green) states. Responses to three different images are depicted. Contrasts (relative to original image contrast) are varied parametrically. Responses are averaged over several cells and several trials with differing initial phases. Abscissa represents speed in degrees per second in log scale, and ordinate, membrane potential relative to rest in millivolts. Data obtained by T. Rainsford & D. O'Carroll.

We subsequently continued to make recordings from HS cells in specimens of *Eristalis*, and ran initial experiments in which small-signal test or probe stimuli were used in a effort to evaluate the front-end gain in the motion system, and its dependence upon parameters of the adapting stimulus (i.e., contrast and speed of motion). The adapting stimulus was large-signal (i.e., full contrast moving image covering much of the receptive field of the neuron under test), and was interleaved with test stimuli in which contrast was reduced by compression of intensity variations about the mean luminance of the scene.

Experiments were carried out using the same 'standard' set of 3 natural panoramic images ('high', 'medium', and 'low' contrast) used previously, as adapting stimuli (at full contrast and various speeds), and as probe stimuli (with artificially compressed (relative) contrasts of 0.1 and 0.12, and at the near-optimal speed of 100°/s). Preferred- and antipreferred-direction adapting stimuli were used. The intention was to use the difference in response to the 0.1 and 0.12 probe contrasts as the measure of gain. Unfortunately, these two contrasts proved to be too weak in the adapted state, so that the results were too noisy to make this analysis meaningful. However, to convey a picture of the small-signal response, the results of the experiments (three

scenes and two reduced contrast values) were simply averaged together for each direction. Results are depicted in figure 9 below:

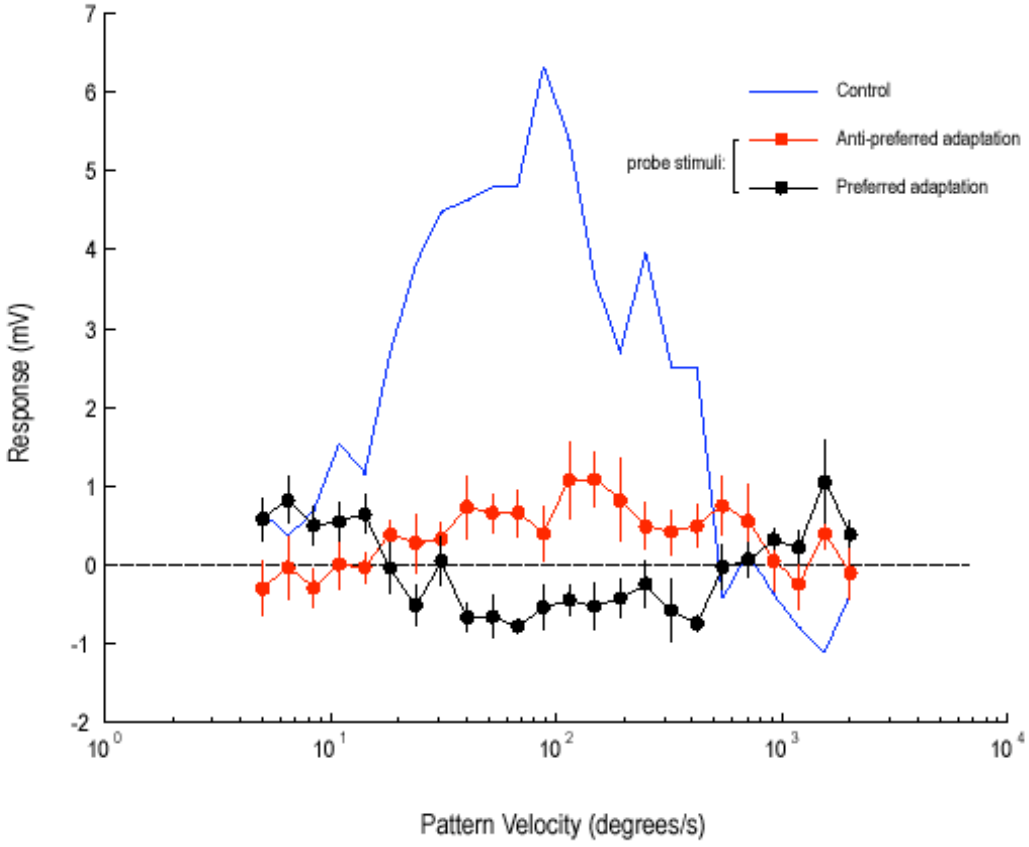

Figure 9: Averaged HS cell responses to low-contrast test stimuli following adaptation. Results for both preferred (black) and antipreferred (red) direction of motion are shown. Control response of the motion-adapted system to full-contrast stimuli is shown in blue. The dashed horizontal line represents the resting potential. Pattern Velocity on the abscissa refers to the velocity of the *adapting* stimulus (probe stimuli were all at 100°/s). Error bars indicate standard error. Data were obtained by T. Rainsford & D. O'Carroll.

These curves clearly show an inverse relation between probe response and the full-contrast tuning curves, which is consistent with an adaptive gain reduction that is dependent upon system output, and thus with the presence of a feedback mechanism. However, the results were not entirely conclusive because they were confounded with changes in the resting potential: while the preferred-direction responses were consistent with a shift downward due to the 'waterfall effect', the anti-preferred direction responses (in which no after-potential effects are expected) were *above* the resting potential for many of the points on the curve. In addition, dependence of the small-signal responses on adapting pattern contrast was not tested directly in these experiments, so definitive answers to the question of what drives contrast gain reduction in adaptation awaits further experiments.

Due to lack of availability of *Eristalis* during the onset of winter no further progress was made on this species (our primary experimental preparation for the project). In experiments on an alternative, the blowfly *Calliphora*, most recordings were made from VS and CH cells rather than HS cells, and involved the test-adapt-test protocol. These data were of poor quality and largely unanalyzed during the period, but suggested similar adaptive behavior and tuning in

their responses with respect to preferred direction stimuli (vertical motion in this case), to what had been observed in HS cells.

2.1.3.3 Small signal contrast gain

In our prior attempts to extract the small-signal contrast gain of HS cells using low-contrast probe stimulus, we mainly demonstrated the difficulty of estimating appropriate test contrast values to elicit responses both above the noise floor and below any saturating effects. In addition, the confounding effects of possible shifts in the 'resting' or baseline membrane potential compounded the difficulty. Because of these unsuccessful experiments, we decided to adopt a more involved method in which a contrast sensitivity curve was generated for each state of adaptation to be investigated, and worked on both the details of the issues involved with this approach and the methodology to implement it. Our intent under this protocol was to apply a standard or canonical form of probe stimulus (such as an optimal frequency grating) in all such experiments, so that all measurements of contrast gain so obtained would be certain to be comparable. This required interleaving of the probe stimulus with the various adapting stimuli, which necessitated some further programming efforts in the Vision Egg stimulus generating system.

We also analyzed a large volume of data previously obtained from *Eristalis* which confirmed tentative conclusions reached from pilot experiments: following adaptation to natural images, which may vary significantly in contrast, a high degree of velocity constancy was observed in the cell response. This conclusion was found to apply even when the velocity of the adapting stimulus was varied over a wide range.

These experiments were carried out using the 'standard' test-adapt-test protocol: an adapting stimulus, consisting of a panoramic image at full natural contrast, was presented at a fixed speed and interleaved with test stimuli of the same image at varying speeds. However, the dimension of the adapting stimulus speed (previously limited to a few different values) was thoroughly explored in a large set of such experiments. These were repeated for both preferred and antipreferred directions.

A summary is presented below in figure 10 in which individual response curves for adapting stimuli at different velocities are shown as smooth unbroken lines, and their averages as heavy lines in which markers indicate individual data points.

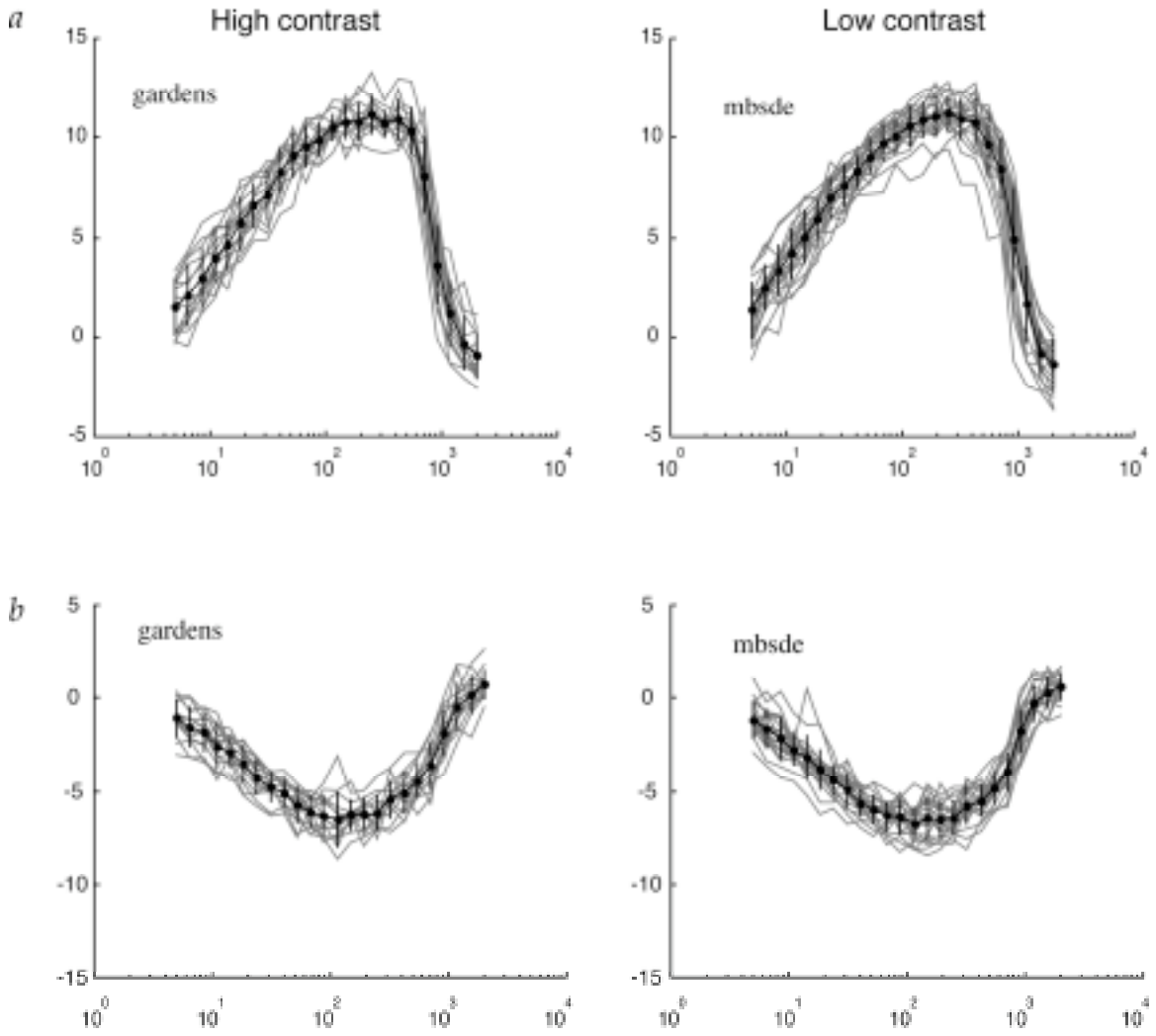

Figure 10: HS cell responses to test stimuli following adaptation to a wide variety of adapting speeds. Individual response curves (smooth unbroken lines) are each for a particular adapting stimuli velocity varied in the range 5-2000 deg/s. The heavy line (with error bars) is the mean for all data. Results are shown for low-contrast ('gardens') and high-contrast ('mbsde') natural images, which has 4 times the contrast of other (as measured by several different contrast metrics). Data are shown for both preferred (a) and anti-preferred (b) directions. Data were obtained by T. Rainsford & D. O'Carroll

The degree of velocity constancy under such a wide range of adapting conditions, even for velocities which induce relatively weak responses in the target cell, is impressive. Further analysis of the same data set showed that deviations from 'perfect' velocity constancy occurred at the limits of the range of speeds over which the HS cell responds. In these cases, responses to the constant probe stimuli were enhanced, in comparison with other adapting stimuli. This supported the notion that strongest adaptation effects are recruited by stimuli that drive the EMDs maximally.

We subsequently obtained a number of additional recordings from HS cells in *Eristalis*. These recordings were done primarily to obtain additional supporting data for the velocity constancy experiments in adapted and unadapted HS cells, to increasing sample sizes to a level acceptable for a published paper. We also began work on a manuscript for publication that will include these results (This paper, Straw, Rainsford and O'Carroll, has subsequently been submitted but has not yet been accepted for publication).

2.1.3.4 New experimental Protocol for evaluating contrast gain in adapted neurons

Due to the difficulties with evaluating contrast gain with the 'contrast sensitivity' experiments discussed in prior periods, we began modifying the 'Vision Egg' stimulus generation and display system to permit more elaborate protocols that will allow unambiguous evaluation of small-signal contrast gain. These modifications included: a) implementing the ability to switch textures in the panoramic image stimulus. This allows a stereotyped test (probe) stimulus such as an optimal frequency sinusoidal grating to be used while adaptation occurs with a natural image; (b) Ability to window the panoramic stimulus to reduced angular extent (with Gaussian window to 'soften' the stimulus edges). This allows testing of the theory that the constancy observed for unadapted velocity tuning derives in part from non-linearity in spatial integration (i.e. local saturation, or the Borst 'gain control' mechanism). It also permits testing of the spatial locality of the possible mechanisms for motion adaptation.

We implemented this probe-adapt-probe experiment protocol in order to quantify the gain change induced by an adapting stimulus. The stimulus was implemented as a modification of a VisionEgg stimulus that projects a textured 'spinning drum' onto the monitor. In previous experiments of this type, we rendered a single texture in order to simulate motion at different speeds. In the new stimulus, we cache two textures, one as the adapting stimulus and one as the probe.

After several pilot experiments, we settled on a sinusoidal grating stimulus as a canonical 'probe' texture. The sinusoid has an integer number (36) of cycles in 360 degrees, so that when mapped onto the cylinder it can be moved continuously without edge effects. The spatial period (10 degrees) is close to optimal for HS neurons when the pattern is presented frontally, and we settled on a velocity (ca. 80 degrees/s) that induces optimal temporal frequency (8 Hz) for male HS neurons, based on earlier work (O'Carroll et al 1997). This sinusoidal stimulus lacks the 'pattern noise' associated with low contrast presentation of natural images. Because it is an 'optimal' stimulus, we were therefore able to estimate response magnitude at low contrasts with relatively little signal averaging.

In initial experiments we obtained recordings from several HS neurons and an interesting VS (vertical system) type neuron. We presented the probe stimulus for 1 second before and after presentation of an adapting stimulus (in this case our default high contrast panoramic natural image), and then varied the contrast of the test pattern over a large range in order to (a) estimate the unadapted contrast/response function (i.e. in response to the first test), and (b) to evaluate the same curve in the motion-adapted state for purposes of establishing ideal contrast values to select in further experiments. In the VS cell, the contrast threshold was very low: significant responses were evoked by contrasts as low as 1% for the canonical test pattern before adaptation. We subsequently presented the stimulus at pairs of probe contrasts, in each case differing by 10% (e.g. 1% and 1.1%). Even though the system has a non-linear 'gain' with respect to contrast, the small difference between these probe contrasts allowed us to define contrast gain within an approximately 'linear' part of the response range:

$$G_c = dR/dC$$

In fact, because of the quadratic non-linearity involved in motion correlation, the square root of G_c would be a measure of the 'input gain' of the system. By measuring the *change* in G_c before and after adaptation, we were able to evaluate a 'tuning curve' for the parameters that drive adaptation.

The biggest problem with this technique was the need to know, in advance, the approximate range of contrasts that are most useful. In our pilot experiments we explored contrast pairs in

the range from 1 or 1.1% to 10 or 11% contrast for the sinusoid. In one recording we held the cell long enough to do this for several different adapting stimulus speeds. These pilot data were used to plan further experiments that were optimized for the task, and thus to obtain complete tuning curves.

We further elaborated our protocol for evaluation of contrast gain based on the responses of wide-field motion-sensitive neurons, as well as a method of analysis that we believe will give a robust indicator of shifts on contrast sensitivity based on a relatively limited number of response data. By limiting the number of data required from each experimental trial, this approach was expected to permit experiments covering a large range of adapting conditions during the typical period of viability of lobula plate cells following electrode penetration. We obtained experimental data and performed analyses for several neurons using these methods.

The experimental procedure consists of two parts. First is a control experiment, where a canonical probe stimulus (a grating with optimal spatial frequency moving in the preferred direction for the neuron) is presented at a series of contrasts from below threshold (i.e. contrasts that produce no measurable response) to the maximum that can be generated (=1.0 for a sinusoid). Between each stimulus, the neuron is unstimulated, and the insect views a blank screen of mean luminance for at least 8s. We then plot response (membrane potential for a graded neuron like HS, or 1/inter-spike interval for a neuron that generates action potentials, such as VS) as a function of the contrast of the stimulus. On the assumption that this 'rest' period negates the effect of adaptation due to the probe stimuli, we called the resulting contrast sensitivity function (CSF) the 'unadapted' CSF.

We fit the unadapted CSF with a Weibull function of the following form, using non-linear function minimization (Nelder-Mead Simplex method):

f(x)=gain(1-(exp(-((x./alpha).^beta))))*;

An example for an HS neuron is shown below in figure 11:

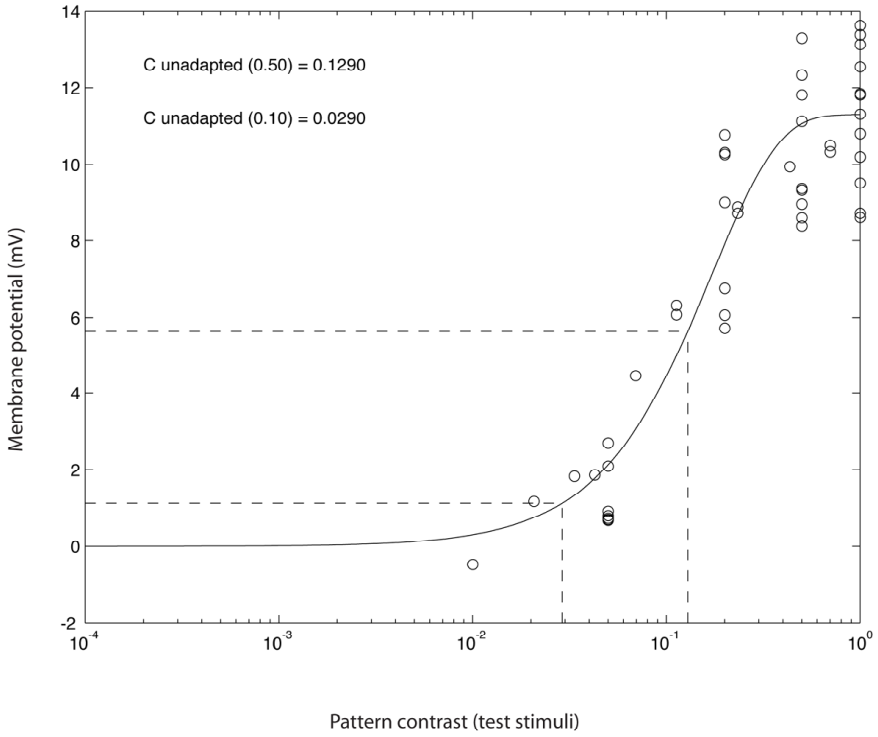

Figure 11: Contrast Sensitivity function for an unadapted HS neuron. Data obtained by T. Rainsford & D. O'Carroll

In agreement with our earlier results evaluating contrast sensitivity in these neurons (O'Carroll et al 1997,Harris et al 2000), we found that the unadapted CSF for both HS and VS neurons indicate they respond down to very low contrasts of just 1-2 %.

The aim of this control experiment is not only to determine the shape of the unadapted CSF, but also the saturation response level for the neuron. In particular for HS neurons, the quality of individual recordings varies, due to the difficulty of inserting the glass microelectrode into the neuron without damage to the surrounding membrane (the neuron diameter is ca. 1μm - 2 μm, while our microelectrode tips are ca. 50nm - 100nm). Hence, the *gain* parameter in the above equation does not correspond to the contrast gain that we are trying to estimate with this experiment, but rather a variable that accounts for the range of membrane potentials over which an individual neuron can depolarize (or maximum firing rate for a spiking neuron). We can then quantify the contrast sensitivity of the neuron by solving the fitted function for response level criteria (10% and 50% of the maximum being illustrated in the curve above). These threshold contrasts give an estimate of the *gain* of the CSF. Since lower gain results in a right-shift in the CSF, it is convenient to take 1/threshold as an estimate of the contrast sensitivity of the system, CS, where CS is directly proportional to contrast gain.

The next step in the protocol is a more demanding probe-adapt-probe sequence, where probe stimulus is similar to that in the control experiment is used, but with several seconds of adaptation to a variable stimulus before the second probe in each case. After each sequence is presented, the neuron is again allowed to recover by viewing a blank screen for several seconds. We compare the CSF obtained for the neuron in the first probe of each sequence with the control to check that the rest interval is adequate. We found that CS solved for such data is indistinguishable from the control if we use rest periods greater than 5s. For these data, we estimate the response to *both* probe stimuli and use Simplex minimization to find the best fit to the data of models for both unadapted and adapted responses:

$f(x)=gain*(1-(exp(-((x./alpha).^beta))))$;
$f_2(x)=gain*(1-(exp(-((x./alpha_2).^beta_2))))$;

where the subscript "*2*" indicates the function that is applied to the adapted response. Note that this double-Weibull model uses a single *gain* parameter for both functions, on the assumption that the basic recording properties of the cell do not change.

We then compute two sum-square error terms, q, q_2, as the difference between $f(x)$, $f_2(x)$ and the actual data measured for the cell to the two probe stimuli:

$q=\Sigma((y-f(x)).^2)$;
$q_2=\Sigma((y_2-(f_2(x)+offset)).^2)$;

where y and y_2 indicate the unadapted- and adapted-state experimental data, respectively. Note that the second term includes an *offset* parameter, which allows us to account for DC membrane potential changes that we frequently observe following powerful adapting stimuli (the so-called waterfall component of adaptation, or motion after-effects). The sum of q and q_2 is then minimized. The resulting minimization thus uses 5 parameters ($alpha,alpha_2,beta,beta_2,offset$). Note also that the *gain* used in the model fits is not varied during minimization, being fixed to the value obtained for the control experiment.

An example of this double-Weibull fit is shown below in figure 12, where the adapting stimulus was a high contrast panoramic natural image moving at 100 deg/s in the preferred direction:

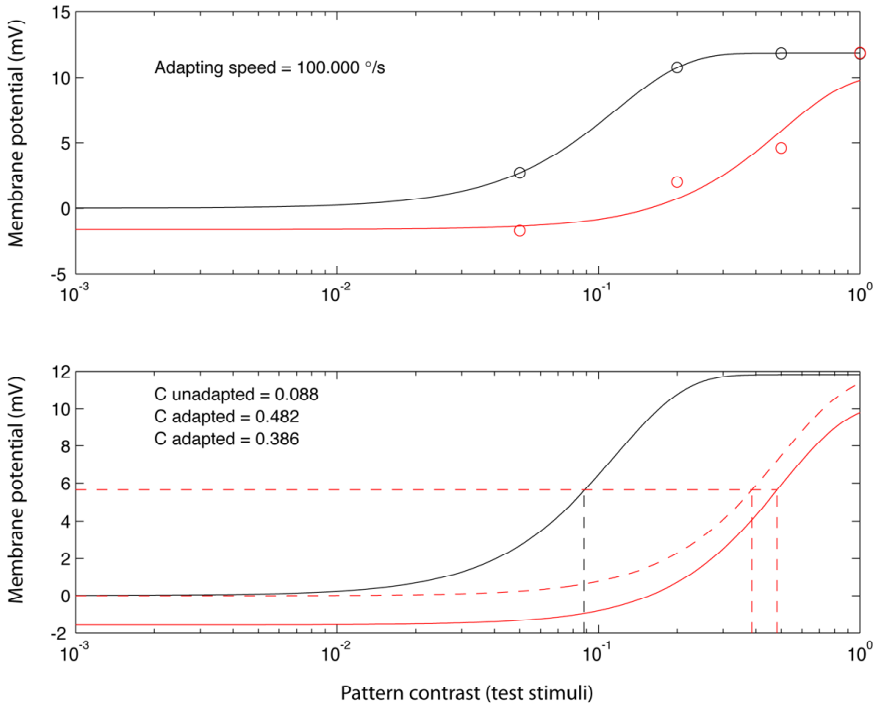

Figure 12: Fits to contrast sensitivity functions using data obtained from the adapted (red) and unadapted (black) states. Data obtained by T. Rainsford & D.O'Carroll

Note that with the addition of the offset back into $f_2(x)$ (solid red lines in above plots) the model provided a convincing fit to the data despite the paucity of points sampled. This reflects the benefit of fixing the gain term based on a control experiment. Providing the recording remains healthy, the Weibull fit was found to be extremely robust when applied to such data.

We then solve the fitted Weibull functions for precise response threshold criteria, either with or without the DC offset term. This allows determination of the *shift* in contrast sensitivity due to both gain reduction and the DC offset component (waterfall effect). As our pilot data show, we were able to obtain good quality fits with as few as 5 sampled points in the contrast domain, greatly reducing the experiment duration compared with that in previous work. This made it feasible to vary the adapting stimulus over a limited range within a typical experiment duration (10 minutes-1 hour).

We were subsequently successful in applying this method to 2 further recorded neurons, one a spiking VS cell, and the other an HS neuron. Typical fits to the VS data are shown for 3 different adapting speeds in Figure 13

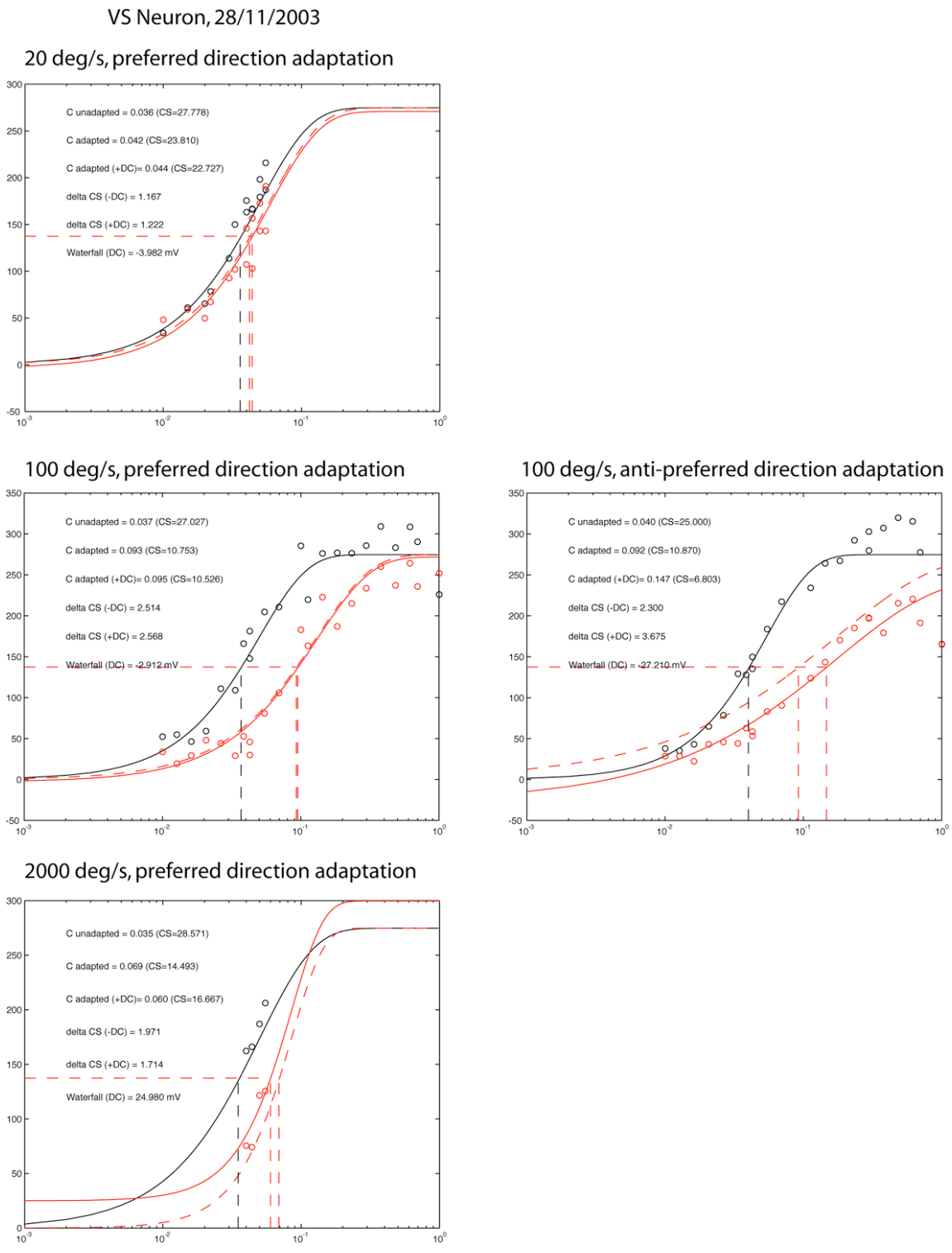

Figure 13: Double Weibull function fits and 50% response criteria computation for a contrast sensitivity of a VS neuron for several adapting stimuli. Data obtained by T. Rainsford & D.O'Carroll

In this case, we were experimenting to find the optimal (subset) set of contrasts at which to evaluate the adapted response in each case (hence the variable number of points for each graph). These data showed that adapting speeds in the vicinity of the response optimum for the cell (100-300 deg/s) produced the most convincing rightward shift in the CSF following adaptation (red data). Note also that even when very few points were sampled (e.g. at 2000 deg/s), the solved contrast sensitivity for the unadapted response (black lines) was similar to

that obtained in control experiments. Interestingly, the effect of reversing the pattern direction during the adapting stimulus produced a similar right-shift in the CSF, but appeared to have a marked effect on the shape of the CSF in this spiking neuron. We did not observe this in our earlier recordings from HS neurons, and it could have been due to additional non-linearity associated with the spike generating mechanism: This throws into some doubt any conclusions based solely on data obtained for spiking responses only (as is always the case for extracellular recordings from cells like H1, commonly used as models for studying insect visual processing). It also emphasizes the strengths of the intracellular recording technique, where we can analyze membrane potential independent of spiking responses.

At this point, we were able to use data of this form to graph contrast sensitivity (CS) following different adapting pattern speeds. An example for the above neuron is shown below in figure 14.

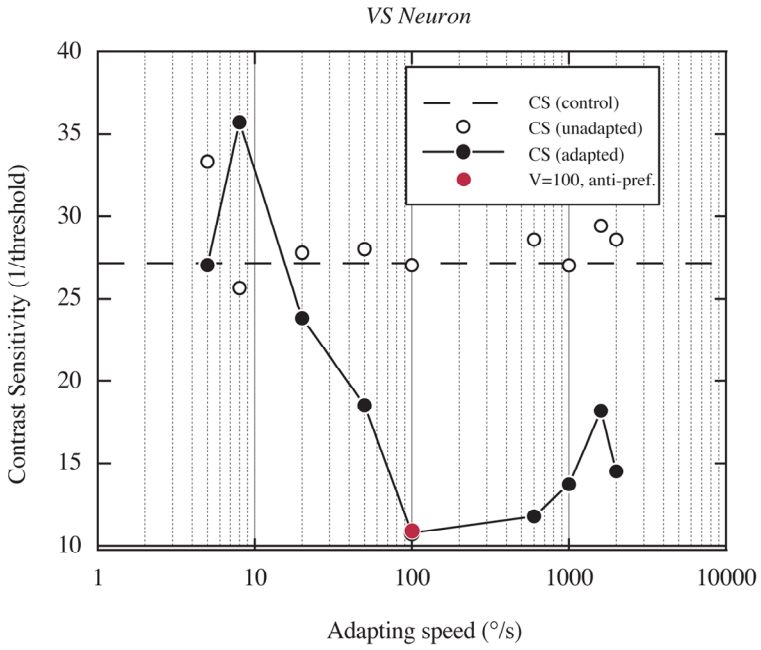

Figure 14: Contrast sensitivity of VS neuron as a function of adapting stimulus speed.

Data for this neuron illustrates 3 important points: (1) The unadapted contrast sensitivity (open symbols) estimated in each short sequence of the probe-adapt-probe stimulus was in good agreement with the control experiment data (dashed line). (2) Direction reversal of the adapting stimulus produced similar shift in contrast sensitivity (red data point) to the preferred direction stimulus, indicating that the gain control mechanism is not inherently direction selective. (3) The strongest adaptation (lowest gain following adaptation) was observed when the adapting stimulus is close to the optimal speed for the neuron. The latter finding generally supports the notion that the adaptation process is driven by feedback from motion detectors, but this conclusion is somewhat contradicted by the fact that the overall 'tuning' of adaptation is very broad, with powerful adaptation still evident at the highest speeds used in this experiment. By contrast, the HS or VS neurons gives little or no sustained, measurable response to such stimuli.

We evaluated the effect of varying the adapting contrast during a probe-test-probe sequence, using the Weibull curve fit experiments outlined above. We obtained partial data sets from several HS neurons, and more complete data sets in 2 cases. Figure 15 shows the results

of curve fits to the data obtained from the two cells, using two different images as the adapting pattern. Each point is the mean of all 4 conditions ± standard error.

Although we considered several metrics for evaluating the gain reduction in these data sets, the simplest (and a theoretically sound) method which was eventually put into use was to evaluate a response threshold in the adapted state. For the data below, this is the probe stimulus contrast required to evoke a 50% maximal response from the neuron, determined from the Weibull curve fit to the contrast/response function. The upper plots in fig. 15 show this metric. As gain was reduced by adaptation, a higher stimulus contrast was needed to evoke this response. The threshold contrast is inversely proportional to contrast gain of the system.

This experiment is technically challenging and very demanding time-wise, in that each point on the resulting curves requires an independent experiment in which contrast of the probe stimulus is varied in sequential presentations. Because it is vital that the adaptation state be dominated by the adapting stimulus, rather than the probe itself, we needed to employ (a) long adapting times and (b) long 'rest' intervals between experiments. In the data obtained during this period, we used a total duty cycle of 16 seconds. Despite these measures (which led to experiment durations of >20 minutes), analysis of the response to the first probe in each case ('unadapted' in fig. 15 below) showed a slight but worrying upward trend in the threshold contrast for the control experiment. This suggested that some of effect of adaptation evoked during each probe-test-probe sequence lasted until the first probe stimulus of the next, at least when the adapting contrast was high. Consequently, in experiments performed after this period, we would increase the interval between experiments in an attempt to abolish this effect.

In spite of these issues, the result of these experiments was very clear: Adaptation was found to be strongly dependent on contrast. Indeed, the threshold contrast appears to increase linearly up to the maximum (unattenuated) contrast of the natural scenes used as adapting stimuli in this instance. The latter observation is particularly interesting because earlier experiments on the unadapted system showed that these higher contrasts lead to saturation of the response. The continued linear (and possibly even supra-linear) contrast dependence of gain reduction could be taken as evidence that the adaptation mechanism incorporates an expansive non-linearity. Since most other non-linearities observed in the motion pathway are compressive (e.g. logarithmic luminance coding, saturation), these findings provide strong support for our computational models, where gain control is either gated by feedback from EMD outputs or directly modulated by it: Under these conditions the non-linear (multiplicative) correlation mechanism explains the dramatic onset in adaptation at higher contrasts.

The method we employed also allowed us to address a second question: Are the so-called 'waterfall effect' and gain reduction components of adaptation similarly driven by contrast? Both components lead to a net decrease in response at a given contrast. The magnitude of the waterfall effect, though, is quantified by the overall DC offset in the Weibull fits to adapted curves. The lower figure shows that this waterfall component increases in magnitude as contrast increases, again in a near-linear manner for larger adapting contrasts. By subtracting this component away from the adapted curves, we were able to determine the gain reduction independent of it (filled triangle symbols in the upper plots). The data show that both components of adaptation are similarly dependent on contrast.

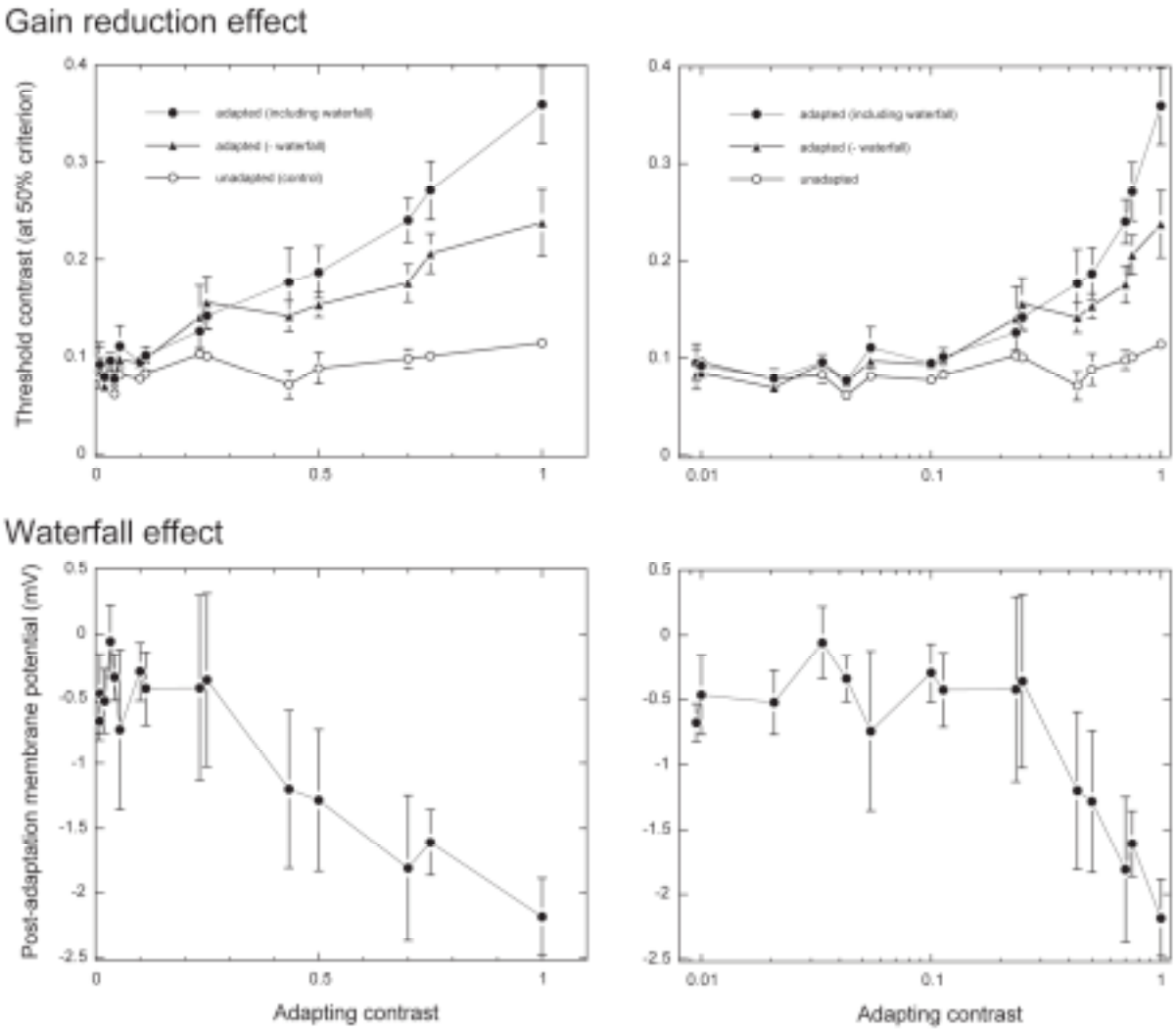

Figure 15: Contrast threshold (top) and post-hyperpolarization (bottom) as a function of adapting stimulus contrast. Data are averaged over two HS cells and two different (contrast-attenuated) natural images. The abscissa is linear at left and logarithmic at right. Data obtained by T. Rainsford & D.O'Carroll.

The data shown above were pooled from both images used as adapting stimuli – the lowest and highest contrast images from the set that we used in the experimental program during this stage of the work. At this point, we did not have sufficient data to differentiate the adaptation generated by these two images, which have intrinsic statistical differences (particularly in the contrast domain), although both were taken from natural habitat that the flies are active in. We planned further experiments to replicate this effect and provide data for a more definitive analysis of the effect of the individual image on the parameters of adaptation.

2.1.3.5 Analysis of Neurobiological Data and Implications for Modeling

Our analysis of the basic behavior of biological motion detectors in response to the velocity of natural scenes was sufficiently complete at this point to begin preparation of several manuscripts for submission to specialized vision research journals. Although our elaborated, adaptive EMD models provided a basis for development of robust biomimetic motion detector arrays that are a clear improvement over previous implementations of the Reichardt model, they have yet to provide a definitive explanation for the remarkable velocity constancy exhibited in the biological system, particularly that observed in (presumed) unadapted

responses. We consider our discovery of the full nature of this phenomenon to be a major finding for understanding biological motion coding and prepared a manuscript summarizing the key findings for submission to the journal *Nature* (rejected and subsequently modified for submission to an alternative journal).

To summarize the basic observations of 'velocity constancy' at this point, responses of fly HS or CH neurons were found to be virtually independent of the natural image selected, even where the 'natural' contrast of those images varies over a large range. Even highly elaborated EMD and tangential cell models that incorporate many of the known static nonlinearities in the biological system (including the HS cell 'gain control' mechanism proposed by Borst et al.) fail to reproduce this behavior (see Modeling). Since static nonlinearities fail to provide a perfect model for the biological system, our data support the hypothesis that dynamic motion adaptation plays a role in the velocity constancy phenomenon.

In addition to the data for two neurons provided in earlier material, in this period we performed analysis of data from a further three, including one recording of exceptional stability. In each case, these newer results used the longer inter-stimulus 'rest' period that we concluded was required following our previously reported data. For that reason, we did not pool the data together at this point, and awaited one or two further stable recordings before doing so.

Figure 16 shows the results of Weibull curve fits (as outlined earlier) using two different images as the adapting pattern. In all cases, the adapting pattern had optimal speed and was presented for 4 seconds prior to presentation of the probe stimulus. One adapting image ("Hamlin woods") is the forest scene with numerous vertical tree trunks visible against a bright background (see fig 3), and has the highest contrast of the set of images that we have available to us as stimuli in our experiments. Several different contrast measures show that the second image ("Gardens") captured under dull light conditions from the Botanic Gardens near the University of Adelaide has 1/4 to 1/3 of the contrast of the Hamlin woods scene. The 'canonical' probe stimulus (an optimal frequency sinusoidal grating) is identical in every case, except for its contrast. The left hand panel shows the raw contrast sensitivity obtained by solving Weibull function fits to individual contrast/response functions at a 50% maximal response criterion. Such functions include both major components – gain reduction and the 'waterfall effect' (an antagonistic DC offset to membrane voltage) of motion adaptation that we identified in our earlier studies (reported in *Neuron*, Harris et al. 2000). It is clear from the data for both images that when contrast of the images is strongly attenuated, there is little observable effect on contrast threshold, suggesting that both of these components are only recruited by relatively high contrast adapting patterns. Note that the adapting contrast referred to is not an absolute value, but is expressed relative to the 'natural' contrast of the adapting scene.

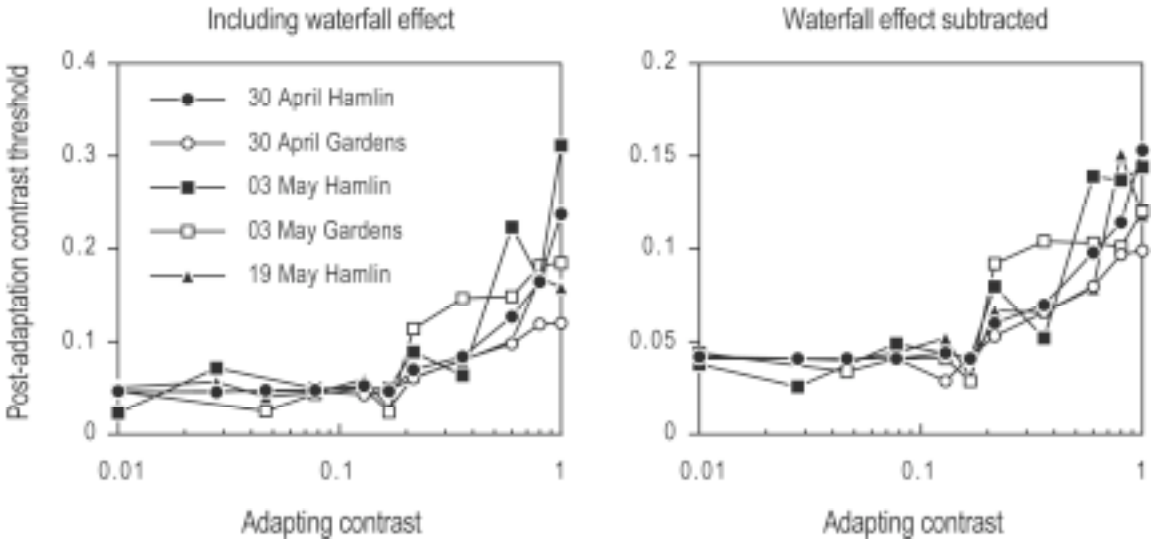

Figure 16: Contrast sensitivity following motion adaptation by natural scenes.

At low contrasts (<0.15 times natural contrast) contrast threshold in the adapted responses in all 5 cases is close to that evaluated in unadapted neurons (threshold ca. 0.04). When we consider that this threshold is evaluated at a 50% maximal response criterion, this highlights the high inherent gain of this system. At relative contrasts for the adaptor (i.e. the natural scene) above 0.15, the threshold starts to rise rapidly. All 5 curves are remarkably flat in the lower part of the curve and are not distinguishable from unadapted responses. This transition from a non-adapting to adapting regime as pattern contrast increases is an interesting observation, suggestive of a possible 'threshold' in the adaptation mechanism. It may, however, also be consistent with a shunting inhibitory mechanism in which the membrane conductance associated with the shunting effect falls below levels associated with other membrane conductances, when adaptation is weak.

The right panel shows effect of subtracting away the DC offset in the response (the 'waterfall effect') and re-solving the criterion response. Although the thresholds are lower, the qualitative shapes of the curves are similar, suggesting that both components of adaptation are similarly sensitive to contrast.

Of great interest, the data show that both images produce a shift from the non-adapting to adapting regime at a similar threshold value (filled versus open symbols), even though the intrinsic contrast of one is at least 3 times lower than the other. Furthermore, if we re-plot the data from the most reliable of the 5 recordings obtained so far (figure 17), it is evident that above this 'onset' contrast for the gain reduction, the rate of increase in threshold (i.e. strength of adaptation) is different for the two images. Hence, we conclude that the adaptation state does depend on the intrinsic contrast of the image. It is worth pointing out that this is the only experiment we have yet conducted using 'true' natural scenes that has yielded a clear difference in response to these two images. Motion-adapted velocity tuning curves superimpose perfectly at any one 'attenuation level' for such scenes, so that the simultaneous presence of velocity constancy and differential adaptation has been demonstrated.

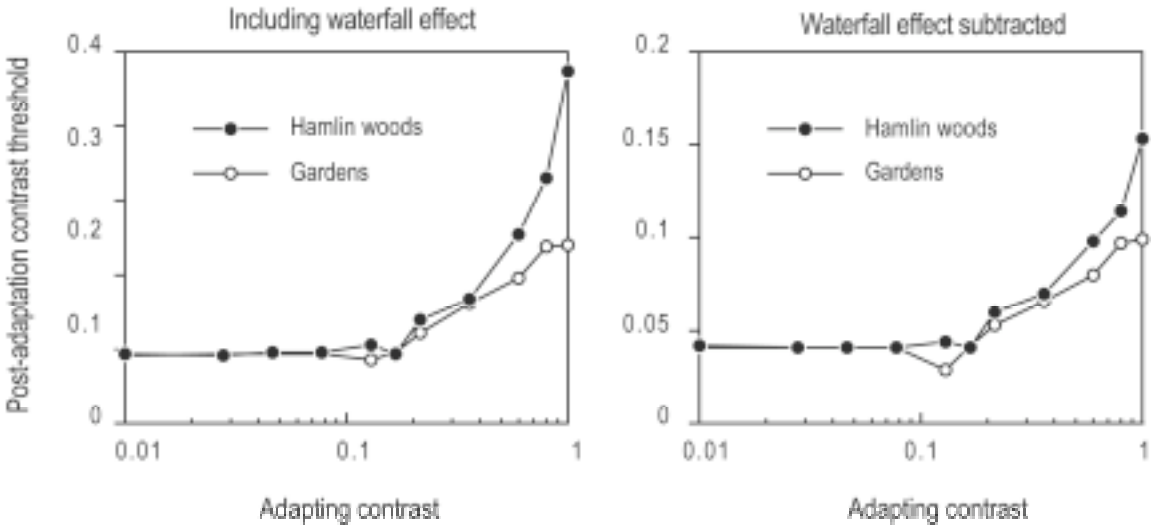

Figure 17: Contrast sensitivity data for a single neuron.

Since the results of these experiments strongly support a role for motion adaptation in the velocity constancy phenomenon, and our models for static nonlinearities fail to reproduce the same behavior, a question that we asked at this stage was, why do (apparently) unadapted neuron responses display near- 'velocity constancy' to the same set of images? With respect to this observation, it must be noted that our standard stimulus techniques for evaluating such responses were not able to exclude the possible contribution of very rapid components of adaptation: This is because probe stimuli were presented after subjecting the neuron to prior 'stimulation' by a blank screen of mean luminance. When the blank screen was replaced with the pattern in motion, response transients were evoked that then dissipate with the time constant of any temporal filters in the motion pathway. Since we need to exclude such transients from our analysis, we needed to discard the first 50-100 ms of data collected. Hence, if adaptation is rapid enough, it may already have influenced the responses that we evaluated.

2.1.3.6 Alternative stimuli for evaluating unadapted responses

Are any alternative stimulus techniques available to evaluate responses of unadapted neurons to high contrast stimuli? One method that we developed previously to avoid the confounding effects of motion adaptation on raw response tuning is the 'contrast ramp' method, in which the contrast of the probe stimulus is increased over time, from an initial zero value. This 'soft' onset of this stimulus avoids the transient behavior referred to above and was regarded as a potentially useful alternative stimulus regime. Unfortunately, this stimulus is not suitable for 'probing' the contrast sensitivity of the adapted response, as it confounds recovery from adaptation (during the early part of the ramp) with gain. Figure illustrates an interesting pilot experiment with this stimulus using a slower ramp than we used previously (5 seconds versus 1 second). In each case the stimulus was a sinusoidal grating which increased in contrast linearly over a 5 second period. An interesting feature of such a stimulus is that as the ramp reaches the contrast threshold for any given speed of the pattern, the weakly stimulated neuron is within the 'Reichardt detector' part of its dynamic range and thus subsequent increase in response is approximately quadratic until either the effects of saturation or adaptation start to distort its shape and response plateaus. This is clearly visible in most of the raw data traces in Figure, at least at lower temporal frequencies (pattern speed).

In such data, the contrast sensitivity at any particular temporal frequency is explicitly represented by the *time* at which responses reach threshold. The solid vertical line in Figure 18 shows that, as expected from the temporal frequency tuning characteristic of a Reichardt-detector based system, this threshold value (say at 50% maximum response criterion) is very similar at very low (e.g. 0.5 Hz) and very high (40Hz) frequencies, while threshold is reached *earlier* (i.e., at lower contrasts) at intermediate (i.e. optimal) frequencies. The most interesting feature that is immediately evident from this experiment is, however, that once threshold has been reached, response time course is very different over the subsequent part of the ramp at very high temporal frequencies. In particular, it never reaches a 'steady state' plateau level as predicted by static models for non-linear 'gain control' (i.e., the Borst model), but rather falls back to the resting membrane potential (dotted line on each trace) and even below at very high contrasts. This suggests that motion adaptation during the ramp is so rapid that it may overcome the quadratic rise in supra-threshold response – but only at high temporal frequencies.

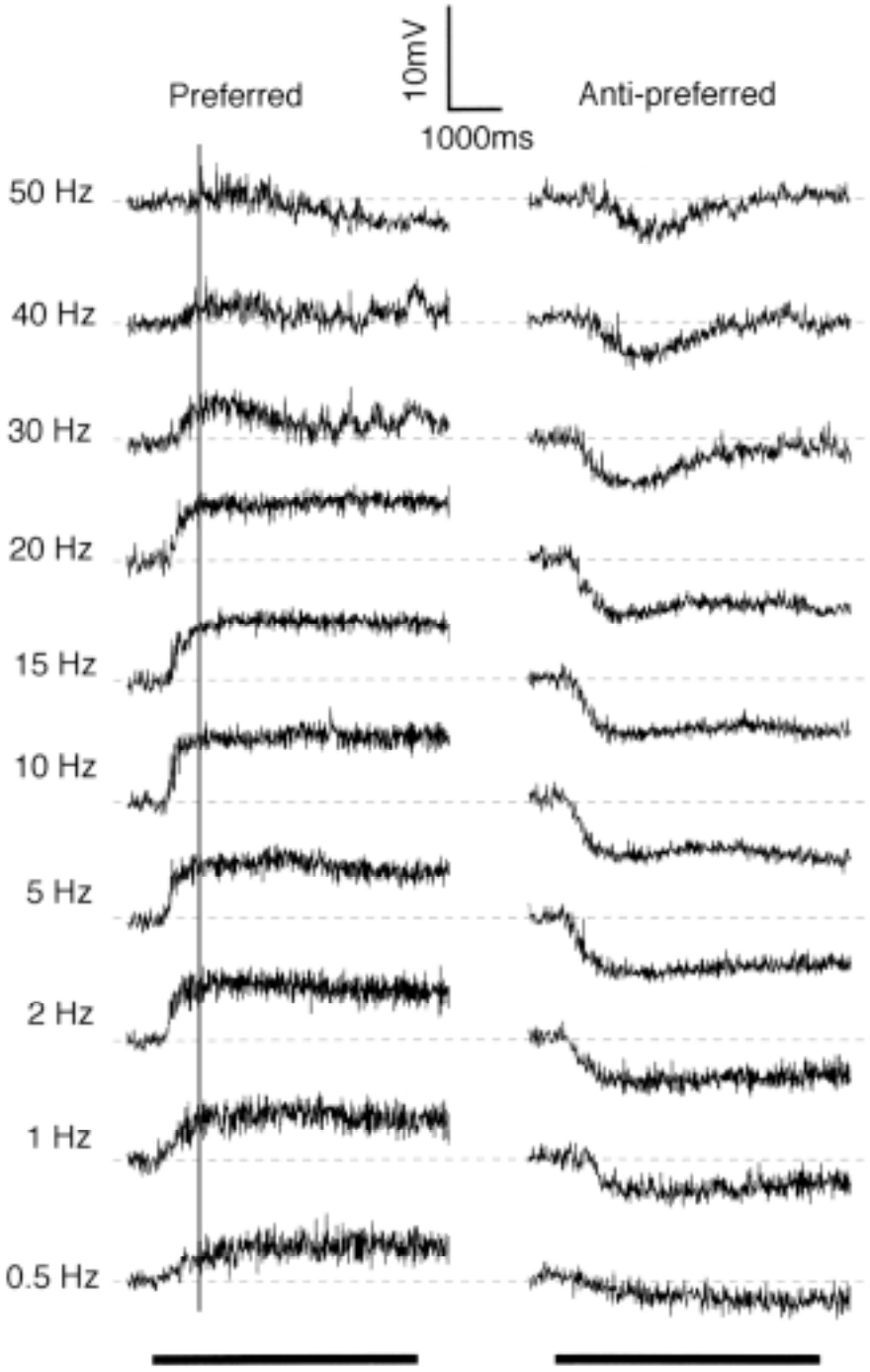

Figure 18: Raw data for a CH neuron in response to 5 second contrast ramps of a sinusoidal grating moving in the preferred direction (left) or anti-preferred direction (right) at a range of temporal frequencies. Data obtained by D. O'Carroll

Is this effect due to the waterfall or gain reduction component of adaptation? The simple test for this is to repeat the experiment in the anti-preferred direction, since our previous work shows that this does not recruit a significant waterfall component. The right column in fig 18 shows that, again, the confounding effect of gain reduction on time-course is very evident at high temporal frequency but even visible at intermediate frequencies, where responses reach saturation, adapt back below this level in the middle of the ramp and then rise again at the end of the ramp (particularly evident at 5-10 Hz). Interestingly, while preferred direction responses at very high temporal frequency fall below resting potential, this is not seen in the anti-

preferred direction. This suggests that both components of adaptation strongly shape the time course even during the stimulus at very high frequencies. The waterfall effect clearly contributes to strong asymmetry of the preferred versus anti-preferred responses at even very low contrasts and within a very short time after onset of the ramp. This is a surprise given that we had previously assumed the waterfall component to be relatively sluggish. Taken together with the data presented earlier in this section (fig 17), our latest data suggests that the 'waterfall' component of adaptation may play a significant role in the velocity constancy phenomenon.

The data are consistent with a hypothesis that the time-scale, and possibly the strength of adaptation, depend on the temporal structure of the stimulus. Specifically, adaptation may be faster (and/or) stronger at higher temporal frequencies. In the context of adaptation to natural images, it is interesting to speculate that this previously unsuspected degree of adaptation to such high temporal frequency stimuli might play a critical role: Such components would be produced by the higher spatial frequency features of natural scenes at a range of image speeds. Given the basic 1/f property of natural scenes, they would only be low contrast elements of such scenes, but fig 18 shows that such adaptation is evident at even low contrasts during the earliest parts of the ramps.

In principle, such a mechanism could produce a constant adaptation level for a variety of adapting speeds in a natural (1/f) image, even if implemented as a feedback gain reduction: As speed increases, the temporal frequency spectrum passed by the low-pass optical filtering of the eye shifts upward (to recruit faster and stronger adaptation). Although such faster patterns may be beyond the optimal speed range of the neuron (and thus produce weak global excitation of the tangential cell) the inherently higher contrast of the low spatial frequencies that produce high temporal frequencies in a fast moving scene could mitigate this effect and still produce strong local adaptation. Such a mechanism would only 'fall out of compliance' at much lower speeds, which would fail to produce any adaptation at all. In this context, it is particularly interesting to note that the pilot experiments we conducted recently (reported several months ago) showed a surprisingly strong and yet constant adaptation level for even the highest adapting speeds we can produce, even though such stimuli produce little steady state response from the neuron. These data, by way of contrast, showed significant decline in the strength of adaptation to slow moving patterns. Thus the 'velocity tuning' of adaptation is *not* identical to the velocity tuning of the tangential cell itself.

This idea clearly requires extensive further physiological work to provide a basis for further modeling. In the shorter term, however, it may be worth reconsidering the present inclusion of a low-pass filter in the adaptive element of our existing EMD models: the latter was included on the assumption that, to provide a gain reduction that compensates for the difference in contrast between different images, local EMDs ought to adapt to a level that reflects the global luminance contrast of the image (a parameter that can be extracted from the signal by a combination of partial or full rectification with low-pass filtering, as in our models). It will be interesting to explore the effect of replacing this low pass-filter with a temporal band-pass mechanism that would reject the lower frequency components of such scenes and introduce a dependence on temporal frequency into the adaptation mechanism. During our earlier work for the concurrent SBIR Phase I effort, we already showed (using Fourier analysis of individual EMD outputs in a relatively unelaborated EMD model) that intermediate temporal frequencies in the output of opponent EMDs were inherently independent of the speed at which the pattern was moved and thus might provide an alternative to seeking the DC response through massive low-pass filtering in the gain control mechanisms. Using a bandpass filter tuned to higher

temporal frequencies (10-50 Hz) as the source of either the gating signal to enable feedforward contrast normalization or a feedback gain control would also yield a much shorter time-constant for adaptation, at least at higher temporal frequencies.

By the onset of winter, we had obtained contrast sensitivity data from a number of further neurons, including 4 HS cells, 1 CH cell, and 1 VS cell. These data included tests in which both velocity and contrast of the adapting stimuli were varied as parameters. Reduction and analysis of the new data continued through the winter, in preparation for presentations by the PI and T. Rainsford at two conferences in Brisbane (August 2004, see below). During this period, T. Rainsford accepted a new position in another laboratory. Experimental work during the remaining part of the reporting period were obtained by a new post-doctoral researcher in the O'Carroll lab, Karin Nordström, who was supported in by by AFOSR funds, but also by the Swedish Research Council. Subsequent experiments were also carried out with AOARD funding by a part-time technical assistant, Irene Moyer, through to the end of the period. The training of these new personnel necessarily introduced some delay into the analysis and execution of further experiments.

From mid-winter (June 2004) in Adelaide, flies were not easily obtained. Although some additional recordings were performed at the start of the period, they were not sufficient to address the major aim of studying further the effect of adapting conditions. Instead we worked up the backlog of data from recent experimental recording periods into figures with high enough quality for use in publications and talks at the 22nd Quadrennial meeting of the International Congress of Entomology (ICE) and subsequent workshop "Insect Sensors & Robotics" (ISR) at the University of Queensland.

We expected flies to be more readily available during the upcoming reporting periods and planned to continue HS recordings using the test-adapt-test approach with the intention of estimating the time constant of adaptation. Given some contemporary simulation results (ijn our concurrent Air Force funded SBIR Phase II project), which suggested that an adaptive time constant of 200ms or even faster may be optimal for controlling contrast gain, we considered it a priority in further recordings to vary the adapting *period*, (using both optimal and non-optimal adapting patterns) in addition to the recent efforts varying adapting contrast and speed.

While little progress was made on actual experiments due to poor availability of *Eristalis* this spring, we did considerable work in upgrading laboratory facilities. Interface software was added to the Vision Egg by an Honours student, Lachlan Dowd, which greatly facilitates the design and running of complex experimental sequences, and which we expected to increase the volume and range of data available from individual experiments. In addition, we furnished a second experimental bench in the lab, enabling parallel experiments to be run.

2.1.4 Year 4 (2005): end of experimental period

An unusually late Spring season meant that little progress was made on experiments due to poor availability of *Eristalis*. As flies became available, we began training our research assistant Irene Moyer, who started work part-time with the intention of recording from HS cells when *Eristalis* became more abundant.

2.1.4.1 Strip test experiments to evaluate waterfall effect

A hitherto poorly studied aspect of the neurons response was the waterfall effect. Successful recordings were made in this period by both Irene Moyer and post-doctoral fellow Karin Nordström and Irene Moyer. Experiments aimed to address 2 key questions relating to the poorly characterized waterfall effect. The first set of experiments ("Strip-test, surround adapt") used a sinusoidal stimulus in a probe-adapt-probe experiment to evaluate gain change

resulting from adaptation, as in the previous experiments on the effect of adapting speed and contrast. As before, data were analysed using a Weibull function fit to the contrast sensitivity function. In each case, the stimulus was the same 'canonical' sinusoidal grating (with approximately optimal spatial and temporal frequency) used as a probe stimulus in the earlier experiments. The difference compared with earlier applications of similar stimuli was that the grating was used as the adapting stimulus, as well as the probe, but probed *different* parts of the receptive field of the HS neuron to that adapted. This was achieved by using a grating with a central 'strip' missing as the adapting stimulus, while probing the central part of the receptive field with the missing strip alone. The rationale behind this approach is that we know from earlier work (e.g. Maddess & Laughlin 1986) that the main effect of adaptation (quantified by ourselves as a contrast gain reduction) is a highly local phenomenon. It is unclear whether the waterfall effect is also locally generated, but because it is a persistent effect, it can potentially influence the membrane potential of the HS cell even when stimuli are presented to previously parts of the receptive field. Hence, the 'surround' adaptation allows us to probe the effect of the waterfall component on 'normal' responses to a part of the visual field that is unaffected by adaptation. Furthermore, because our earlier work (Harris et al 2000) had shown that the waterfall effect is direction selective, we can control in these experiments by using different combinations of adapt and test stimuli in the preferred and anti-preferred (null) direction. A clear prediction based on our earlier work would be that null-direction adaptation of the surround would recruit no waterfall effect and thus affect neither contrast gain, nor global membrane potential. We would thus expect to observe no effect of such adaptation on contrast sensitivity functions in either preferred or null directions. By contrast, any 'global' contribution of the waterfall effect accumulating during preferred direction adaptation would cause an effective DC (downward) offset in the contrast sensitivity functions (for either stimulus direction), and thus we can quantify their contribution to gain reduction.

The basic stimulus and examples of responses in raw trials are shown below, with data illustrated for 3 contrasts (1,0.1 and the control of 0). In each case, data are illustrated for (a) null direction test and adapt (b) null direction test, but preferred adapt (c) preferred direction test, null adapt and (d) preferred direction test and adapt. The test periods are indicated by gray boxes, adapt by the black stimulus bar. It is immediately evident from the raw data that effects on the second test stimulus are rather subtle, even at the low contrast illustrated. This is especially noticeable compared with previous test-adapt-test experiments that we conducted (e.g. Harris et al 2000). Strong adaptation is evident in both test and adapt stimuli during the time course.

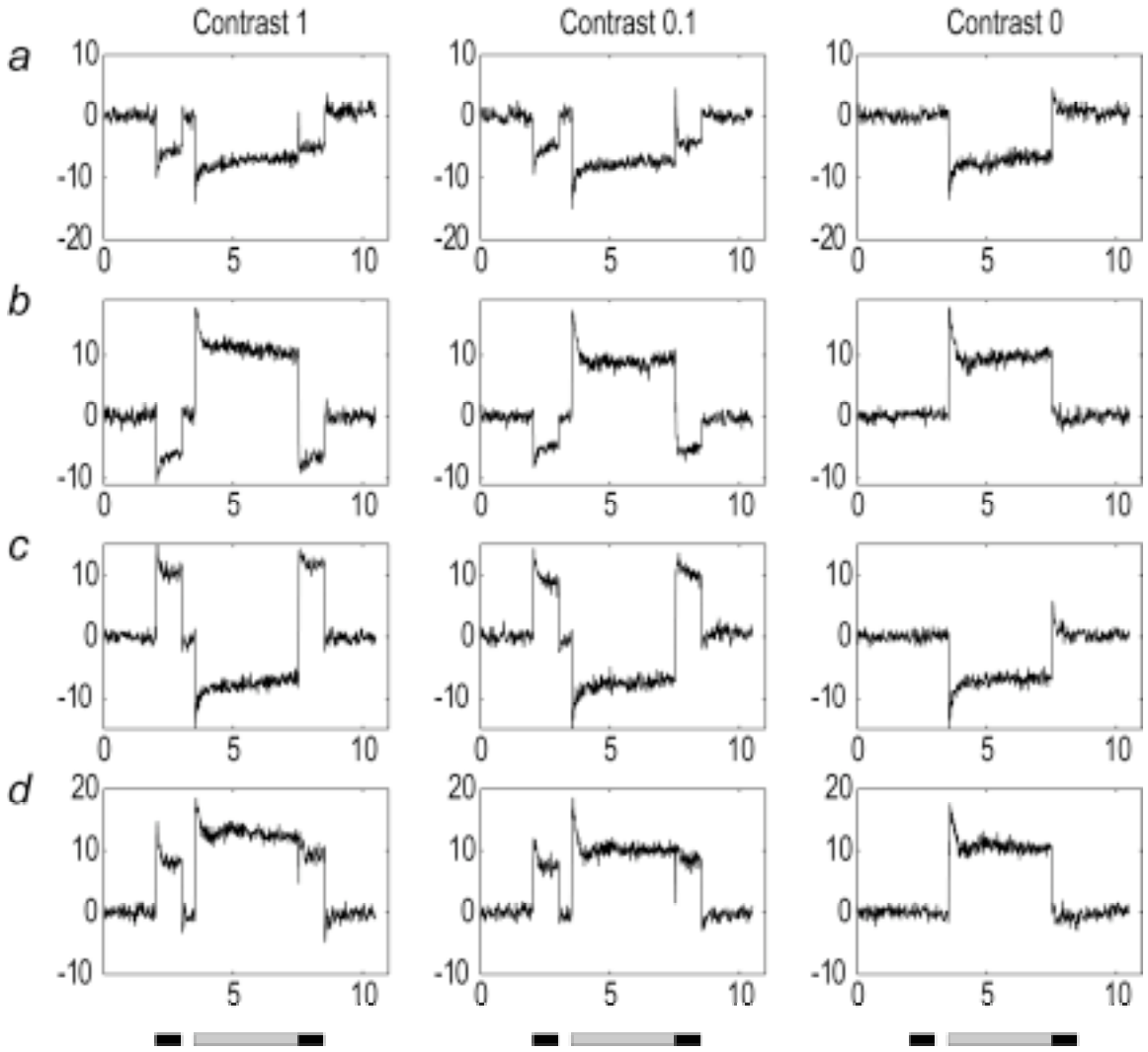

Figure 19: Raw data for an HS neuron in test-adapt-test experiments using a surround adapting stimulus and strip test. Data are shown for 3 test contrasts (test periods indicated by gray bars) and 4 combinations of adapt and test direction.

Figure 20 below illustrates results for a single HSE neuron in *Eristalis*. This data illustrates the main findings of the overall set of data recorded from 18 HS neurons to date. In each case, there is little or no evidence for any right shift in adapted contrast sensitivity functions, confirming earlier findings that contrast gain reduction is a local phenomenon.

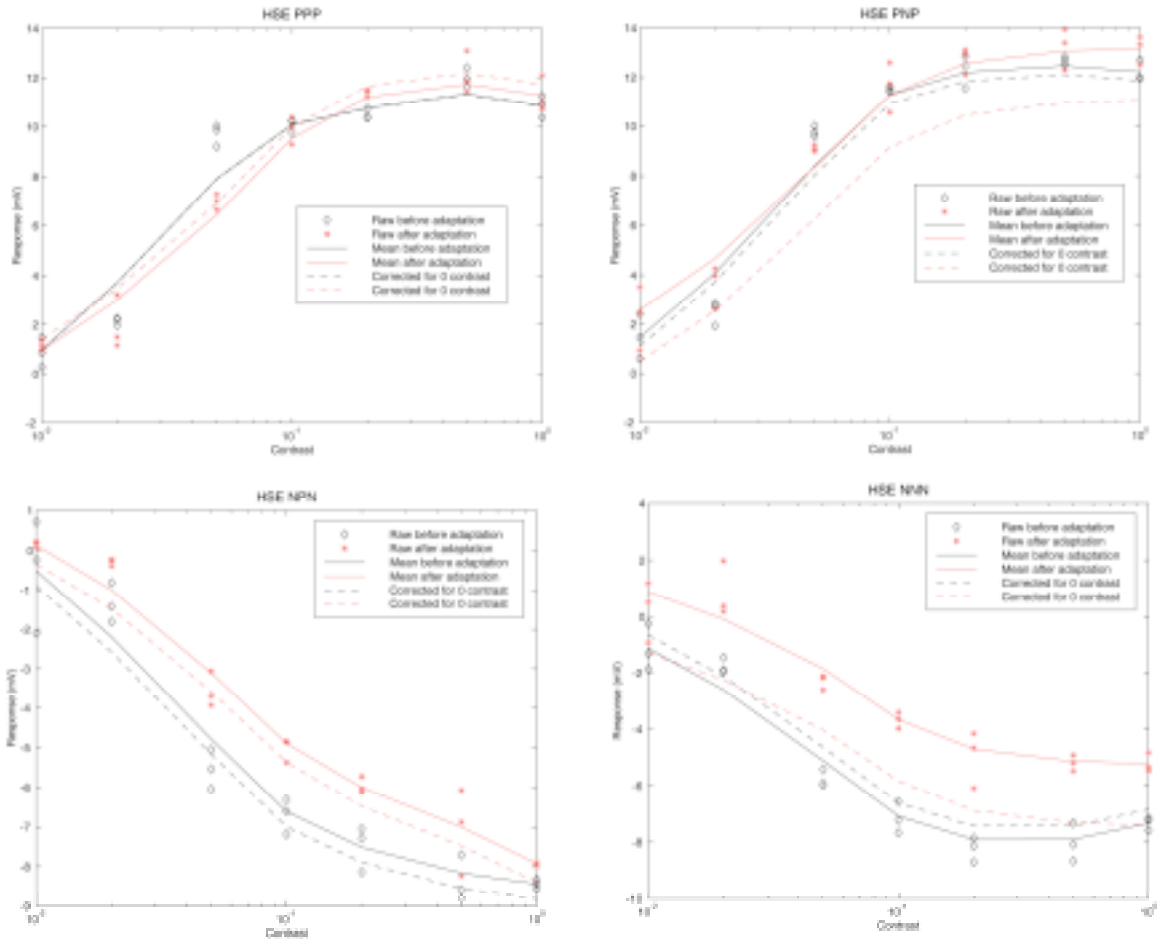

Figure 20: Contrast sensitivity data for a single HS neuron recorded in test-adapt-test experiments using a surround adapting stimulus and strip test. Data are shown for 4 combinations of adapt and test in preferred (P) and null (N) directions. Individual data points are shown together with means from all trials at each contrast. The dotted lines represent the same data after subtracting away the response at contrast=0 (the control experiments shown in the right hand side of the previous figure). Data recorded by Karin Nordström, Irene Moyer.

Figure 21 below shows similar data averaged across 6 HSE/HSNE neurons, after normalizing each curve to take account of differences in maximum response (due to differences in penetration quality, as outlined in the earlier reporting periods). Perhaps the biggest surprise from these experiments is that the surround adaptation reveals antagonistic afterpotentials een when adapting stimuli are presented in the null direction. This partially contradicts our earlier findings (Harris et al 2000). Note that the very 'early' response period used for this analysis (between 100 and 300 ms after stimulus onset) may pick up a brief, transient 'burst' of spikelets in some recordings upon relaxation from the hyperpolarizing adapting stimulus: such transients are clearly evident in the raw data illustrated earlier.

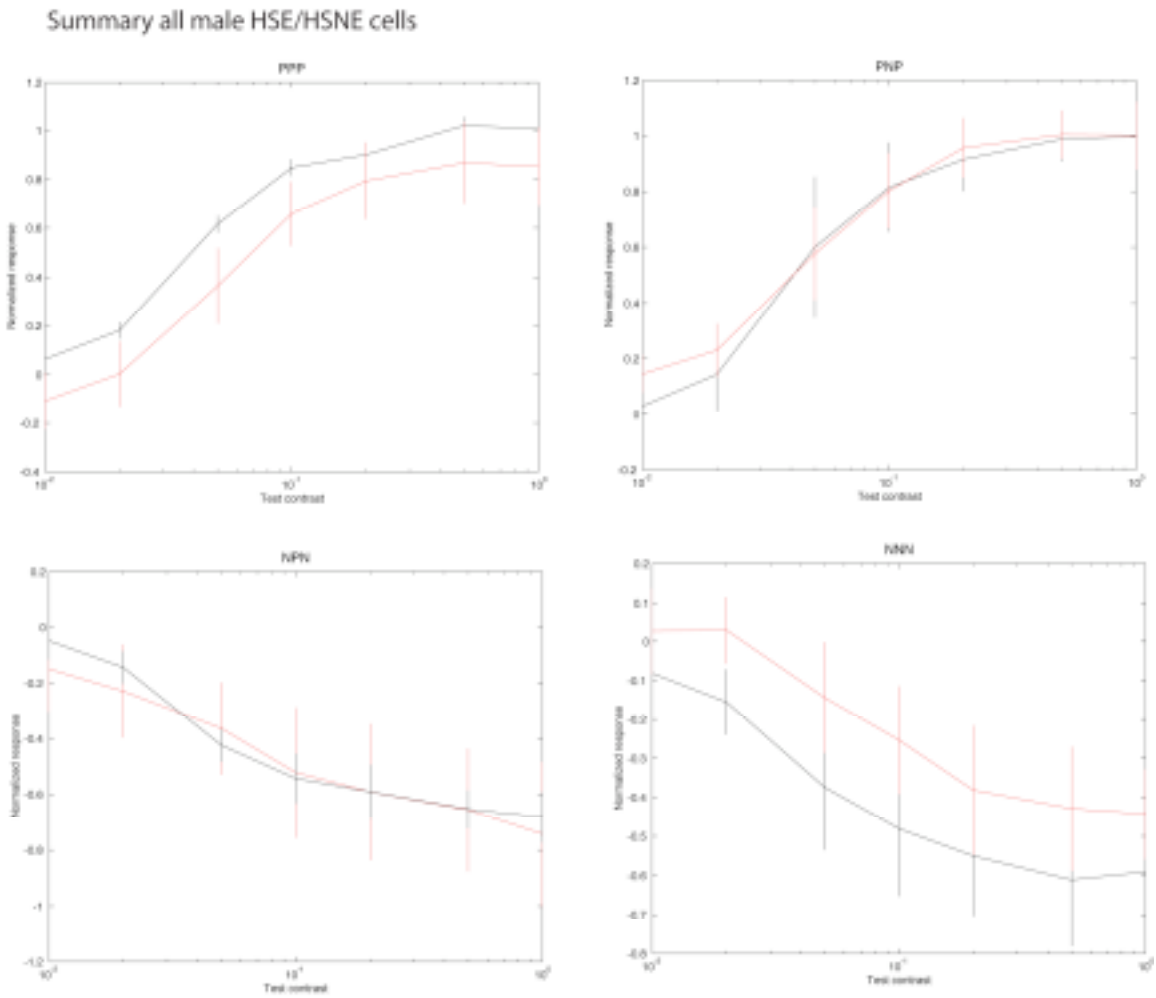

Figure 21: Contrast sensitivity data (as in previous figure) but averaged across 6 neurons. Error bars denote s.e.m. Data are shown for 4 combinations of adapt and test in preferred (P) and null (N) directions. Individual data points are shown together with means from all trials at each contrast. The dotted lines represent the same data after subtracting away the response at contrast=0 (the control experiments shown in the right hand side of the previous figure). Data recorded by Karin Nordström, Irene Moyer.

To summarize the results of these experiments, the recordings show that the waterfall effect, when present, adds a DC offset to the response only when test stimuli are presented in the same direction as the adapting stimuli (PPP, NNN). In this case, the offset persists even at the highest test contrasts (i.e. even when the underlying responses are fully saturated). This suggests that the waterfall effect is independent of the site of response saturation in the motion pathway. When test stimuli are different in direction to the adaptor (NPN, PNP), a DC offset is still evident at very low contrast, but responses at higher contrasts saturate at the same level as before adaptation. This makes sense since in this case the waterfall effect offset is antagonistic to the adaptor and thus adds to the test response measured. At very low contrasts, there is no response to the test stimulus itself, so the waterfall effect is the only measurable voltage.

The final set of experiments used a simpler experimental approach of a long stimulus (4 seconds duration) applied to an unadapted neuron, using the 3 images ('Hamlin', 'Close' and 'Gardens') that represent the extremes of contrast in our set of natural panoramas, as well as for our canonical sinusoidal stimulus. Response was simply evaluated in response windows very early in the stimulus (*Initial* in figure 22 below) at the end of 4 seconds (*Adapted*) and the antagonistic response immediately after stimulus end (*waterfall*)

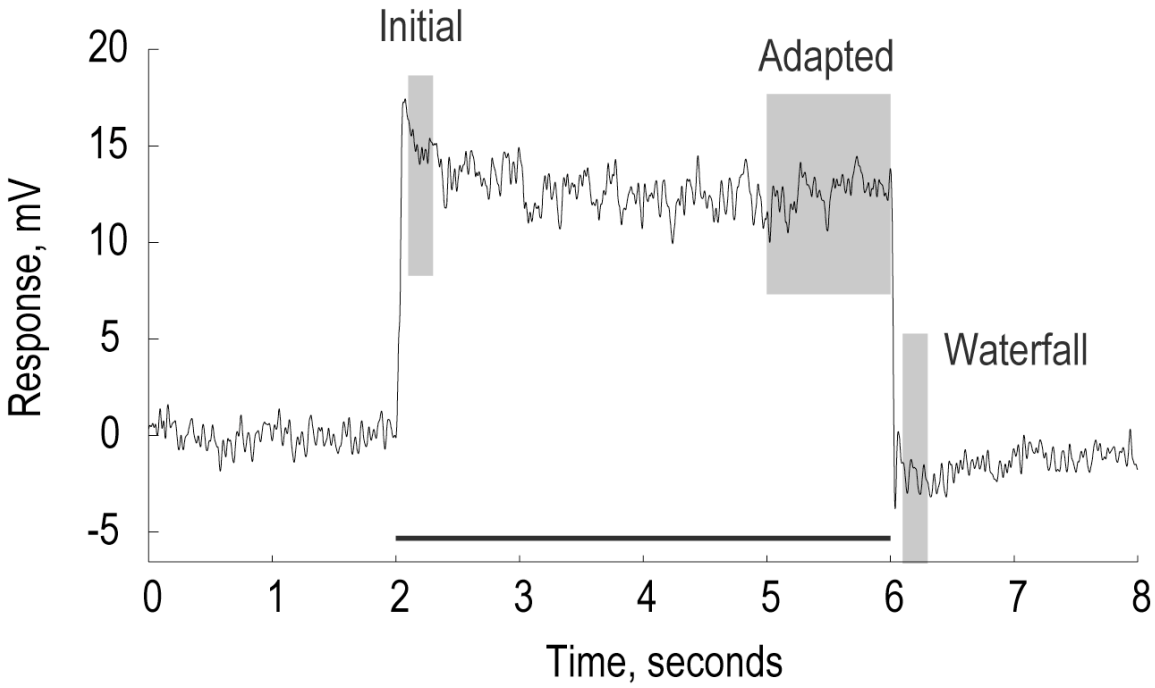

Figure 22: Averaged responses of an HS neuron to 4 seconds of stimulation with panoramic natural scenes, illustrating the 3 periods (indicated in gray) used to evaluate responses. Data recorded by Karin Nordström.

Figure 23 below shows the response averaged across these 3 windows when the speed of the pattern is varied, for each of the 3 images and also for the sinusoidal image. The data are the mean of 3 HS neurons, each normalized to account for responsiveness (as before). Both initial and adapted responses show clear velocity constancy, as expected from our earlier experiments. Adapted responses, however, are substantially weaker due to the combined effects of both gain reduction and the waterfall component. Interestingly, the shape of the responses are similar in each case if they are re-normalized to their own maximum (bottom right).

The main point of this experiment is illustrated by the top right panel: It can be seen that the waterfall effect is largest at the same velocities that the underlying response is strong. Again, if we invert this curve and normalize it to its own maximum, the resultant function nearly overlies the basic velocity tuning of the HS cell. In this respect the waterfall effect is clearly distinct from the gain reduction that we quantified in the earlier reporting periods, which showed somewhat more tuning to higher image velocities. Taken together with the results above, we conclude that the waterfall effect is clearly a separate component to the gain reduction and is most likely a property of the HS neuron itself, probably being generated within the axon, since the offset it introduces does not prevent underlying responses from saturating.

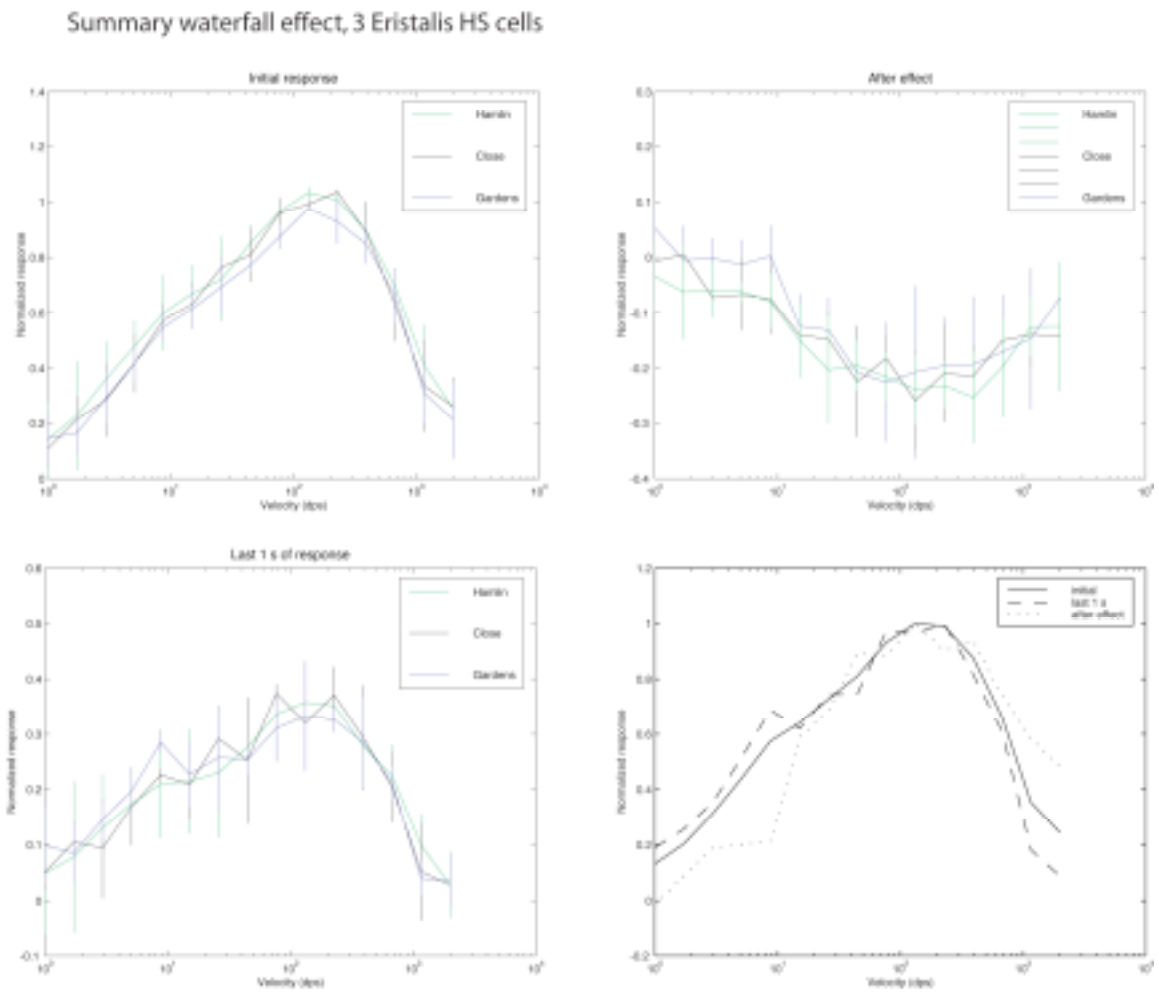

Figure 23: Averaged responses of 3 HS neuron to 4 seconds of stimulation with panoramic natural scenes, evaluated in the response periods indicated in the previous figure. The bottom right panel shows the data normalized by dividing through by their maximum. Data recorded by Karin Nordström.

2.1.4.2 Duration of adapting stimuli

Perhaps the most intriguing aspect of the project to this point was the observation that the (apparently) unadapted responses of neurons presented with natural images already display velocity constancy within the first few hundred milliseconds of the experiment (figs 6-8). This property is summarized for all of the neurons studied so far in figures 24 and 25 below, taken from our submitted manuscript (Straw, Rainsford & O'Carroll, presently under consideration by the journal Current Biology).

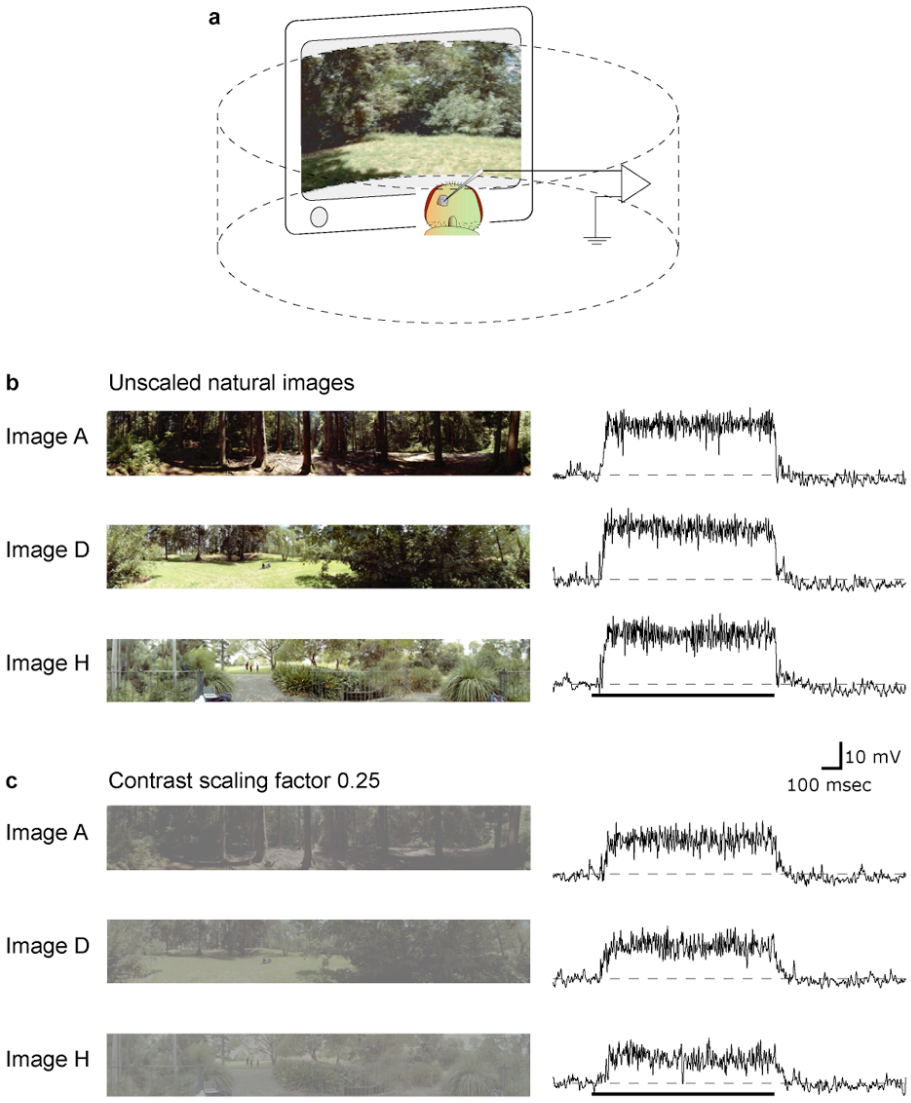

Figure 24: Unadapted responses in an HS neuron to 1 second of stimulation with panoramic natural scenes. A shows the experimental system. B,C responses to unscaled and contrast reduced versions of images A,D,H (see figure 3) (from Straw, Rainsford & O'Carroll 2005, submitted).

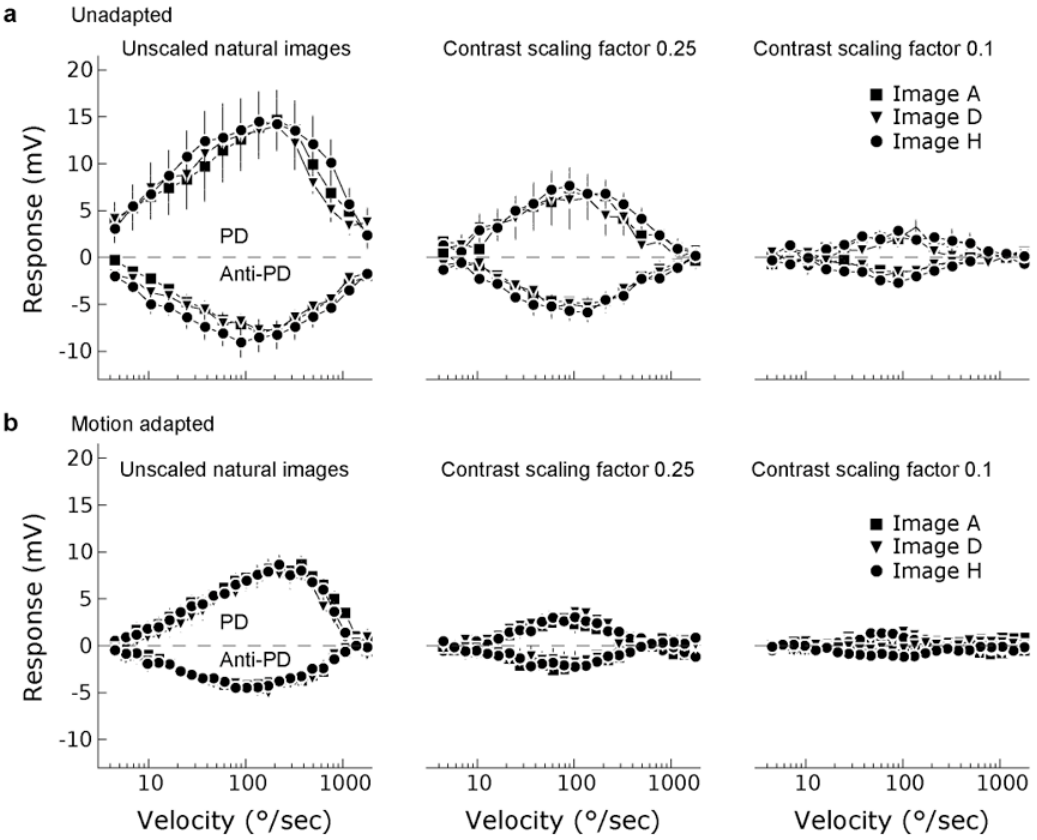

Figure 25: Velocity tuning (showing velocity constancy) in unadapted and motion adapted responses of HS neurons to both preferred and anti-preferred directions of motion. A shows the unadapted responses to scaled (left) and two degrees of artificial contrast compression (right). B shows similar data for neurons adapted using the the monotonic stimulus sequence described earlier (and see also figure 26) (from Straw, Rainsford & O'Carroll 2005, submitted).

These data make a very clear case for velocity constancy, but yet are enigmatic because the artificially contrast-reduced experiments are always consistent with one of the basic predictions of the Reichardt model – that lower contrast stimuli should produce lower contrast responses. Intriguingly, at no point do the reduced contrast responses fall out of compliance with respect to one another. This argues strongly against the velocity constancy being due solely to saturation nonlinearities.

An interesting insight into this problem comes from examination of our 'population' data for large numbers of repetitions of experiments in the adapted state, using the monotonic method (figure 26). Because this method is quick to generate results, we are able to evaluate a larger set of images. What is most interesting is that the artificial images – those taken from man-made scenes (images E and I, shown with open symbols to distinguish them from the natural scene panoramas) are outliers in the contrast reduced set, with obviously larger responses at all speeds. This is less evident but perhaps still present in the unscaled images. This observation is significant because these images are by no means the highest global contrast of the set. Indeed, image I is the lowest, with 1/4 the global contrast of image A by several measures. This trend is thus the complete opposite of what one would expect from a Reichardt based EMD. Indeed, we confirmed this in our recently submitted paper by using a contrast measure that was based on a simple EMD model.

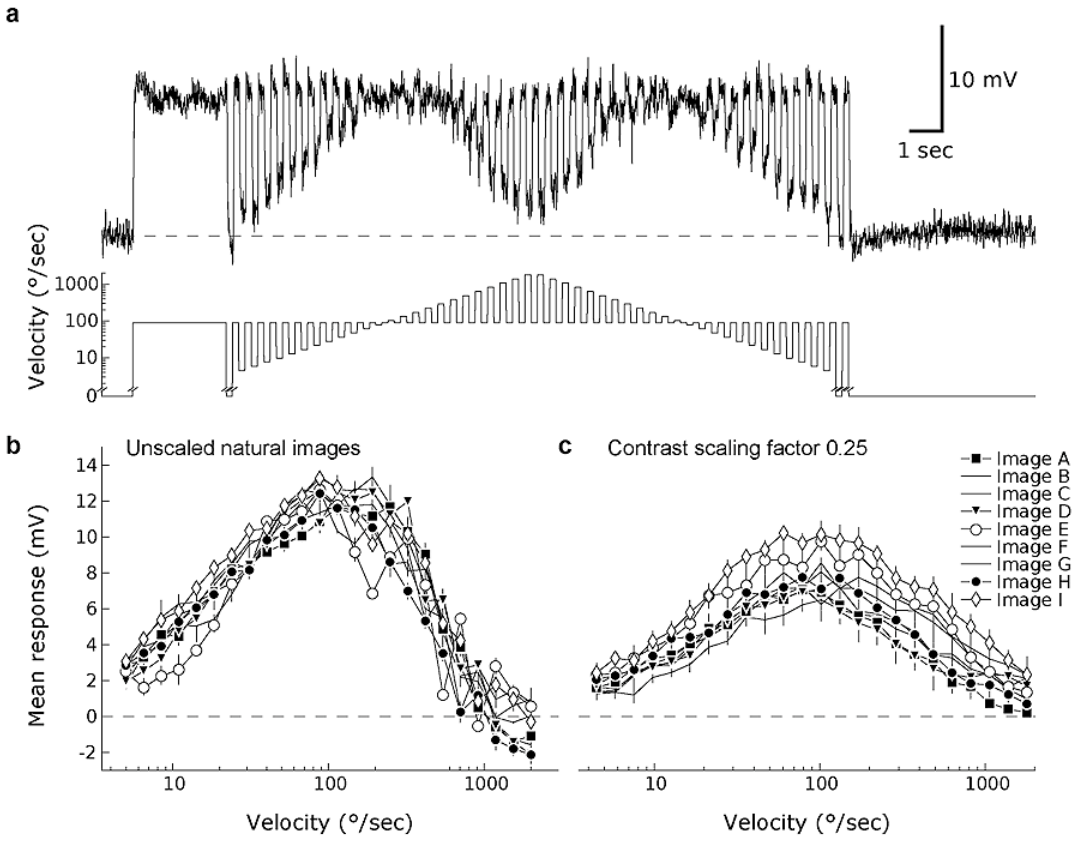

Figure 26: Velocity tuning (showing velocity constancy) in motion adapted responses of HS neurons to preferred direction of motion. A shows the monotonic stimulus sequence from which velocity tuning was obtained (as described earlier). (from Straw, Rainsford & O'Carroll 2005, submitted).

This observation is suggestive that dynamic motion adaptation does play a role in velocity constancy, yet seems to contradict the observation that supposedly unadapted neurons (fig 24, 25) already display similar velocity constancy. This interpretation is confounded by the difficulty of carrying out experiments that evaluate a 'true' unadapted neuron since we must expose the neuron to motion (which could induce rapid adaptation) in order to evaluate its response. An interesting observation in even the raw data (figure 24) is that little adaptation is *evident* during the 1 second stimulus presentation in these experiments, either in normal contrast (b) or reduced contrast (c) images. This raises the interesting possibilities that adaptation is so fast with these natural scenes that the gain reduction component of adaptation is already in 'steady state' within the initial response period. The slower reduction in response observed in many earlier studies may be less associated with the gain reduction component of adaptation than with the waterfall effect.

The rapid adaptation evident in the contrast ramp responses illustrated in fig 18 is consistent with this hypothesis, but does not permit is to evaluate the speed of adaptation quantitatively. To test the hypothesis that there may be 'fast' components of motion adaptation more directly, we therefore returned to the probe-adapt-probe method and contrast sensitivity (=gain) estimation method used to evaluate the effect of adapting contrast and adapting pattern speed. In this case, however, we varied the duration of the adapting stimulus in the range from

0.05 to 5 seconds. At the time of writing, we have obtained several pilot experimental data sets with this stimulus, but have (as yet) evaluated only one of these in detail. The raw results at several different adaptation times are illustrated in figure 27 below.

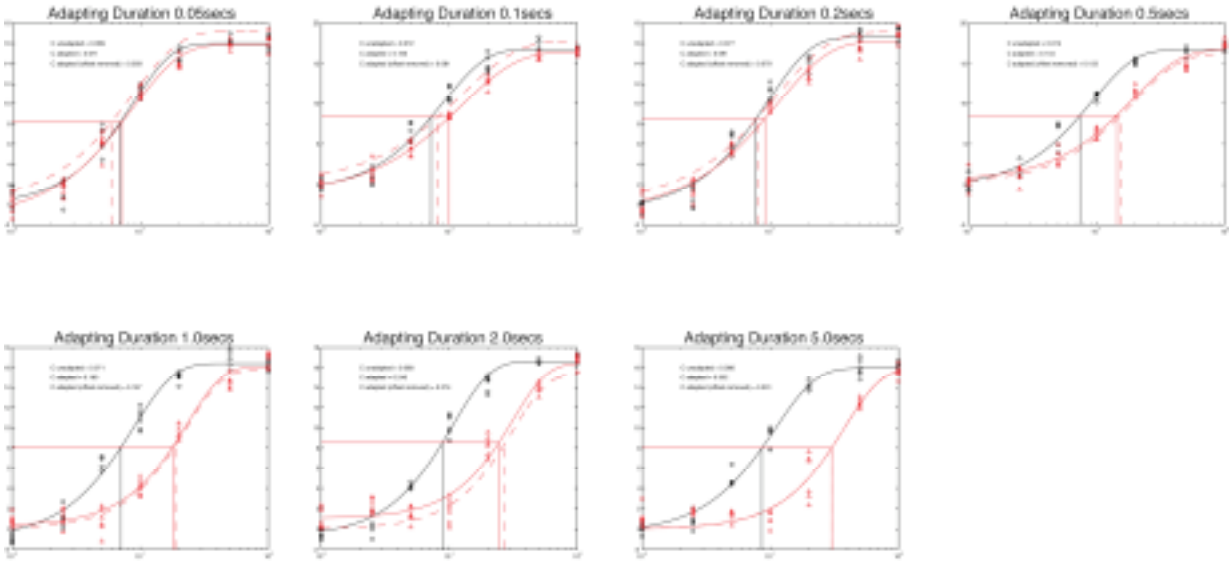

Figure 27: Contrast sensitivity of an HS neuron before (black) and after (red) different durations of adaptation in test-adapt-test experiments. The adapting duration is shown in the captions. Data from Irene Moyer & D. O'Carroll.

The right shift in the curves shows the amount of contrast gain reduction induced by the adapting stimulus. Two surprising observations emerge: (1) even by the longest adapting stimulus used in this pilot study, the right shift is still continuing to enlarge, suggesting (as hinted at in an earlier experiment) contrast gain reduction continues for many seconds after stimulus onset. (2) Even very short adapting stimuli induce a measurable gain reduction. Much further work is required to elaborate this finding, but it is clear that contrast gain reduction begins very rapidly but continues slowly over many seconds.

The results are summarized by figure 28 below, which shows contrast sensitivity (1/contrast threshold @ 50% maximal response) extracted from Weibull function fits to the data in fig 27. The blue line shows the adapted response after allowing for the confounding effect of the waterfall component (fitted by the offset term in the Weibull curves see fig 12 and associated discussion). Unadapted and adapted curves only converge for the shortest adapting stimulus (0.05 seconds). Importantly, this latter value is close to the estimated delay time constant of the underlying motion detectors. This suggests that adaptation begins on the same time course as the response of the EMDs themselves. If so, this confounds our attempts to quantify any 'truly' unadapted responses, and we cannot rule out this mechanism playing a key role in velocity constancy observed in our earlier work (e.g. figures 24-26).

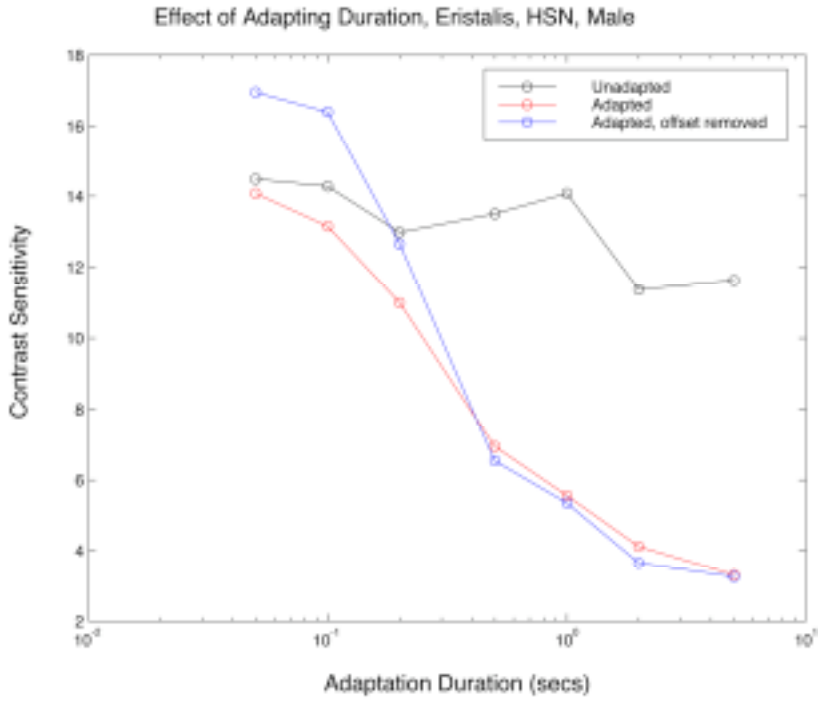

Figure 28: Contrast sensitivity of an HS neuron before (black) and after (red) different durations of adaptation in test-adapt-test experiments. The adapting duration is shown in the captions. Data from Irene Moyer & D. O'Carroll.

One obvious deficiency of this experimental design, at least for the long adapting stimuli, is that we are not allowing sufficient time for recovery from adaptation in one repetition of this stimulus before hitting the neuron with the next: This is evident from the downward trend in contrast sensitivity of the 'unadapted' response, which signifies reduced gain in these cases. We clearly need to do further experiments with yet longer adapting stimuli still as well as longer 'rest' periods between trials to allow neurons to fully recover.

2.2 Simulation and Modeling

2.2.1 Year 1

2.2.1.1 1-dimensional EMD model with adaptive (feedback) gain control

Work began on development of an EMD array simulation based on an elaborated Reichardt model as used in our previous work (Dror et al 2000). This was implemented in the MATLAB environment. This EMD model includes specific features designed to mimic the obvious known features of the neurobiology, e.g., with prefiltering based on models for photoreceptor and laminar temporal responses. The array was initially one-dimensional but was intended for expansion to two dimensions in the future. Adaptation was not initially enabled, but would be included as experimental work was done, and data to refine our models of adaptation became available. The basic framework employed for development of this adaptive EMD is illustrated below in figure 29:

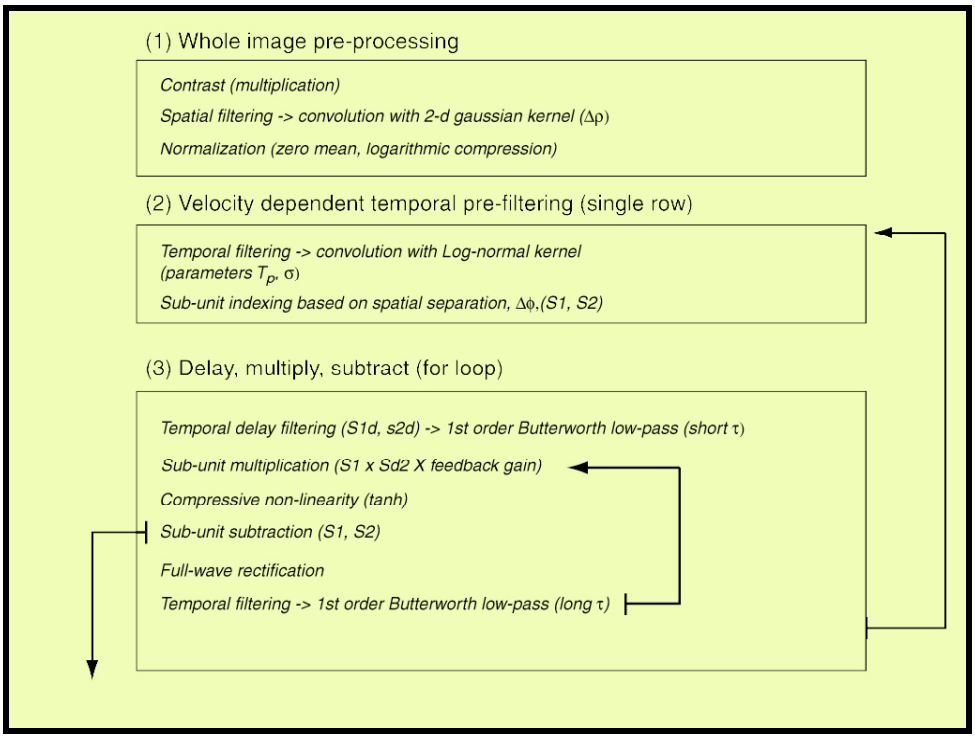

Figure 29: Summary of 3 key components of elaborated EMD model developed in Matlab. D. O'Carroll.

The model begins with the panoramic imagery used in the neurobiology experiments. Although we desire a fully 'biomimetic' front end for such a model, this isn't practical if we are to use the same stimuli in both model and experiments, because the camera used to capture the images necessarily imposes some limitations on the data obtained. For example, in nature, each and every photoreceptor (or second order neuron) adapts locally to the luminance so that image sampling cannot be defined by a single global gain terms, whereas in our camera, a single gain governs the value sampled by every pixel (within the limited dynamic range of the sensor). Hence, in setting the camera to 'optimal' exposure for the sampled scene, we are already biasing the subsequent model by the inherently linear sampling strategy of a CCD device. In converting the image (grayscale) to input values for the model , we need to make assumptions about the way that luminance is coded. The first stage of the model "Whole image pre-processing" is thus an attempt to re-encode the image into a biologically plausible form. In the initial model, this involved adjustment of the contrast (if desired to mimic the reduction in contrast of the images as in our experiments), spatial pre-filtering (specifically low-pass filtering to mimic spatial blur in insect vision) and image normalization to a zero mean and with a logarithmic compression to mimic the logarithmic encoding of luminance by photoreceptors.

In the second stage, the model takes account of the temporal filtering properties of the insect photoreceptors, by animating the image one row at a time (in a manner to mimic the desired experiment) and then introducing temporal blur by convolution with a lognormal impulse response derived from experimental data for insect photoreceptors (Howard et al). Indexing of the output of this operation then provided the inputs to the two arms of the elaborated EMD (S in figure 30 below). The index onto the animated luminance sequence for each image row allowed the inter-receptor angle (delta phi in fig 30 below) to be matched appropriately to the amount of spatial blur introduced into the image. For all simulations, these

were set to values based on 'typical' fly photoreceptors, with delta phi of 1.5 degrees, while the spatial blur was fixed with a Gaussian blur of half-width 2 degrees. All models were carried out using full resolution panoramic images, with approximately 8200 pixels wide (thus approx. 23 pixels/degree). The model thus provided an array of 240 EMDs to cover the full 360 degrees of each image. Animating the whole array simultaneously avoided simulations suffering from any confounding effect of pattern noise, as the same features were always present at all times in the field of view of the (assumed) circular EMD array.

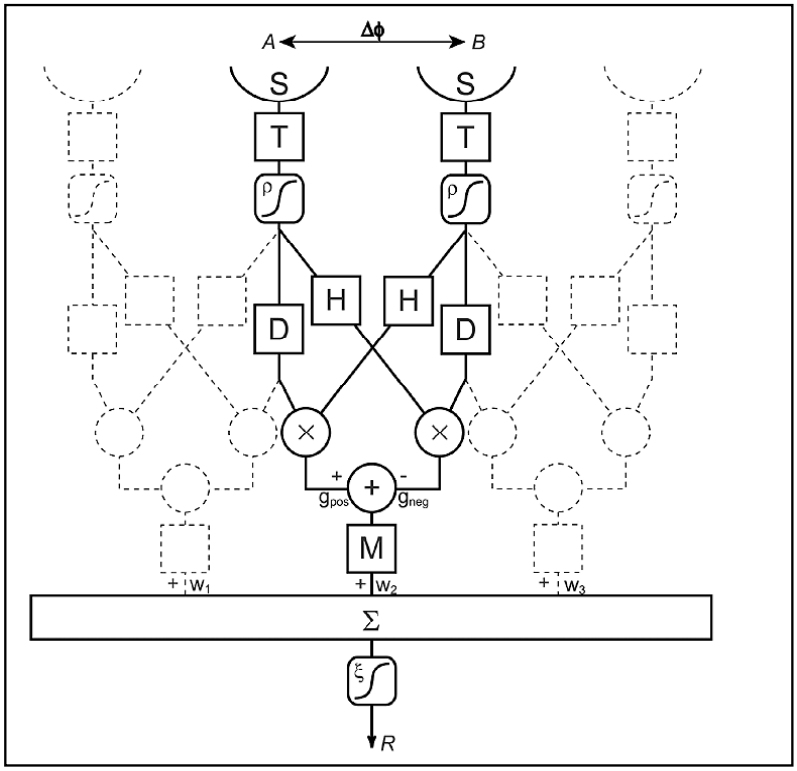

Figure 30: Block diagram for an elaborated 1-dimensional EMD array model

Following 'sampling' of the animated pattern, the delayed (D in fig 30) and undelayed EMD arms were implemented by low-pass filters applied inside a FOR loop in Matlab for each modeled time step. Although the limitations of our digital simulation required discrete time sampling, we used a high sample rate (500 samples per second minimum) compared with any of the time constants of the simulated elements, to approximate a continuous time series. The for loop allowed for local EMD outputs to be fed-back to control the input gain (see fig 29). Local outputs were multiplied and subtracted to produce the opponent EMD output. In the initial adaptive model, outputs were then rectified and fed back to control the input gain. At each time step, the output of opponent EMDs was then taken as the overall system output, either independently or after summation across all 240 EMDs in the row.

Figure 31 below shows the output of 100 EMDs in this model for several different image speeds, and both with (red) and without the adaptive feedback turned on in the model. The trace shows the typical 'pattern noise' of a Reichardt based EMD system, despite the large number of local units averaged – large fluctuations in output, but the basic velocity tuning is also evident, with a response maximum seen at ca. 200 degrees/second.

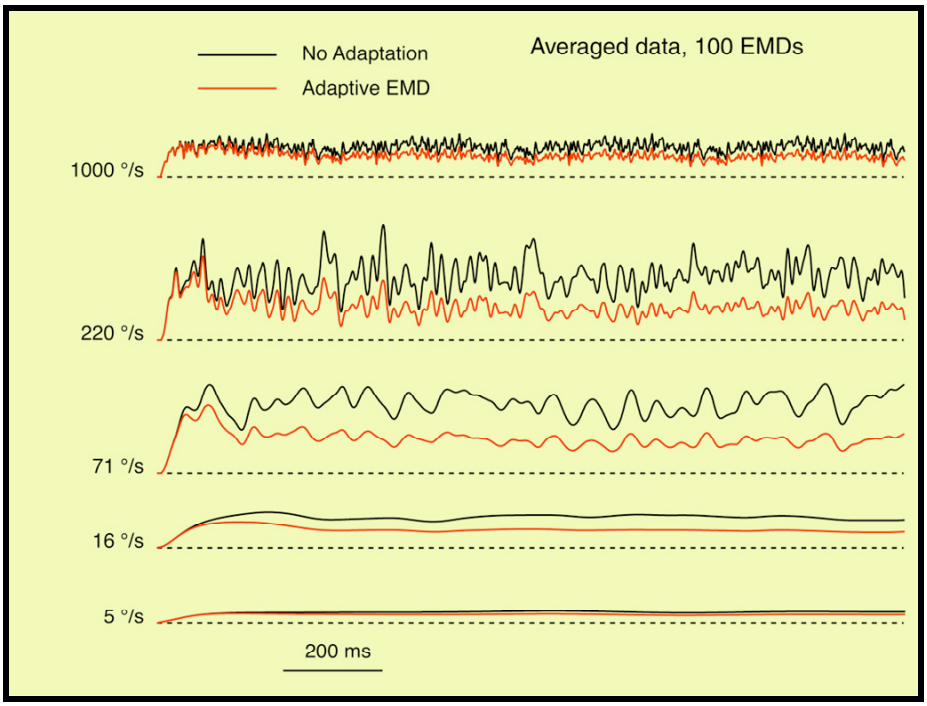

Figure 31: Output of the basic 1-dimensional adaptive feedback model, averaged across 100 EMDs

2.2.1.2 2-dimensional elaboration of the adaptive feedback model

We subsequently developed a 2-dimensional EMD model into a large retinotopic array of elaborated EMDs. Using an inter-receptor spacing of 1.5 degrees as before (an average value for fly optics), we were able to simulate a retinotopic EMD array 240 wide by 36 high. The vertical number was limited by the angular extent of our panoramic images which are limited to 57 degrees by the field of view of the original camera used to capture them. A major advantage of the approach adopted is that the input data are assumed to be panoramic images, oriented across the equator of the yaw plane, so that the array views 360 degrees of space horizontally (and 54 degrees or the overall 57 degrees of the images vertically). This 'receptive field' is similar to that achieved by the combined receptive fields of the two HSE neurons in the (left and right) lobula plate of the fly. By averaging EMD outputs across the full 360-degree horizon, pattern noise (due to local differences in luminance of form) such as that evident in figure 31 was virtually eliminated in the output, greatly facilitating the use of the model to measure 'tuning' characteristics of the system (e.g. velocity tuning) for comparison with that of the biological system.

One improvement on the 1-d modeling approach was a method developed for handling of the original image data. Computation time in execution of the earlier model trades off against the resolution with which simulations are run, in both space and time. Because the simulations are discrete in both domains, while the biological system is discrete only in the space domain, some effort was put into determining the detrimental effects of using low sample rates, combined with appropriate anti-aliasing techniques to improve efficiency. Although we had acquired a large set of panoramic images for the biological experiments at very high spatial resolution our initial models required the use of downscaled images (to 1024 pixels or less) to simulate responses in an acceptable time frame. To achieve acceptable efficiency, we found it necessary to use a variable sample rate depending on the velocity of the pattern, even after optimized compilation of key limiting stages. While this worked, and allowed us to verify the

effectiveness of the contrast-adaptation algorithm to a limited degree, it limited simulations to a single constant velocity stimulus. In order to simulate the experiments carried out on the biological system, and in particular the "monotonic" series of experiments for testing motion adaptation and velocity constancy (where the neuron is tested with short bursts of 'test' motion at variable speed against a background of an adapting speed – see figure 1), we required an approach that utilizes a constant temporal sample rate.

The approach developed permits the use of the original image at its full resolution, avoiding any statistical artifacts introduced by interpolation. By using the very high spatial sample rate of this image, we were able to generate a realistic simulation of even very slow motion (such as during hovering) at a constant (and acceptably high) temporal sample rate, without the time-consuming interpolation methods required in the earlier model. This latter point was was important because the neurobiological experiments harnessed the real-time interpolation power of the Open GL graphics card, and thus was able to provide responses to very low stimulus speeds. The general organization of this revised model is as follows:

1. Spatial Prefiltering: The panoramic image is spatially pre-filtered by 2-dimensional convolution with Gaussian kernels to mimic insect optics (low pass) and lateral spatial interactions (lateral inhibition, high-pass) by lamina monopolar cells (LMCs). These filters are applied sequentially to the green channel of the original RGB image in integer form, with unity gain, outside Matlab, using a difference of Gaussian filter applied in Adobe Photoshop. In practise, the DOG filter is not applied in one pass, but rather we construct two Gaussian filtered versions of the image, 1 with 2 degree half-width and one at 6 degrees. This gives the Matlab model flexibility to use either low pass or band pass spatial filters by applying the difference operation, as desired.
2. The two integer (1 byte per pixel) images are then loaded into Matlab. An EMD 'framework' is set up for sub-sampling the image in two dimensions, onto a retinotopic array based on the ommatidial separation of the fly eye. At present the array is rectangular to aid further development of the model without the complexity of a hexagonal lattice as present in the fly, but elaboration into a hexagonal mosaic at a later stage should be straightforward, since this can be modeled as a pari of interleaved rectangular mosaics (with one offset vertically by half an 'ommatadium'..
3. Based on the retinotopic framework, the inputs to a single row of ommatidia in time are generated from a single row of the image, converted to floating-point and then animated in space-time according to a pre-defined vector of velocities, as in the 1-d model.
4. The space-time matrix is then temporally filtered using a 2-dimensional convolution with a separable kernel. The kernel is based on a difference of log-normal functions, to simulate the impulse response of a fly lamina monopolar cell (LMC).
5. A copy of the temporally filtered matrix is then convolved a second time with a kernel to implement the delay filter.
6. The two matrices are then multiplied after column-wise offset by a single subscript value and the same operation is carried out in mirror image.

7. The two products are then subtracted to produce the opponent outputs for all 240 EMDs. This matrix is then added to a 3 dimensional 'stack' matrix.
8. Additional image rows are processed in sequence until the 3 dimensional matrix is full.
9. Slices across the resultant output matrix can be considered slices at single instants in time for the output of all EMDs in the 36 x 240 EMD array.

In a simulation whose results are detailed below, the panorama was rotated in the yaw axis at a temporal sample rate of 500Hz for 8 seconds. During this period, the pattern was is incremented logarithmically in 200 ms bursts, interspersed with bursts of an adapting speed. The entire simulation took approximately 4 minutes to generate using a 900Mhz CPU running Matlab.

Figure 2 below shows the mean output of this simulation, averaged for all EMDs in the 240x36 array, and demonstrates how spatial summation across the panorama reveals the underlying response with superb rejection of pattern noise. During the early part of the response period, responses during the adapting 'bursts' are stronger than during the (low speed) test patterns, but as speed of the test bursts increases, the response rises to a maximum (around 2500 ms, corresponding to a burst speed of ca. 300 degrees/s). This trace already mimics many of the features of the neurobiological recordings in monotonic experiments (e.g. figure 1), including prominent response 'transients' at the change of speed between adapting and test bursts of motion.

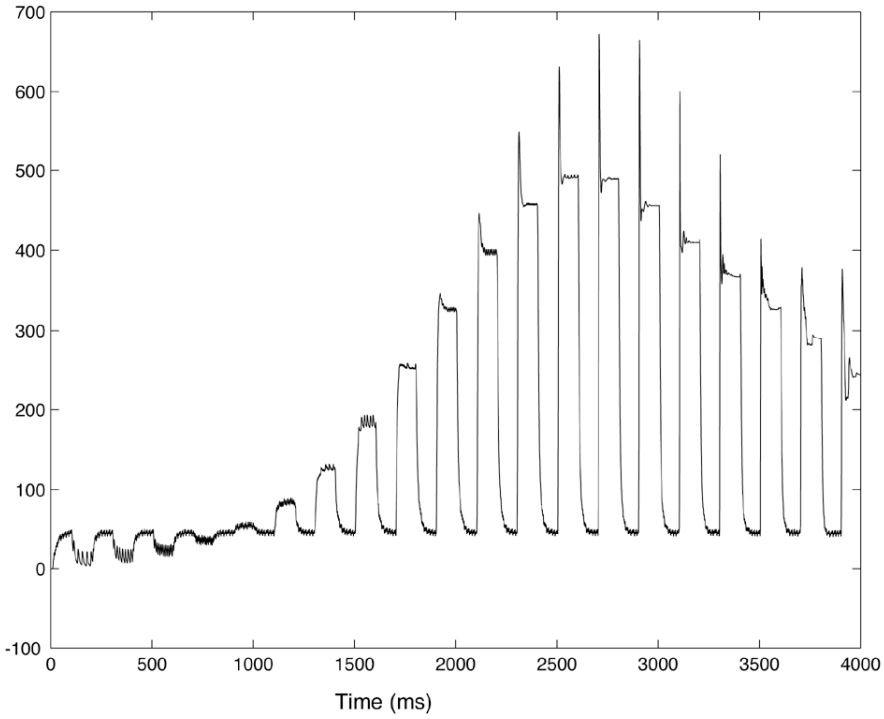

Figure 32: Spatially averaged EMD responses to interleaved 'monotonic' protocol for panoramic image motion, as used in the neurobiological experiments.

We initially setup this model using no adaptive feedback, but then refined the neurobiological model as reported during the last period to include the adaptive feedback behavior. Two time-slices from the output matrix of a simulation of the adaptive model are shown in figure 33 below, taken from a matrix movie showing the evolving output of the 2 dimensional EMD array over time. The movie itself is embedded into figure 34 (requires the QuickTime engine to run - a separate copy of the movie is included in the accompanying CD). The simulation was for 36 x 240 EMDs, subtending the full 360 degree panoramic 'scene' in the horizontal dimension, and corresponding approximately to the field of view of the two equatorial HS neurons (HSE) of the fly motion pathway.

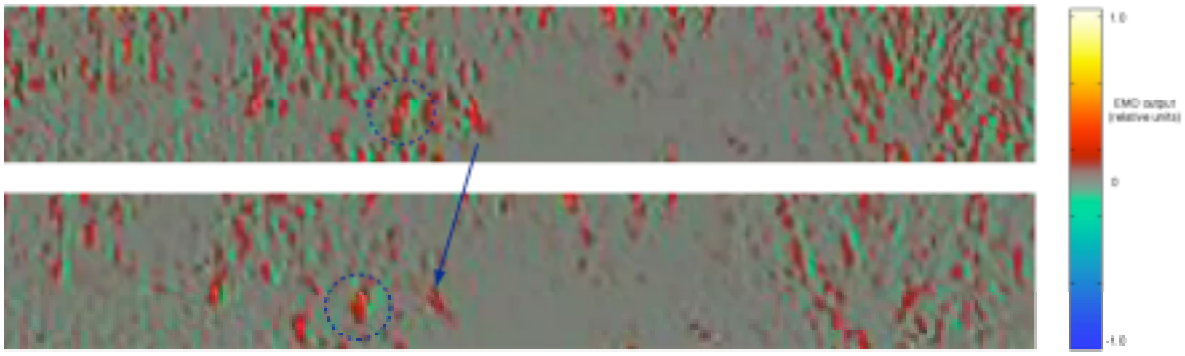

Figure 33: Adaptive EMD responses to moving natural imagery.

The first frame shows the EMD array response 100ms after a transition in speed from motion at an adapting speed (in this case a low adapting speed of 5 degrees per second was selected) to a higher test speed (150 degrees/s). The low speed of the adapting pattern produces little response of EMDs and thus little motion adaptation, so that local EMD gain is in the default 'high' state, as observed in the fly under similar coniditions. By the time of this 1st 'snapshot', local EMDs are responding strongly to the onset of the faster pattern. By the time of the second frame (100 ms later still) local motion adaptation has selectively reduced the gain of local EMDs that previously viewed high contrast features. The overall gain reduction is apparent from the general decrease in EMD activity. One interesting observation here is that high contrast features, which produce the largest response (and greatest local adaptation) are not randomly distributed within the scene, but tend to be clustered.

Figure 34: Animation showing adaptive EMD model responses to moving natural imagery (as in fig 33). Double click to play (requires Apple Quicktime engine).

Thus for optic flow of the kind simulated (in this case 'rigid' yaw) any EMD which is initially stimulated strongly (and thus adapts) may have a significant effect on the subsequent response, since additional high-contrast features are likely to pass across its field of view while it remains adapted. One such case is illustrated in figure 33, where a high-contrast local feature (circled) is 'followed' by two others. Initially, this leads to 3 distinct 'patches' of local excitation (hot colors), but following adaptation, the rightmost pair of these features (arrow)

produce only weak excitation, since they pass across the adapted EMD initially excited by the left-most patch. This illustrates the fact that the effect of adaptation on the global response of a collator neuron, such as an HS cell, depends on a complex (and non-linear) interaction between local adaptive properties and the particular statistical distribution of contrasting features in the image.

It is difficult to make empirical predictions about how such a complex set of interactions will behave in the presence of more complex optical flow sequences, such as might be experienced during complex behavior. For this reason, we also commenced, during this period, construction of an even more elaborated and generalized class of EMD models, in which we would be able to supply arbitrary sequences of discrete-time sampled data to test responses to more complex optic flow (e.g. combinations of translation and rotational motion). During this period, we constructed the 'front end' to permitting modeling of the spatial imaging properties of the EMD array given an arbitrary 'movie' as the data source. We tested this with optic flow sequences generated by flight simulator software running on a modern accelerated PC graphics card. One problem with such simulations is that the limited frame rate at which such data can be rendered limits the temporal sample rate for simulations based on their output in real time. 'Flying' in slow motion and then scaling the simulation to higher speeds would enable us to simulate effective frame rates up to 1000Hz, sufficient to approximate a continuous-time system with time constants of the order of those seen in the biological system. However, this approach would be limited to simulation of relatively fast moving scenes. This was regarded as sufficient for testing model EMD array responses in a variety of interesting scenarios, but we planned to eventually move to more explicit rendering of 3-D motion stimuli in order to simulate the full range of image speeds to which neurons are able to respond

2.2.2 Year 2

2.2.2.1 Elaboration of EMD output stages

With the neurobiological experiments suggesting a degree of 'velocity constancy', attention in modeling turned to quantifying the behavior of the adaptive model in the context of different images from the set in figure 3. Discussion with our collaborators over the concurrent SBIR effort considered two alternative models, one based on feedforward contrast gain and one using feedback (as modeled above), and the features known to be present in motion adapted neurons from our experiments. We concluded that a model based on a feed-forward contrast normalization algorithm may not be able to explain the observation that gain reduction during brief 'bursts' of motion at a variety of speeds appears greatest at those speeds where HS neurons generate maximal responses. On the other hand, it was not clear how an alternative mechanism, such as the feedback mechanism described above which is based on direct control of gain by a signal fed back from EMD outputs, could produce velocity constancy over any but a limited range of speeds. The issue is confounded by the observation that the biological system shows two distinct components to motion adaptation, one of which being a gain reduction and the other (the so-called 'waterfall effect') the addition of an apparent DC offset. The latter is only recruited by motion in the optimum direction, whereas gain reduction is recruited by motion in any direction. At this point, our biological experiments suggested velocity constancy but had all been carried out with preferred-direction stimuli. We concluded that further neurobiological experiments to repeat such stimulus trains in the anti-preferred direction would be an excellent way to tease these components apart.

Prior to completion of such experiments, the 'correct' model approach was undecided, with both feed-forward and feedback models having both desirable and undesirable features. We

agreed that the feedforward model would be explored in detail in the concurrent SBIR project, while we would explore further elaborations of the feedback model in this project..

A set of simulations was therefore performed with a large adaptive EMD array operating on natural image data, which suggest that a gain control scheme based on feedback of EMD outputs can result in at least some degree of velocity constancy. In addition to feedback, this model featured biologically plausible prefiltering, and limiting or squashing nonlinearities applied at several stages in the processing chain, including a *tanh* compression of the individual EMD outputs, and a mild compressive nonlinearity to the summed EMD outputs, which represents nonlinear 'HS cell' processing. This was similar to the compression used by us in earlier modeling efforts (Dror et al 2000). In the feedback adaptation, each EMD output was rectified, lowpass filtered, and passed through a decreasing nonlinear function that starts at unity for small arguments, and decreases toward zero for larger ones. Specific functions used included 0.5*(1–tanh[k(x-m)]) and SQRT(1-bx), where x is the argument and k, m, and b are constants. (In practice, values for b were chosen so that negative for values of the argument of the square root did not occur.) The output of this function then multiplied the inputs to the EMD to effect the adaptive gain reduction.

Simulations based on this model followed the 'test-adapt-test' protocol used experimentally. Some example outputs are shown below in figure 35. The output variable is the (compressed) sum of all EMD outputs in the array, and the tuning curves are generated based upon the output values during 'test phases' at various image velocities.

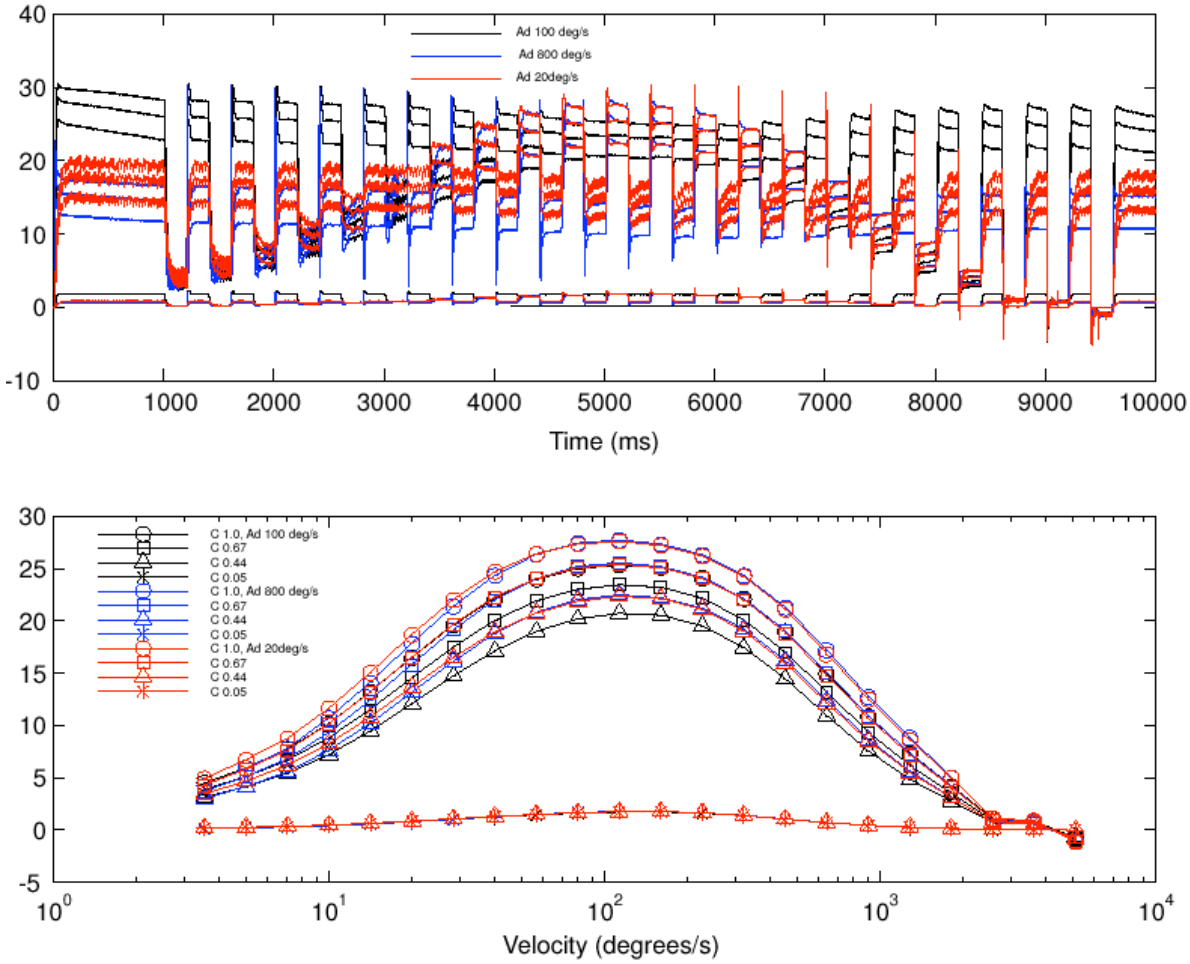

Figure 35: Results of a simulation of an EMD array with adaptive feedback, subject to the test-adapt-test protocol used to determine HS cell velocity tuning. The output is a (compressed) sum of the individual EMDs in the array. Nonlinear feedback uses the squareroot-based function described in the text. Top is the time domain response, and bottom the velocity tuning. Various contrasts and adapting speeds are indicated in the legends.

The model shows firstly that it is possible to obtain a reasonable fit to the observed velocity tuning of HS neurons simply by choosing parameters for key filter stages measured directly in the fly visual system. Secondly, it shows that it is possible to explain some deviation from the predictions of the classical Reichardt model for variable contrast using a feedback gain control. However, when tested at very low contrasts, the model displays the expected contrast dependence (quadratic) resulting from the multiplication mechanism.

These simulations suggested that a gain control scheme based on feedback of EMD outputs can result in at least some degree of velocity constancy. We found the model behavior to be strongly affected by the image-prefiltering applied. We began exploring possible alternatives to replacing simple logarithmic compression at the 'photoreceptor' level (which provides a poor model for the behavior of real photoreceptors at very high luminances, or of the Delbrück and Mead -type adaptive photocircuit that our hardware efforts utilize) with more biologically plausible non-linear compression.

2.2.2.2 Elaborations of delay filter element

The 'baseline' EMD model used at this point incorporated a relatively simple first-order low-pass filter as the delay element. However, additional work around this time (O'Carroll in

conjunction with former PhD student Rob Harris) suggested that a simple delay model might be inadequate to explain the shape of observed HS neuron temporal frequency tuning curves. In a related project (Navy funded, N00014-02-M-0247) we explored the use of higher-order delay filters based on a log-normal model, and found that these explain several features of the temporal tuning observed in nocturnal moth motion detectors. During a visit by former Ph.D. student Rob Harris to the O'Carroll laboratory, we considered similar delay filters for fly motion detectors. Our new models show excellent fits of such filters to fly temporal tuning, so this type of delay mechanism may be widespread within insects. Temporal tuning so derived is characterized by rapid roll-off at high frequencies, suggestive of a relatively high filter order, and very broad temporal tuning. We have found that in modeling Calliphorid fly HS responses, a complex delay filter consisting of two such delay elements in parallel provides a better fit than a single delay model.

In subsequent modeling, we tried to produce implementable forms of this lognormal delay mechanism. Using Prony's method, we fitted arbitrary infinite impulse response filters to the 'ideal' lognormal impulse response, and found that we were able to mimic its characteristic time-course by filters of 6th order. We planned further analysis of these filters with a view to deriving a transfer function with discrete poles that would be useful for biomimetic implementation.

2.2.2.3 Modeling receptive field shape to reduce pattern noise effects

We further quantified the effects of receptive field shape on pattern noise, measured as 'relative error' (see Dror, O'Carroll & Laughlin 2001, J. Opt.Soc.Am.A 18:241-252). We defined this error as the residual variance over time in the response due to the local structure of the image, divided by the mean (DC level) of that response. The assumption here is that the DC level of the summed outputs of an EMD array represents the desired velocity signal, while time-variation due to the pattern structure is effectively noise, so that relative error is a measure of signal-to-noise ratio in the context of the task of velocity coding.

Our hypothesis was that the semi-circular (fully circular if summation at the steering muscles is taken into account), strip-like nature of the HS cell receptive field plays a functional role in encoding velocity. Because the circular array of EMDs is parallel to the preferred direction of motion, a purely circular optical flow pattern (i.e. yaw for an HS neuron) would produce the same temporal sequence of stimulation of individual photoreceptors. Hence if a high contrast feature were present within the receptive field at one point in time, it would also be very likely to be present at future times. By summing across such an array, pattern noise would be largely reduced.

To test this hypothesis, we ran simulations of the 2-d model, with an array size of 240 by 37 EMDs, each with an inter-receptor angle of 1.5 degrees, and subtending a total of 360 degrees of visual angle. We ‘stimulated’ the array with a panoramic yaw stimulus with a fixed velocity, for 2 seconds. We ran the simulation for 4 different panoramic images and 12 different speeds for each. We then sampled the matrix of EMD outputs in one of 4 ways. The first (labeled ‘total’ in the figures below) is the sum (across the time dimension) of all EMDs. The second used a circular linear array with just 240 EMDs, representing one of the 37 possible rows of EMDs, selected at random. The third was a randomly selected rectangular grid of 15x16 EMDs (i.e. 240 total). The 4th consisted of 240 EMDs selected randomly from the 240x37 array. In each of these subsampled EMD sets, we repeated our estimate 20 times, using a different

random number seed in each case. Relative error (as defined above) was then estimated for the linear sum of the EMDs in each sample and averaged across the 20 trials.

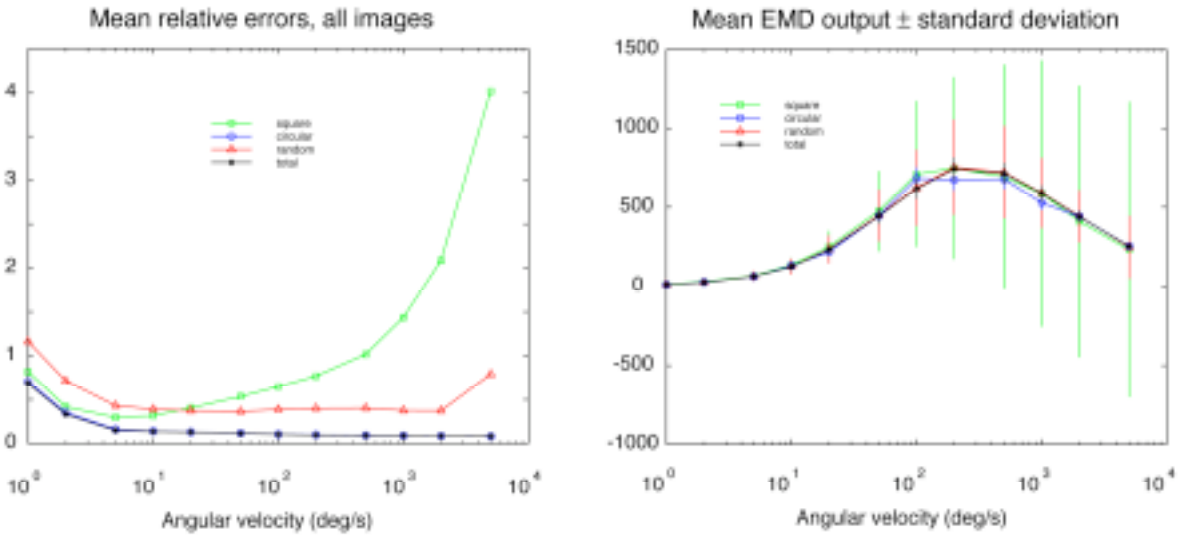

Figure 36 Relative errors (left) and average outputs (right) of several array topologies as defined in the text. Modeling By O'Carroll and Sreeja Rajesh (PhD student, O'Carroll lab)

As can be seen, the circular linear array achieved a very similar variance in velocity estimation to that of the 'full' EMD set, and (depending on speed) 10 or more times lower than the other two strategies for sampling EMDs. We concluded that a circular, linear detector array may be the ideal and most efficient way to sample outputs from EMDs of the correlator type, at least with respect to reduction of pattern noise in rotational motion. This suggested that a small detector array with as few as 240 pixels could provide robust estimates of speed under natural image conditions.

2.2.2.4 Elaboration of input compressive nonlinearity

Further modification was made to the 2-d model to add elaborations to the scaling of luminance in the model inputs. Our previous modeling efforts made the assumption that biological photoreceptors encode luminance logarithmically. Our elaborated EMD model showed (desirable) reduced sensitivity to image contrast when we placed saturation at any of several locations in the EMD. Since strict logarithmic encoding is non-saturating (and biologically unrealistic), we thus began working with implementation of the Naka-Rushton (or Lipetz) equation:

$$R = I^n / (X^n + I^n),$$

where I is the raw luminance value, X is the intensity giving 50% response (midpoint for the dynamic range) and n is the slope of the 'linear' region. Values for n were selected to give a logarithmic intensity code over two base-10 log units of intensity. This curve provides a sigmoidal (on log intensity scale) relationship between input and output that closely fits the observed V/Log(I) curves of biological photoreceptors. Incidentally, the same equation gives an excellent fit to the V/Log(I) function for adaptive photocircuits of the Delbrück and Mead type, as implemented in our silicon models.

2.2.2.5 Modeling the waterfall effect

Thus far, no attempt had been made to 'fit' the amount of adaptive behavior in the model to any of the observed biological data. Modeling efforts thus turned to using the HS data obtained in our earlier work (Harris, O'Carroll, Laughlin, 2000, Contrast gain reduction in fly motion adaptation, *Neuron* 28: 595-606). The experiment in that paper consisted of the test-adapt-test protocol. This was implemented in a model as a variable contrast test pattern presented for 1 second before and after a 4 second adapting stimulus. The adapting pattern had maximal contrast, high temporal frequency (20Hz) and low spatial frequency (0.02 cycles/degree). Although a 'non-optimal' stimulus for the HS cell, this stimulus produces powerful motion adaptation and is fast enough that it avoids confounding 'afterimage' effects. We used this as a standard adapting stimulus during all of our earlier experiments.

The responses were evaluated during a 100ms 'window' 25ms after the commencement of the test stimulus, and then plotted against the contrast of the test pattern.

In four 'virtual experiments' designed to mimic the experiments in the previous neurobiological study, we varied the test and adapting patterns in all four possible combinations of preferred and antipreferred directions. The direction selectivity of the motion aftereffect (waterfall effect) was very evident in the neurobiological data as a downward (negative) shift in the control response (lowest contrast) for post-adaptation responses. Note that this was only observed when the adapting stimulus was moving in the preferred direction (as seen in the top left and bottom right panels in Figure 37 below). In all four cases there was a pronounced contrast gain reduction, evident as a rightward shift in the entire contrast response function (increased contrast threshold). Other experiments (not shown) demonstrated that this effect is motion dependent.

We modeled this system as circular array of 240 EMDs, viewing a sinusoidal pattern that subtends 360 degrees and was assumed to be panoramic, i.e., the pattern contained an integer number of stimulus cycles, matched to that used in the experiments. Each EMD within the array was elaborated (as described in previous reports) by inclusion of biologically inspired elements. The image was low-pass filtered by a Gaussian kernel of 2-degree half-width, then animated to mimic the exact sequence of stimuli in the HS experiments. The model included a saturating logarithmic 'photoreceptor' stage, modeled using the Lipetz (or Naka-Rushden) equation. The slope n in the log-linear region was set to give a dynamic range (logarithmic region) spanning 2 log units of intensity, as observed in recordings from typical diurnal apposition eyes such as that in the fly.

In the case of the sinusoidal images used in these simulations, the images were scaled to range from 0-255, with a mean of 128, in order to match the range of luminance values in typical 8-bit images. This allowed the same model to be applied to any other arbitrary image, including the panoramic natural scenes used in other concurrent experiments. After transformation through the Naka-Rushden curve, the image is rescaled to a range from 0-1.

The animated image was temporally band-pass filtered by a linear kernel based on the double log-normal equation fitted to Eristalis lamina monopolar cell (LMC) responses. EMDs were then constructed using multiplication of the pre-filtered data with a delayed version (first-order low-pass, time constant=35 ms). The multiplication on each EMD subunit included a saturation mechanism (based on a simple *tanh* transformation of the output). Each EMD incorporated two adaptive mechanisms. The first was a feedback gain control, as described earlier. The second was a direction-selective offset, applied as a linear function of depolarizing EMD outputs. In this version of the model, this was applied locally to each EMD, based on the

half-wave rectified EMD output, after low-pass filtering (1st order, 0.2Hz corner frequency). An alternative form, where this offset is applied to the low-pass filtered sum of all EMDs in the array (a 'global' mechanism) would be equally plausible for the biological system and could not be excluded based on any experimental results obtained to this point. These two alternatives would have similar quantitative effects.

After subtraction of the two mirror symmetrical subunits in each EMD, local EMDs were then summed using a non-linear spatial summation mechanism, here modeled as a simple saturation in the summation mechanism.

Simulations were run for the same set of test contrasts as used in HS recordings. The gain of the feedforward stages was set to match the contrast threshold (contrast required to evoke a 50% maximal response) in the unadapted response to stimuli moving in the preferred direction (i.e. the data illustrated by square symbols in the top left panel of the figure). The gain of the feedback loop that acts to reduce contrast sensitivity following motion adaptation was then adjusted to match the right-shift in contrast/response functions following preferred direction adaptation. An additional adjustment was made to match the observed DC offset (the motion aftereffect). Note that apart from adjustment of these two parameters, no explicit attempt was made to fit the dynamic range of the contrast sensitivity curves: The observed excellent fit in both cases was due entirely to the quadratic nature of the essential non-linearity of the local motion detectors (i.e. the multiplication stage), the dynamic range of the underlying photoreceptors (modeled closely on that observed in real recordings from insect photoreceptors), and the various saturation stages built into the model, each of which was based on published or measured values from the physiological data.

The same model was then applied to the other three experimental conditions. This model provided a surprisingly good fit to several interesting phenomena in the physiological data. Firstly, the model nicely captured the response range compression and slope reduction noted in null-direction test following preferred direction adaptation (bottom right in Figure 1), where the DC offset (motion aftereffect) in effect adds to the response to test stimuli. It failed, however, to produce pronounced response range compression in other situations, suggesting that contrast gain reduction may be weaker in the biological system than in this 'best fit' model. It is likely that this deficiency could be addressed by a more 'biomimetic' implementation of the non-linear saturation mechanism in the spatial summation stage, to better match the biophysical properties of the HS dendritic tree. This may actually be simpler in a hardware implementation of this model than in the present (Matlab-based) simulation.

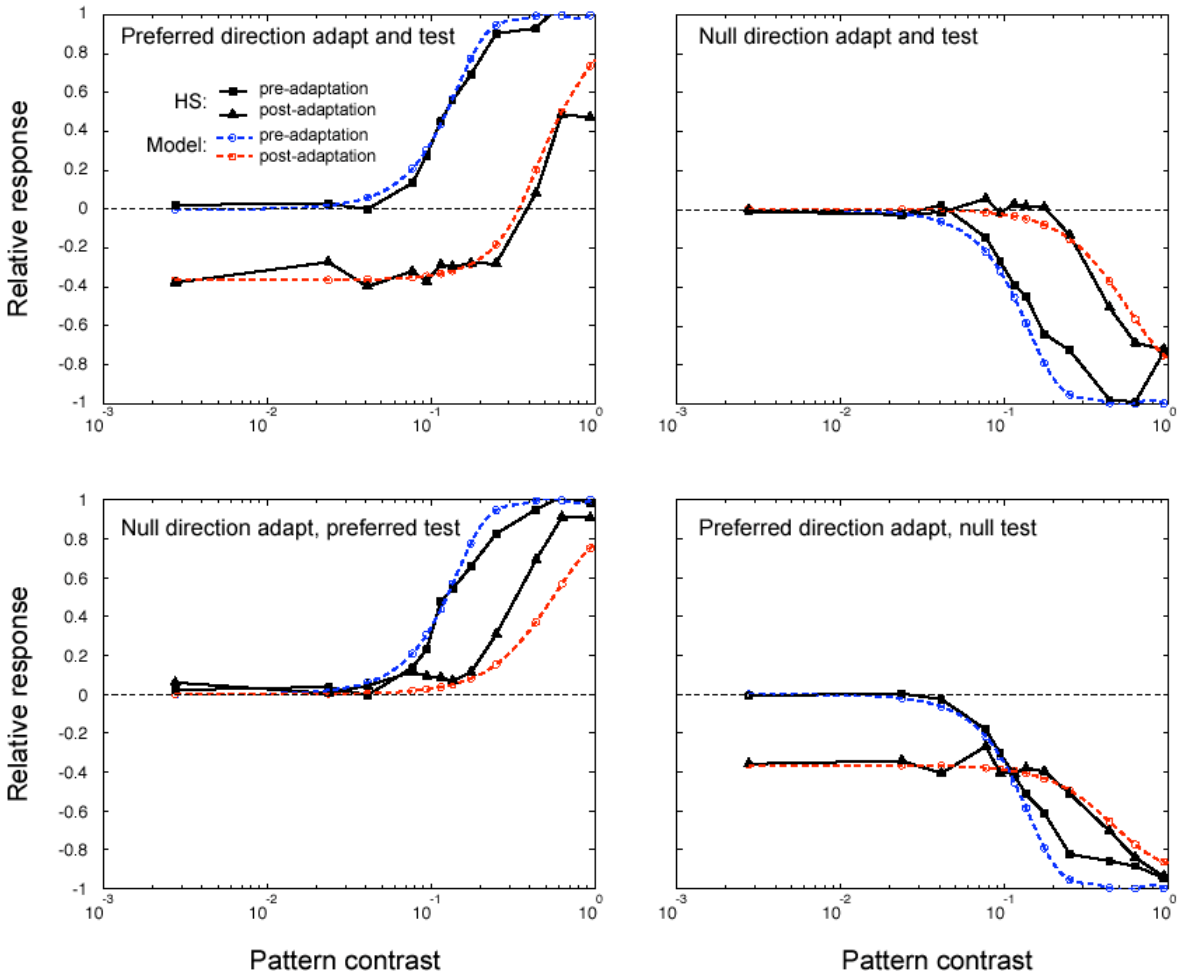

Figure 37: Experimental and modeled contrast sensitivity curves for combinations of preferred- and antipreferred (null)-direction adapting and test stimuli. Both actual and modeled results are depicted.

2.2.3 Year 3

2.2.3.1 Analysis of Results to Date

At this point in the effort, we collated and examined the modeled tangential cell responses in work to this point. While many experimentally observed characteristics had been reporduced, none of the biologically plausible models had achieved the degree of velocity constancy seen in the biological neuron with natural imagery. While a high degree of velocity constancy could be obtained with very high gain and saturating nonlinearity at the inputs to the multiplication stages of the EMD, such models would be expected to perform poorly in the real world, since they would be susceptible to noise about the threshold value, which must, by definition, lie close to the mean luminance in a given image. Velocity constancy was only achieved by saturating at contrasts below those observed in the natural scenes that we had sampled to date; with these parameters, saturation in response to spatially narrow-band scenes (i.e. sinusoidal gratings) was also observed at contrasts much lower than those at which

complete saturation is observed in the biological system. Furthermore, the saturating model failed to display one of the most striking observations of the biological data: reducing the contrast of the natural image by re-scaling its luminance distribution produces a reduction in response to any one image (whereas the highly saturating model would not) and yet the neurons still display robust velocity constancy with respect to different images.

Simulations were run in which both components of adaptation – post-stimulus changes in membrane potential (the 'waterfall effect') and contrast gain reduction – were incorporated in a feedback adaptive model. This elaboration was observed to result in velocity constancy for natural imagery in preferred-direction motion. However, due to symmetry of the gain-reduction part of the model and the fact that the waterfall effect is not observed in antipreferred direction motion, we did not expect velocity constancy to hold for antipreferred direction stimuli (as it does in the biological neuron).

Further elaborations of the model were deferred to our concurrent SBIR effort, while the remainder of this project focused on in-depth analysis of possible physiological drivers for adaptation. Again, the primary conclusion drawn from the results of this study was that, while all of the test features reduced interscene scatter of 'tangential cell' outputs relative to the most basic version of the model, in no case did the model approach velocity constancy as closely as does the biological system. Combining our efforts from both AOARD and SBIR projects, we submitted a summary of our model outputs as a paper which was subsequently accepted for publication by the journal Biological Cybernetics. The key findings are illustrated below in figure 38.

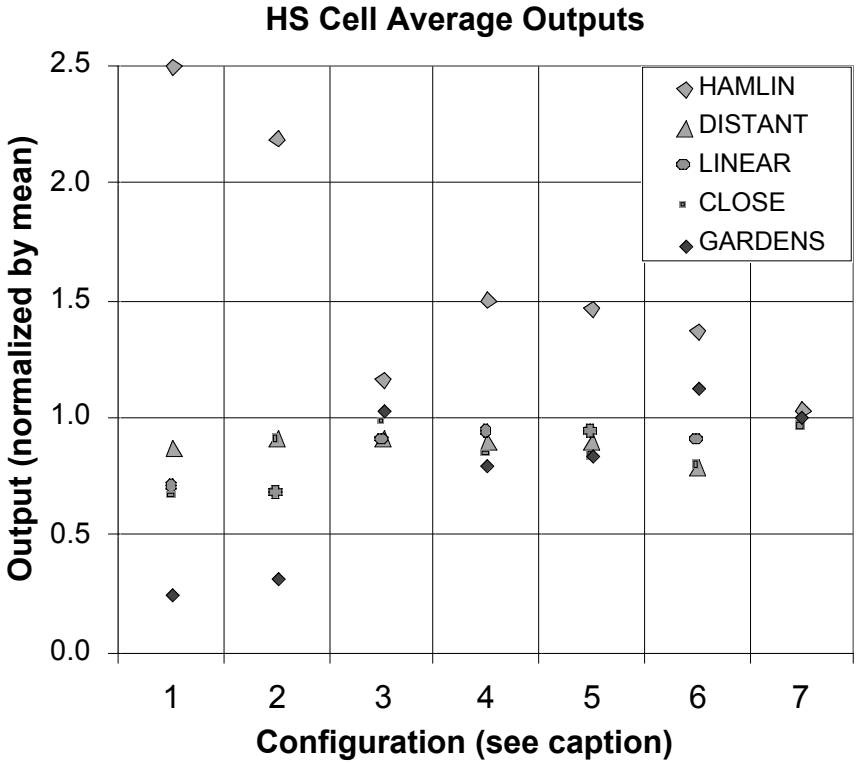

Figur 38: Scatter of responses between different animated scenes of the model in various configurations, at the near-optimal speed of 50º/s. In each column of the graph are displayed responses to a set of five different images for a particular model configuration, normalized by the mean over all five. Configurations include each of the test features individually: 1. basic model; 2. with spatial highpass filtering; 3. with motion adaptation (gain control) with time constant τ_A = 200ms; 4. with saturation of early vision signals; 5. with saturation of EMD correlator outputs; 6. with Borst 'gain control' in the HS cell. Column 7 shows mean responses of biological HS cells in the hoverfly *Eristalis tenax* to yaw stimuli with the three of the images, at a speed of 100º/s.

Also shown in Figur are three data obtained from biological HSNE cells in the hoverfly *Eristalis tenax*, for the images *hamlin*, *close*, and *gardens* in simulated yaw rotation at 100º/s. Experimental preparation was as described in Harris *et al.* (2000). Results are averaged over the time period 0.25s to 0.4s following onset of motion at 100º/s (preceded by motion stimuli at slightly different speeds), over four stimulus presentations at four phases varying by 90°, and over five neurons.

Of the nonlinear test features, the simple gain-control-based motion adaptation model provided the greatest reduction in interscene scatter relative to the baseline model. Spatial highpass filtering significantly improved the performance of the model in combination with one or more of the nonlinear features, although it resulted in little reduction in scatter by itself. This we suggested is due to reduction of the amplitude of low spatial frequency components of natural imagery, which tend to have large interscene variance. Finally, we found that combining multiple nonlinear features did not generally improve performance.

2.3 Milestones and Metrics

2.3.1 Publications

(* asterisks denote work partially or fully funded by this AOARD project_

2.3.1.1 Refereed Papers

*Shoemaker, P.A., O'Carroll, D.C. and Straw, A. (2005) Velocity constancy and models for wide-field motion detection in insects. ***Biological Cybernetics***, (in press: http://dx.doi.org/10.1007/s00422-005-0007-y).

*Mah, E.L., Brinkworth R. and O'Carroll, D.C. (2005) Bio-inspired analog circuitry model of insect photoreceptor cells. ***Proc. SPIE*** 5839 (in press).

*Rajesh, S., Straw, A., O'Carroll, D.C. and Abbott, D. (2005) Effect of spatial sampling on pattern noise in insect-based motion detection. ***Proc. SPIE*** 5649, p. 811-825

*Rajesh, S., Straw, A., O'Carroll, D.C. and Abbott, D. (2005) Effects of compressive nonlinearity on insect-based motion detection. ***Proc. SPIE*** Vol. 5649, p. 798-810

*Rajesh, S., Straw, A., Rainsford, T. and O'Carroll, D.C., (2005) Modeling pattern noise in responses of fly motion detectors to naturalistic scenes. ***Proc. SPIE*** Vol. 5651, p. 160-173

Mah, E.L. and O'Carroll, D.C. (2005) Implementation of an adaptive photodetector circuit inspired by insect visual systems. ***Proc. SPIE*** Vol. 5649, p. 839-848

*Rajesh, S., O'Carroll, D.C. and Abbott, D. (2004) Effects of nonlinear elaborations on the performance of a Reichardt correlator. ***Proc. SPIE*** Vol. 5275, p. 287-303

*Rajesh, S., O'Carroll, D.C. and Abbott, D. (2003) Velocity estimation and comparison of two insect-vision-based motion-detection models. ***Proc. SPIE*** Vol. 5062, p. 401-412

*Rajesh, S., O'Carroll, D.C. and Abbott, D. (2002) Elaborated Reichardt correlators for velocity estimation tasks. ***Proc. SPIE*** Vol. 4937, p. 241-253

2.3.1.2 Conference Presentations and Posters

2005

*Moyer de Miguel, I, Nordström, K, O'Carroll, D C. "Local motion adaptation in insect visual systems." Society for Experimental Biology Annual Main Meeting, Barcelona, Spain. 2005 (pending)

Nordström, K and O'Carroll, D C. "Asymmetric receptive fields of target neurons in the dragonfly lobula." Society for Experimental Biology Annual Main Meeting Barcelona, Spain 2005 (pending)

*Shoemaker, P.A., O'Carroll, D.C. (2005) Insect-based visual motion detection with contrast adaptation. To appear, ***Proc. SPIE*** Vol. 5783, *Defense and Security Symposium, Infrared Technology and Applications Conference* (Orlando, FL, March-April 2005).

2004

*O'Carroll, DC, Shoemaker, PA, Rainsford, T, Straw, AD, Mah, EL and Rajesh, S. Motion detection and velocity coding of natural scenes by the insect visual system. Invited talk, *International Conference on Intelligent Sensors, Sensor Networks and Information Processing (ISSNIP)* (Melbourne, December 2004).

*Shoemaker, P.A. and O'Carroll, D.C. (2004) Silicon and abstract modeling of elementary motion detection. *Workshop on Insect Sensors and Robotics* (Brisbane, August 2004).

*O'Carroll, DC, Shoemaker, PA, Rainsford, T, Straw, AD, Mah, EL and Rajesh, S. Motion detection and velocity coding of natural scenes by the insect visual system. Invited talk, *Workshop on Insect Sensors and Robotics* (Brisbane, August 2004).

*Mah, EL & O'Carroll, DC, Implementation of Biomimetic Models for Adaptive Photoreceptors Based on Insect Neurobiology. Poster, *Workshop on Insect Sensors and Robotics* (Brisbane, August 2004).

*Rainsford, T, & O'Carroll, DC Pattern Noise in Neural Coding of Natural Moving Images. Talk, *Workshop on Insect Sensors and Robotics* (Brisbane, August 2004).

*Dowd, L., Ali, I., Straw, AD & O'Carroll, DC Interfacing VisionEgg-based Stimulus Generators for Testing Responses of Biological and Artificial Vision Systems. Poster, *Workshop on Insect Sensors and Robotics* (Brisbane, August 2004).

Nordström, K. & O'Carroll, DC Detection of small low-contrast targets across cluttered and moving backgrounds. Poster, *Workshop on Insect Sensors and Robotics* (Brisbane, August 2004).

*Rainsford,TJ, Moyer, IM, Browning, M, & O'Carroll, DC. Does the neuroanatomy of visual neurons in hoverfly match visual ecology? (poster) XXII International Congress of Entomology, Brisbane, August 2004

Nordström, K and O'Carroll, D C. "Characterization of small motion detection neurons of Eristalis tenax." XXII International Congress of Entomology, Brisbane, Australia, abstract S12F57 + PS2S1205. Brisbane, August 2004

Nordström, K, Swan, L, Mayrhofer, S and O'Carroll, D C. "Comparisons of the image-step response in flies and humans." XXII International Congress of Entomology, Brisbane, Australia, abstract PS2S1209. Brisbane, August 2004

*O'Carroll DC & Rainsford, TJ What drives adaptive gain control in insect motion detection. Invited talk, XXII International Congress of Entomology, Brisbane, Australia, August 2004

Nordström, K and O'Carroll, D C. "Small target motion detector neurons are present in female hoverflies." The 7th Congress of the International Society for Neuroethology, Nyborg, Denmark, July 2004, abstract PO163

2003

*O'Carroll, D.C., Straw, A.D., & Shoemaker, P.A. Adaptive gain control in insect motion detection. In N. Elsner & H. Zimmermann, Eds., *The Neurosciences – From Basic Research to Therapy: Proceedings of the 29th Göttingen Neurobiology Conference* (Germany), Georg Thieme, Verlag, Stuttgart, pp. 546-547. (2003)

DuBois, RA., O'Carroll, D.C., & Shoemaker, P.A. Spatio-temporal tuning for small targets from a simulated array of elementary motion detectors. In N. Elsner & H. Zimmermann, Eds., *The Neurosciences – From Basic Research to Therapy: Proceedings of the 29th Göttingen Neurobiology Conference* (Germany), Georg Thieme, Verlag, Stuttgart, pp. 547-548. (2003)

*Straw, AD & O'Carroll, D.C. Ghosting and aliasing artifacts in apparent motion displays eliminated with motion blur. In N. Elsner & H. Zimmermann, Eds., *The Neurosciences – From Basic Research to Therapy: Proceedings of the 29th Göttingen Neurobiology Conference* (Germany), Georg Thieme, Verlag, Stuttgart, pp. 601-602. (2003)

*Straw AD, O'Carroll DC Robust velocity estimates by fly motion detectors following motion adaptation . Annual meeting, Association for Research in Vision and Ophthalmology , Fort Lauderdale USA., 2002. Published in: Investigative Ophthalmology & Visual Science 44: 4131 Suppl. 2 May 2003

2002

*Straw AD, O'Carroll DC Adaptation of wide-field movement detecting neurons in hoverflies produces velocity constancy to natural scenes. Annual meeting, Vision Science Society, Sarasota, Florida, 2002. Published in Integrative & Comparative Biology 42 (6): 1320-1320 DEC 2002

*Straw, A.D., O'Carroll, D.C., & Shoemaker, P.A. (2002) Adaptive Motion Detectors Inspired by Insect Vision. *Proceedings of the First World Congress on Biomimetics and Artificial Muscles* (Albuquerque, NM, December 2002).

2.3.2 Students and Post-Doctoral Fellows Supported and Advised

Andrew Straw: Ph.D. student. Supported by a Howard Hughes Medical Institute Pre-doctoral Fellowship, but advisorship supported by SBIR and IRI (AOARD) funds. Worked extensively on the study of velocity constancy in coding of velocity in natural scenes. Developed the VisionEgg software that is now key to current and future experimental work in this area. Received the Ph.D. degree in August 2004; currently a post-doctoral fellow in the Dickinson laboratory at California Institute of Technology.

Roger DuBois: Postdoctoral Research Associate. Dec 2001-2003. Supported by AFOSR funds to work on target detection, but also contributed to the SBIR and AOARD efforts by helping develop optimized filter routines in C for compilation into Matlab models.

Tamath Rainsford: Postdoctoral fellow. Supported by IRI (AOARD) and SBIR funds Feb 2003 - August 2004. Was initially to work on an AFOSR project, but subsequently worked on HS cell recordings for the AOARD effort. Her main role in the project was to 'flesh out' the numbers of recordings for the velocity constancy data for Straw's thesis work (hence her co-authorship of the primary manuscript on this topic (initially rejected by Current Biology but is currently under revision)). She also performed a suite of experiments looking at the effect of adapting speed and adapting contrast on the 'right shift' of contrast sensitivity curves (contrast gain reduction), using natural images. These experiments were incomplete at the time that she accepted a longer-term position in the T-Ray lab (with Derek Abbott) at the University of Adelaide in July 2004.

Irene Moyer: Paid part-time using SBIR funds after Rainsford's departure, in order to complete recordings left unfinished. She has subsequently started looking at the influence of the 'waterfall effect' component of adaptation on contrast sensitivity, using prolonged test stimuli and a modification of the probe-adapt-probe stimulus using a 'strip-surround-strip' stimulus, that invokes the waterfall effect, but not local contrast gain control. These experiments are nearing completion. Despite termination of the SBIR project, she will continue work under other support (carried forward) until these questions have been adequately addressed to make a definitive paper.

Russell Brinkworth: Post-Doctoral Fellow. Commenced full-time in January 2005 under AFOSR funding. He has also played a valuable support role in the SBIR project since that time and has become heavily involved in construction of the optical head for the Yaw Sensor as well as developing grant proposals to local (ARC) sources to continue work in this area.

Sreeja Rajesh: Ph.D. student. Under stipend support from the University, but IRI funds have supported advisorship (i.e. O'Carroll's salary) and research infrastructure used in her work. She is completing a PhD project modeling pattern noise and the effects of non-linear components of EMDs in a 'yaw simulation' of the HS receptive field.

Eng Leng Mah: Ph.D. student. Supported by a University of Adelaide scholarship, but SBIR/IRI funds again have supported advisorship and research infrastructure used in his work. He is an electrical engineer working on discrete circuit designs based on insect vision. His project is primarily focused on models (based on van Hateren and Snippe) for luminance and contrast adaptation at the early vision stage (photoreceptors and LMCs). He has also worked with Brinkworth in the last few months of the SBIR project on the construction of a prototype optical head for a Yaw Sensor based directly on the models developed for this project.

Lachlan Dowd: Honors Student. Paid part time from SBIR funds since late 2004, in order to provide VisionEgg programming support to the O'Carroll laboratory.

2.4 Partial Bibliography

Collett, T.S. and Land, M.F. (1975) "Visual control of flight behaviour in the hoverfly, *Syritta pipiens*." **J. Comp. Physiol. A**, vol **99**: 1-66.

Dror, R.O., O'Carroll, D.C. & Laughlin, S.B. (2000) "The role of natural image statistics in biological motion estimation." **Springer Lecture Notes in Computer Science 1811**: 492-501

Dror, R.O., O'Carroll, D.C., and Laughlin, S.B. (2001) "Accuracy of velocity estimation by Reichardt correlators" **J. Opt. Soc. Amer. A**, (in press).

Harris, R. A., O'Carroll, D. C. & Laughlin, S. B. (1999). "Adaptation and the temporal delay filter of fly motion detectors," **Vision Research 39,** 2603-2613

Harris, R.A., O'Carroll, D. C. & Laughlin, S.B. (2000) "Contrast Gain Reduction in Fly Motion Adaptation." **Neuron** vol**. 28**, pp. 595-606.

Harrison, R. R., and Koch, C. (2000a) "A robust analog VLSI Reichardt motion sensor," **Analog Integrated Circuits and Signal Processing**, 2000 (in press).

Harrison, R. R., and Koch, C. (2000b) "A silicon implementation of the fly's optomotor control system," To appear in **Neural Computation**, 2000 (in press).

Hausen, K. & Egelhaaf, M. (1989). "Neural Mechanisms of Visual Course Control in Insects." In Stavenga, D. G. & Hardie, R. C. (Eds), **Facets of Vision** (pp. 360-390). Berlin: Springer-Verlag

Hassenstein, B., and Reichardt, W. (1956) "Systemtheoretische analyse der Zeit-, Reihenfolgen-, und Vorseichenauswertung bei der Berwegungsperzeption des Rüsselkäfers *Chlorophanus*," **Z. Naturforch**. Vol. **11b**, pp. 513-524.

Ibbotson, M.R. & Goodman, L.J. (1990) "Response characteristics of four wide-field motion sensitive descending interneurons in *Apis mellifera,"* **J. Exp. Biol. 148**, 255-279.

Krapp, H. G., Hengstenberg, B. & Hengstenberg, R. (1998), "Dendritic structure and receptive-field organization of optic flow processing interneurons in the fly," **Journal of Neurophysiology**, **79**, 1902-1917

O'Carroll, D. C., Bidwell, N. J., Laughlin, S.B. & Warrant, E.J. (1996) "Insect motion detectors matched to visual ecology," **Nature** (London) **382**: 63-66

O'Carroll, D.C., Laughlin, S.B., Bidwell, N.J., & Harris, R.A. (1997) "Spatiotemporal properties of motion detectors matched to low image velocities in hovering insects," **Vision Research**. **37**: 3427-3439

O'Carroll, D.C. (2001) "Motion adaptation and evidence for parallel processing in the lobula plate of the bee-fly *Bombylius major*," in Zanker, J.M., Zeil, J., (Eds.) **Motion Vision, Computational, Neural, and Ecological Constraints**. Springer Verlag, Berlin, Heidelberg & New York, pp. 381-394.

Srinivasan, M.V., (1990) "Generalized gradient schemes for the measurement of image motion," **Biol. Cybernetics**. **63**: 421-431

Srinivasan, M. V., Zhang, .S. W., Lehrer, M. & Collett, T. S.(1996) ''Honeybee navigation en route to the goal: visual flight control and odometry,'' **J. Exp. Biol. 199**, 237–244 .